Improvement of the beam quality of high-power broad area semiconductor diode lasers by means of an external resonator

vorgelegt von
Diplom-Ingenieur
Ahmad Ibrahim Bawamia
aus Port-Louis, Mauritius

Von der Fakultät IV – Elektrotechnik und Informatik
der Technischen Universität Berlin
zur Erlangung des akademischen Grades
Doktor der Naturwissenschaften
- Dr. rer. nat -

genehmigte Dissertation

Promotionsausschuss:

Vorsitzender:	Prof. Dr. Heinrich Klar
Berichter:	Prof. Dr. Günther Tränkle
	Prof. Dr. Serge Mottet

Tag der wissenschaftlichen Aussprache: 18. November 2011

Berlin, 2011

D 83

Acknowledgment

First of all, i would like to express my gratitude to the Prof. Dr. G. Tränkle for having offered me the opportunity to carry out my PhD. work at the Ferdinand-Braun-Institut, Leibniz Institut für Höchstfrequenztechnik (FBH), and for supervising the present work. His constant advice, his encouragement, and the fruitful thematic discussions have been of great help during the course of this work.

My thanks also go to Prof. Dr. Serge Mottet for having accepted to act as second appraiser of the PhD. thesis.

I am indebted to Dr. G. Erbert for his guidance and for his valuable advice, especially in the choice of the diode lasers used in the frame of this work.

I am deeply grateful to Dr. B. Eppich and Dr. K. Paschke for their telling contribution at all levels of this work. Their permanent availability, their advice, and their constructive ideas are duly appreciated.

I wish to thank Dr. F. Schnieder and Dr. H. Wenzel for the thermal simulations, and Agnieszka Pietrzak for the waveguide calculations, encountered in this work.

To all colleagues at the FBH, who have directly or indirectly contributed to this PhD. work, i would like to thank you warmly for the help, for the advice, and for the excellent working atmosphere that prevails at the institute.

The opportunity for me to study in Germany has been made possible by the Deutscher Akademischer Austausch Dienst (DAAD), who have provided me with a doctoral scholarship.

Without the help and the encouragement of my family in Mauritius, i would simply never have had the opportunity to pursue my studies. I am grateful to them for having supported my ideas and aspirations.

Last but not least, i am indebted to my wife Andrea for her unconditional support, her selflessness, and her perpetual encouragement, albeit sporadic well-deserved reality checks.

Berlin, 2010. Ahmad Ibrahim Bawamia

Abstract

The operation of high-power broad area laser diodes in an external resonator is studied with respect to the improvement of their lateral beam quality. A simple setup with a broad area laser diode as gain medium, two lenses and an external mirror is considered. The concept relies on the ability of the active region of the laser diode to act as a spatial filter for higher order modes oscillating inside the resonator.

The geometries of the external cavity laser that favor fundamental mode operation in the lateral direction are inferred with the help of a theoretical model based on the ABCD-matrix treatment of Gaussian beams in a passive stable resonator. Thermal lensing that arises in the broad area laser diode is included in the model. The simulation results show that, for a given strength of the thermal lens arising inside the broad area laser diode, there exists one geometry of the external resonator that produces single mode operation as well as a high overlap between the optical mode and the gain medium of the laser diode.

A novel experimental procedure that quantifies the thermal lens arising in the broad area laser diode to be used inside the external resonator is developed. The thermal lens coefficient is determined for different injection currents and pulse widths. The reliability of the method is validated by the comparison of the obtained results with values of the thermal lens coefficient derived from independent measurements and from the simulation of the temperature distribution inside the laser diode. Furthermore, the latter simulation at different pulse widths enables to explain the observed saturation of the thermal lens coefficient as injection current and pulse width are increased.

The external cavity laser comprising a test broad area laser diode that emits at a wavelength in the region of $1.06\,\mu m$, two lenses, and an external mirror is implemented. Additionally, an adjustable intra-cavity slit that serves as a supplementary spatial filter is inserted in the setup. The evolution of the output power and of the beam quality of the device as a function of the length of the resonator and of the width of the slit is studied at injection currents of $1\,A$ (close to laser threshold) and $5\,A$ (high power operation).

It is observed that at both injection currents, the beam quality of the emission is significantly improved when the length of the resonator and the width of the slit are adjusted to their optimal values. In the case of the experiments at an injection current of $1\,A$, the optimal conditions for the operation of the external resonator correspond to the theoretical predictions, but, at an injection current of $5\,A$, they have to be determined experimentally since the behavior of the laser cannot be explained by the model of the passive resonator anymore.

The criterion used to assess the performance of the external cavity laser, as compared to a similar free running laser, is the maximum output power weighted by the M^2 value. In that respect, at an injection current of $1\,A$, the M^2 value is improved from 9.0 to 3.5, with an output power of $0.35\,W$. At the injection current of $5\,A$, the M^2 value is improved from 18.7 to 5.6, with a corresponding output power of $2.5\,W$. The latter result compares with the best values reported in the literature for the operation of broad area laser diodes in an external resonator.

Zusammenfassung

Das Verhalten von Hochleistungsbreitstreifenlasern in einem externen Resonator wird im Hinblick auf Verbesserungen der lateralen Strahlqualität untersucht. Dazu wird ein einfacher Messaufbau verwendet, der aus einer Breitstreifenlaserdiode als Gainmedium, zwei Linsen und einem externen Spiegel besteht. Das vorgestellte Konzept basiert darauf, dass die aktive Zone der Laserdiode als räumlicher Filter für höhere Resonatormoden dient.

Geometrien des externen Resonators, welche für einen lateralen Grundmodebetrieb geeignet sind, werden aus einem theoretischen Modell abgeleitet, das auf dem ABCD-Matrix Verfahren für Gaussstrahlen beruht und die sich in Breitstreifenlasern ausbildende thermische Linse beinhaltet. Die Simulationsergebnisse zeigen, dass es für eine vorgegebene Stärke der thermischen Linse in der Breitstreifenlaserdiode nur eine externe Resonatorgeometrie gibt, welche sowohl zu einem single-mode Betrieb als auch zu einer groSSen Überlappung der optischen Mode und des Gewinnmediums führt.

Ein neuartiges experimentelles Verfahren, welches die thermische Linse einer Breitstreifenlaserdiode in einem externen Resonator quantifiziert, wird entwickelt. Der thermische Linsenkoeffizient wird, für verschiedene Injektionsströme und Pulsbreiten, bestimmt. Die Verlässlichkeit dieser Methode wird, durch den Vergleich der erhaltenen Ergebnisse mit den Werten von unabhängigen Messungen zur Ermittlung des thermischen Linsenkoeffizienten und durch die Simulation der Temperaturverteilung in der Laserdiode, verifiziert. Des Weiteren, lässt sich durch diese Simulation bei verschiedenen Pulsbreiten die Sättigung des thermischen Linsenkoeffizienten für höhere Injektionsströme und größere Pulsbreiten erklären.

Der Laser mit externem Resonator besteht aus der zu untersuchenden Breitstreifenlaserdiode mit einer Emissionswellenlänge von ungefähr 1.06 μm, zwei Linsen und einem Spiegel. Des Weiteren dient ein justierbarer Spalt innerhalb des Resonators als zusätzlicher Raumfilter. Die Abhängigkeit der Ausgangsleistung und der Strahlqualität von der Resonatorlänge und der Spaltbreite wird bei Injektionsströmen von 1 A (nahe der Laserschwelle) und 5 A (Betrieb bei hoher Ausgansleistung) untersucht.

Bei beiden Injektionsströmen verbessert sich die Strahlqualität deutlich, wenn die Länge des Resonators und die Breite des Spaltes auf die optimalen Werte eingestellt werden. Bei den Experimenten mit einem Injektionsstrom von 1 A entsprechen die optimalen Bedingungen den theoretischen Voraussagen. Bei 5 A Injektionsstrom müssen sie jedoch experimentell bestimmt werden, da das Verhalten des Lasers nicht mehr durch das Modell des passiven Resonators erklärt werden kann.

Den Maßstab zur Beurteilung der Laserperformance stellt, im Gegensatz zu identischen freilaufenden Lasern, die maximale Ausgangsleistung gewichtet mit dem M^2-Wert dar. Unter diesem Gesichtspunkt wird, bei einen Injektionsstrom von $1\,A$ und einer Ausgangsleistung von $0.35\,W$, der M^2 Wert von 9.0 auf 3.5 verbessert. Bei einem Injektionsstrom von $5\,A$ und einer Ausgangsleistung von $2.5\,W$ wird der M^2-Wert von 18.7 auf 5.6 verbessert. Das zweite Resultat ist, mit den besten Ergebnissen von Breitstreifenlaserdioden in einem externen Resonator über die in der Literatur berichtet wird, vergleichbar.

Contents

1 Introduction **11**

2 The high power broad area semiconductor laser **15**
2.1 General aspects of semiconductor lasers 16
2.2 Assessment of the maximum output power level of a laser diode 19
2.3 A BA laser for high power operation 22
2.3.1 Epitaxial structure and layout 22
2.3.2 Preparation of the BA laser chips for operation 25
2.4 Characterization of the free running BA laser 26
2.4.1 Power-current characteristics and spectrum 26
2.4.2 Beam quality in the lateral direction 27
2.5 Means of improving the lateral beam quality of BA lasers 29

3 Broad area semiconductor laser with an external resonator **31**
3.1 Model for a passive resonator 32
3.1.1 Vertical axis 32
3.1.2 Lateral axis 37
3.2 Modes of the lateral resonator 37
3.2.1 The fundamental mode 37
3.2.2 Higher order modes 38
3.3 Spatial mode filtering 39
3.4 The passive resonator with a non-uniform refractive index profile 40
3.4.1 Nonlinearities in the laser diode 41
3.4.2 Influence of the thermal lens on the passive resonator 42

4 Definition and measurement of laser beam characteristics **51**
4.1 Measurement of power and spectrum 52
4.2 Measurement of the beam quality 53
4.2.1 Definition of the beam width 54
4.2.2 Extracting the M^2 value from the beam width measurements . . 55
4.2.3 Experimental setup for the characterization of beam quality . . . 58
4.2.4 Estimation of the uncertainty in the measurement of the beam quality 61

5 Determination of the thermal lens in a BA laser diode **65**
5.1 The experimental setup 66
5.1.1 Vertical axis 66
5.1.2 Lateral axis 66
5.2 The measurement principle 67
5.3 Beam shaping inside the amplifier 69

5.4 Experimental procedure and results 72
5.4.1 The experimental procedure 72
5.4.2 Experimental results 73
5.5 Validation of the experimental results 75
5.5.1 Estimation of the beam quality of a laser diode 75
5.5.2 Validation through simulation 76

6 Implementation of the external resonator laser 81
6.1 The experimental setup 81
6.2 Stability of the resonator and output power 82
6.3 Influence on the beam quality 84
6.3.1 The active zone as modal filter 84
6.3.2 Addition of an intra-cavity slit 87
6.4 The resonator at an injection current of 5A 95
6.4.1 The active zone as modal filter 95
6.4.2 Addition of an intra-cavity slit 96

7 Conclusion 103

List of abbreviations and symbols 107

Bibliography 111

Chapter 1

Introduction

The market demand for high-power diode lasers with a highly focusable beam in applications such as free space optical communications, medical therapy, display technologies and material processing is in constant rise. Their popularity stems from the inherent high electrical to optical conversion efficiency, their small size, their high reliability, and their cost-effectiveness [1].

The determining factor in how tightly the emission of a laser can be focused is the beam quality [2]. One common measure of the latter, set by the ISO standard [3], is the beam propagation ratio, denoted by M^2 that takes values greater or equal to one. A beam of optimal quality has an M^2 value of one, corresponding to a Gaussian distribution of the intensity. Owing to the geometry of their optical resonator, diode lasers emit such a beam in the fundamental mode. Therefore, the design of diode lasers, meant to have a very good beam quality, includes a mechanism that ensures fundamental mode operation. In the vertical axis (perpendicular to the p-n junction), optical confinement is provided by a waveguide structure built in the epitaxial layers. In the present work, a large optical cavity (LOC) structure is used, which yields a near-Gaussian mode [2, 4].

One design strategy used to force single-mode operation in the lateral axis of diode lasers is the ridge-waveguide (RW) laser. The RW is defined by two etched trenches, whose depth and separation are tailored in such a way that the thus created waveguide cuts off the propagation of higher order modes. Depending on the depth of the trenches (that create a refractive index step) and the emission wavelength, the ridge is typically some micrometers wide. The maximum output power achieved by such a device is limited by catastrophic optical mirror damage (COMD) and/or thermal rollover, and does not exceed $2\,W$ [5].

When it comes to raising the maximum output power of RW lasers, the most effective solution lies in the broadening of the active region of the diode in the lateral direction [6]. Such lasers, called broad area (BA) lasers, have been demonstrated to emit up to $20\,W$ of output power in continuous wave (CW) operation with a stripe width of $96\,\mu m$ [7]. However, in such a case, it is not possible to maintain single mode operation and, as a consequence of the apparition of higher order modes and the influence of non-linear effects [8], the beam quality is seriously degraded, with M^2 values lying typically above 10 [9].

A method of improving the beam quality of BA lasers while maintaining the high output power is the use of an external resonator. Here, one of the facets of the laser diode is anti-reflection (AR) coated and the laser resonator is bounded by the remaining facet with a given reflectivity R (5 % in the present study), and an external mirror with high reflectivity (HR). The facet with reflectivity R acts as output coupler. It is a very simple and versatile scheme since the geometry of the external resonator can be modified and optical elements can be added into it without requiring further wafer processing.

The aim of this work is to study the feasibility of such external cavity lasers (ECL) with test BA laser diodes that are 1.3 mm long and have a width of the active region of 100 μm. The choice of the external resonator concept should take the following into account:

- An 'on-axis' design is required, since the far-field profile of the laser emission is centered on the optical axis.
- The number of intra-cavity elements should be small so as to minimize internal losses, to enable an eventual miniaturization of the concept, and to reduce the cost of assembly.

To date, the highest output power reported for a BA laser with an external resonator that yields a near-diffraction-limited output beam is 2.46 W [10]. However, the optical setup is designed off-axis, making it suitable only for BA lasers that emit in a double-lobed far-field. Furthermore, in addition to the laser diode and a collimation lens, two volume Bragg gratings (VBG) are required inside the external cavity laser (ECL), that make it relatively expensive to assemble.

Sharfin et al. [11] have proposed a simple ECL that consists only of a lens and a conventional external mirror in addition to the laser diode. The concept, where the filtering of higher order modes is achieved by the active region of the diode itself, is compatible with an 'on-axis' design. Due to its small amount of intra-cavity elements, this ECL offers potential advantages such as minimized internal losses, ease of alignment and a possibility for miniaturization. However, the maximum output power obtained with this scheme in a laterally single mode beam is 100 mW.

The above-named concept is investigated at output powers in the Watt range. In particular, the principles underlying the spatial mode filtering process inside the laser and their validity at high power operation are studied. The theoretical model is refined in order to accommodate thermal lensing, the main contribution to non-linear effects that gain in influence inside the gain medium (the BA laser diode) as the injection current is increased. Subsequently, an additional lens is included inside the setup in order to optimize the mode filtering. The concept is implemented with a test BA laser diode that emits in the wavelength region of 1.06 μm.

This thesis is organized as follows: chapter two deals with the BA laser diode as a free running laser. Generalities about semiconductor lasers are briefly presented, followed by a description of the laser structure used as gain medium inside the ECL. Its characterization (as free running laser) and a brief discussion on different means of improving the beam quality of BA lasers complete the chapter.

Chapter three goes into the details of the theoretical model, based on the ABCD-matrix treatment of Gaussian beams, underlying the functioning of the external resonator. The conditions for spatial mode filtering are looked into, and the limitations of the model at high power operation are discussed. A novel resonator geometry is presented, that takes into account the thermal lensing arising inside the gain medium, and its influence on the mode formation is studied.

Chapter four comprises a description of the experimental setup used for the measurement of the power, the spectrum and the beam quality of the different laser diodes used in the study. The definitions used for the characterization of the spatial distribution of the modes are set, and the ensuing measurement procedure is detailed.

Chapter five deals with the measurement of the thermal lens inside the laser diodes acting as a gain medium inside the ECL. A novel method that allows the determination of the thermal lens coefficient in a laser diode is presented. The experimental results are validated by two methods. The first one is based on the thermal lens dependent M^2 value of a free running laser, while the second one uses a finite element method (FEM) simulation of the temperature distribution inside the laser diode.

In chapter six, the implementation of the ECL is discussed and, with the help of the theory developed in chapter three, and the values of the thermal lens obtained in chapter five, the geometries that yield optimal spatial mode filtering are investigated. In order to monitor the beam diameter inside the resonator, and at the same time to increase the effectiveness of the spatial mode filtering, a series of measurements is carried out with an intra-cavity slit. The different experimental results are compared with each other, and with the free running BA laser.

Chapter seven comprises a summary of the main themes encountered in the present work and a conclusion about the feasibility of the BA laser in such an external resonator at high power operation.

Chapter 2

The high power broad area semiconductor laser

The broad area (BA) semiconductor laser is the central device in the study of the external cavity laser (ECL). In fact, the main goal of the ECL is going to be the improvement of the lateral beam quality of the BA laser, while maintaining the same output power levels. The present work can also be seen as a comparison between a BA laser with both its mirrors lying on the facets (free running laser), and one operated in an external resonator. So, the BA laser diode acts both as reference value for the ECL and as its gain medium.

While it is not in the scope of this work to study the BA laser in depth, it is however important to explain how it functions and how its design has evolved to the present version that is capable of supplying several Watts of optical power. The tools used to assess the performance of a BA laser are introduced next. Based on its electro-optical and thermal properties, a particular BA laser structure is chosen for the purposes of the study. Its epitaxial structure, the layout of the chips, the different facet coatings and the packaging are shortly introduced.

The free running version of the chosen laser structure is characterized with respect to output power, spectrum, and lateral beam quality. The chapter is concluded with a concise literature review of the different methods used for the improvement of the lateral beam quality of high power diode lasers.

2.1 General aspects of semiconductor lasers

Laser radiation is achieved when three conditions are fulfilled, namely [12]:

- The presence of an active medium that, under population inversion, coherently amplifies a beam of radiation (stimulated emission).
- A process, commonly named as 'pumping', that enables the population inversion in the active medium.
- An optical feedback mechanism that allows the radiation to repeatedly bounce back and forth inside the active region.

The overwhelming majority of semiconductor lasers are grown with the so-called III-V materials, that is materials from the columns III and V of the periodic table. A mixture of binary, ternary and quaternary materials are used, examples of those being $GaAs$, $In_xGa_{1-x}As$, $Al_xGa_{1-x}As$ or $In_xGa_{1-x}As_yP_{1-y}$. The indices (x,y,..) represent the fractions of the given element in the material. The extended used of III-V materials lies in the fact that they have a direct band gap [2], which implies that the efficiency of the radiative recombination between the conduction band and the valence band is high relative to materials with an indirect band gap.

In semiconductor lasers, the active medium lies in the space charge zone at the pn-junction when a p-doped semiconductor layer and a n-doped semiconductor layer are brought together. Population inversion comes in the form of electrons and holes that are made to gather at the junction. For the sake of high confinement of the carriers in the space charge zone, which in turn improves the internal efficiency and thermal stability, semiconductor lasers are nowadays built as double heterostructure, where an intrinsic layer of semiconductor material with a given band gap energy E_g is sandwiched between a p-doped layer and a n-doped layer of another semiconductor material with a higher band gap energy [13–15]. A simplified energy band diagram of a double heterostructure is sketched in figure 2.1 [16]. When a forward voltage V is applied, such that $qV \gtrsim E_g$ (q being the charge of the electron), the Fermi levels of the electrons (E_{F_c}) and of the holes (E_{F_v}) in the region of the intrinsic layer lie in the conduction band (E_c) and in the valence band (E_v) respectively, such that the respective carriers can flow there, where they remain confined due to the barrier created by the higher band gap energy of the doped layers. The pumping process is the flow of electric current across the p-i-n diode, that in turn induces the bias voltage. The three transition processes between the conduction band E_c and the valence band E_v involving carriers and photons are absorption, spontaneous emission and stimulated emission. In the latter process, a stimulating photon with energy $h\nu$, with h being the Planck constant and ν the frequency of the photon, induces the emission of another photon with identical wave function. This happens via the radiative recombination of an electron-hole pair at respective energies that fulfill the condition of Bernard et Duraffourg [17]:

$$E_g \leq h\nu \leq E_{F_c} - E_{F_v} \tag{2.1}$$

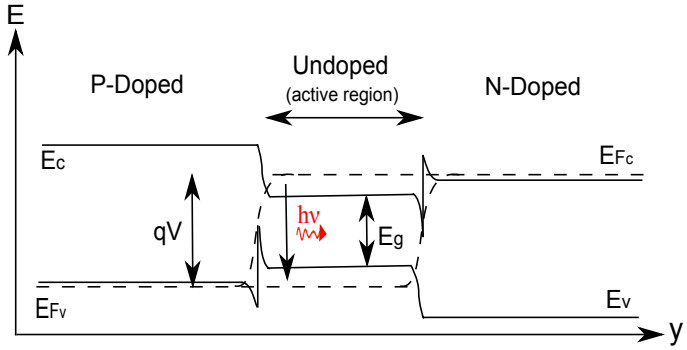

Figure 2.1: Simplified energy band diagram of a double heterostructure in the growth direction of the layers (y).

If the thickness of the active region, that is the intrinsic semiconductor layer, is reduced to the order of the De Broglie wavelength of the electrons in the material, quantum confinement of the carriers occurs in the direction along the thickness of the layer and their energy levels become discrete, yielding a quantum well structure [2,18]. Due to their small active volume as compared to bulk materials, quantum well lasers characteristically have a reduced threshold current density with respect to bulk heterostructure lasers. Moreover, the lattice mismatch between the quantum well material and the neighboring layers can be chosen so as to induce strain in the former. Strained quantum wells enable the enlargement of the spectrum of semiconductor laser diodes to wavelengths not available with standard materials [19] and reduce the threshold current density further than with unstrained quantum wells [20, 21].

For the optimization of the efficiency of the diode laser, the photons should be confined as much as possible in the active region. Due to the extremely thin active region in quantum well lasers, the separate confinement heterostructure (SCH) is widely used, where the confinement of the optical mode is provided by waveguiding layers directly adjacent to the active layer, and an additional cladding layer, with a lower refractive index, adjacent to the waveguide layer [22]. The refractive indices and the thicknesses of the waveguide and cladding layers are adjusted such that only the fundamental mode is guided. Furthermore, it is desirable that the guided mode be large enough in order to reduce the facet load of the device. Additionally, a large optical mode ensures a reduced far-field angle of the emission in that dimension. Therefore, the concept of large optical cavity (LOC) is often implemented [2, 4, 23]. The waveguide layer is broadened while its single-mode operation is maintained. The confinement factor of the mode however falls to very small values (typically under $1\,\%$), thus reducing the modal gain. However it is compensated by the very small losses in the waveguide structure such that long resonator lengths are possible, thus maintaining the overall efficiency of the laser. The number of quantum wells in the device can also be increased in order to yield higher efficiencies.

Until now, the semiconductor laser has been considered only in the dimension perpendicular to the plane of the pn-junction. This direction shall be referred to as the vertical direction. Current is injected inside the device via a metal contact stripe that extends along the lateral dimension, and, to the exception of some current spreading, it remains confined into the area defined by the stripe. The width of the active region in

that direction will then approximately be defined by the width of the stripe. In fact, stimulated emission will occur only in regions pumped by the electric current. Optical confinement also takes place under the current injection stripe. Modes that propagate within its width experience gain and are amplified whereas those propagating beyond it suffer high losses and progressively decay. In steady-state operation, only those modes who experience net gain oscillate in the laser resonator. Such an optical confinement process is called gain guiding. The current stripe can be made small enough such that only the fundamental mode experiences net gain. An alternative to gain guiding under the current injection stripe is index guiding of the optical modes. Just like in the vertical direction, a waveguide structure can be built in the lateral dimension. Its width and the refractive index step can be set such that only the fundamental mode is guided.

Stimulated emission only is not sufficient to guarantee steady-state laser emission. Optical feedback, which increases the photon density inside the active material, is a prerequisite. It comes most often in the form of a Fabry-P$\acute{e}$rot resonator, where the cleaved facets of the semiconductor material act as resonator mirrors. The Fresnel reflectivity of these facets lies in the region of $30\,\%$, for typical effective refractive indices around 3.3 encountered by the laser beam inside the diode.
Based on the principles mentioned in the previous section, semiconductor laser diodes with near-single mode operation in both the vertical and the lateral dimensions have been demonstrated up to a power of approximately $2\,W$ [5]. This result has been achieved by a ridge-waveguide (RW) laser, where the lateral confinement of the optical mode is achieved by index guiding. However, The narrow width of the output facet inherently limits the output power because of the small light-emitting area and the high optical intensity, which induces catastrophic optical mirror damage (COMD) [24]. Moreover, the small contact area (perpendicular to the plane of the p-n junction) results in high values for the thermal resistance and the series resistance of the device. Thermal rollover may then become the main limiting factor to the high power output, especially when the facets are passivated [25], which drives the optical intensity required for COMD higher. When higher output power is required, the broadening of the region of optical confinement in the lateral dimension is opted for. The current injection stripe is made much wider, such that the broader spot falling on the facet reduces the incident intensity significantly and, at the same time, the thermal resistance and series resistance are lower, implying higher output powers are possible before thermal rollover appears (also dependent on the packaging scheme of the device). Due to their extended width in the lateral direction, such lasers are called broad area (BA) lasers. A maximum output power of $20\,W$ in continuous-wave (CW) operation has been demonstrated for a width of the active region of $96\,\mu m$ in the lateral dimension and a diode length of $4\,mm$. The maximum COMD level in that case has been registered to be $31\,MWcm^{-2}$ [7].

With the broadening of the current injection stripe in the lateral direction, the extended active region enables higher order modes to oscillate in the laser resonator. The emission is no more single-mode in that direction, which results in the broadening of the far-field profile of the emission, and consequently a higher M^2 value [26]. Hence the present study, where the operation of a BA laser diode in an external cavity should improve the beam quality of the system whilst maintaining the high power output level as in an identical free running laser (except for the facet reflectivities).

2.2 Assessment of the maximum output power level of a laser diode

A prerequisite for the BA laser diode that is to be implemented as gain medium in the ECL is its ability to operate at high power levels in the order of several Watts. Several aspects, such as the laser structure, the width of the active region, the resonator length, the facet reflectivities and the packaging have to be taken into consideration in the choice of a laser diode that suits the purpose of the experiment. It is therefore important to be able to assess their impact on the output power of the laser diode. For this purpose, a simple model that predicts the power-current characteristics of a laser diode as a function of the above-named considerations is applied.

In a first step, the power-current characteristics of the laser diode is considered to be a linear dependency of the optical power on the current (thermal effects are introduced later, whereas the contribution of spontaneous emission is neglected throughout). The optical power (P) is given as a function of the injection current (I) as:

$$P = \begin{cases} 0 & \text{if } I \leq I_{th}; \\ S(I - I_{th}) & \text{if } I > I_{th}., \end{cases} \tag{2.2}$$

where I_{th} is the threshold current and S is the slope efficiency. I_{th} and S are unknown, so they have to be expressed in terms of parameters that have already been determined.

The BA laser diode is considered to be an active Fabry-P$\acute{e}$rot resonator of length l, with its mirrors, with reflectivities R_f and R_r, being respectively on the front and rear facets. The modal gain at laser threshold (Γg_{th}), where Γ is the confinement factor and g_{th} the gain at threshold, is given in terms of the internal losses (α_i) and the losses through the mirrors (α_m) as [27]:

$$\Gamma g_{th} = \alpha_i + \alpha_m, \qquad \alpha_m = \frac{1}{2l} \ln \left[\frac{1}{R_f R_r} \right] \tag{2.3}$$

The dependence of the material gain (g) below laser threshold of the quantum well active region of the laser with injected current density (J) can be approximated to be logarithmic [28, 29]:

$$g = g_0 \ln \left[\frac{J}{J_{tr}} \right], \tag{2.4}$$

where g_0 is the differential gain and J_{tr} is the transparency current density. By combining equations 2.3 and 2.4, the threshold current density J_{th} can then be written as:

$$J_{th} = J_{tr} \exp \left[\frac{\alpha_i + \alpha_m}{\Gamma g_0} \right] \tag{2.5}$$

The threshold current I_{th} is then obtained by multiplying J_{th} with the cross-sectional contact area of the diode, that is the length l times the width W_x of the active zone in the lateral dimension. The slope efficiency (S) of the power-current characteristics, as it would be measured at the front facet (output facet) of the diode, is given by:

$$S = \frac{h\nu}{q} \eta_i \frac{\alpha_m}{\alpha_i + \alpha_m} \frac{1}{1 + \xi}, \qquad \xi = \frac{(1 - R_r)\sqrt{R_f}}{(1 - R_f)\sqrt{R_r}}, \tag{2.6}$$

where h is the Planck constant, ν is the frequency of the emission, q is the charge of the electron and η_i is the internal quantum efficiency of the laser material.

For a laser with a given vertical structure, the geometry and facet-reflectivity-independent material parameters α_i, η_i, Γg_0 and J_{tr} can all be measured on uncoated and unmounted diode samples of different lengths by either the cavity length dependency of the differential efficiency [2] for α_i and η_i, or by the inverse cavity-length dependency of the threshold current density [30] for Γg_0 and J_{tr}. The emission wavelength is also inferred from sample diodes with a similar vertical structure. The power-current characteristics of different geometries and facet reflectivities can then be investigated. However, the above equations do not take into account the heat produced inside the active zone of the diode during operation. Since it influences both the threshold current and the slope efficiency significantly, it has to be included in a realistic simulation of the power-current characteristics.

The temperature-dependent power-current characteristics can be approximated as [2]:

$$P = S \exp\left(\frac{-\Delta T}{T_1}\right)\left[I - I_{th} \exp\left(\frac{\Delta T}{T_0}\right)\right] \tag{2.7}$$

In the above equation, the values of I_{th} and S used are those corresponding to the heat sink temperature. ΔT is the increase in temperature in the active zone of the diode with respect to the heat sink temperature. T_0 and T_1 are characteristic temperatures of the laser material and they respectively quantify the dependency of the threshold current density and the slope efficiency on an increase in temperature in the active zone. They are also considered to be geometry and facet-reflectivity-independent material parameters of a given laser structure and are measured as follows: the threshold current density and slope efficiency of a sample diode are measured at different heat sink temperatures. The measurements are carried out in pulsed regime with a low duty cycle in order to minimize temperature rise in the active zone other than that contributed by the heat sink. The logarithms of the measured J_{th} and S are plotted against the heat sink temperature. A linear fit on the data yields T_0 in the case of the measurement of the threshold current density and T_1 in the case of the measurement of the slope efficiency.

The temperature rise ΔT in equation 2.7 can be expressed as [2]:

$$\Delta T = R_{th}\Big[I(V_0 + IR_s) - P\Big], \tag{2.8}$$

where R_{th} is the thermal resistance of the device, V_0 is the voltage across the p-n junction and R_s is the dynamic series resistance. In practice, V_0 and R_s are derived from the voltage-current characteristics [2] of the device under test (or estimated from a similar one). R_{th} is determined by a linear fit on the temperature rise in the active zone of the diode with heat power produced. The temperature rise (ΔT) inside the active area as a function of injection current is obtained from the measured increase in the emission wavelength (λ) with current:

$$\Delta T = \frac{d\lambda}{dI}\frac{dT}{d\lambda}, \tag{2.9}$$

where $\dfrac{d\lambda}{dT}$ is the wavelength drift with temperature and it is a constant for the laser material. It is obtained from the measurement of the peak of the spontaneous emission

spectrum with heat sink temperature. The heat power P_{th} is derived from the power-current-voltage characteristics of the device:

$$P_H = IV - P, \tag{2.10}$$

where V is the voltage across the device. Finally, for a given range of currents, the corresponding ΔT is plotted against P_{th} and the slope of the graph yields the value of R_{th}.

Equation 2.8 is injected in equation 2.7 and the latter is solved numerically in order to extract the value of P as a function of I. An example is shown in figure 2.2 below. The measured power-current characteristics (full lines) of a 1.3 mm long BA laser diode with a stripe width of 100 μm is compared with the simulations (dotted lines). The reflectivities are 5 $\%$ and 95 $\%$ for the front facet and rear facet respectively. These values have been chosen after running the simulations for different pairs of facet reflectivities. The output power at the front facet is maximal for this particular pairing of the reflectivities. The diode is mounted p-side up on a CuW sub-mount, which is in turn mounted on a C-mount. The latter is fastened on a copper heat sink, which is kept at a temperature of 25 $^{\circ}C$. The laser is operated in quasi-continuous wave (QCW) regime, with a pulse width of 100 μs and a repetition rate of 25 Hz. The parameters used in the calculations are shown in table 2.1.

The simulation results are in good agreement with the measurements until an injection current of approximately 7 A. Above this point, the measurements show the beginning of thermal roll-over, whereas this behavior is not present in the simulated curve. The principal reasons for this discrepancy are that, in the simulations, R_{th} and T_1 are taken to be constant over the whole current range whereas the former normally increases and the latter decreases as the current, and therefore the heating inside the diode, is increased [31, 32].

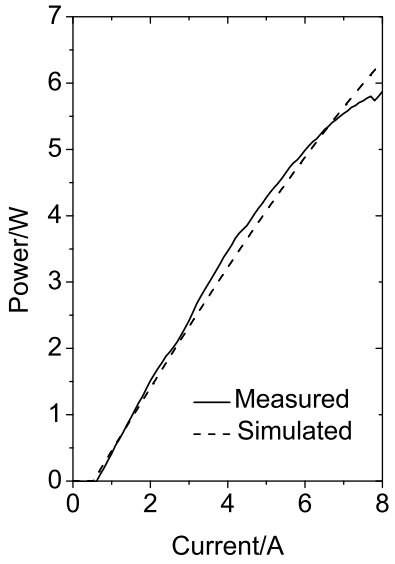

Parameter	Measured	Simulated
I_{th}/A	0.60	0.57
S/WA^{-1}	0.83	0.83

Figure 2.2: Measured (full lines) and simulated (dotted lines) power-current characteristics of a BA laser diode

J_{tr}/Acm^{-2}	η_i	α_i/cm^{-1}	$\Gamma g_0/cm^{-1}$	λ/nm	T_0/K	T_1/K	$\frac{d\lambda}{dT}/KW^{-1}$	R_{th}/KW^{-1}	R_s/Ω	V_0/V
134	0.95	1.56	11.2	1053	85	450	0.41	4.3	0.08	1.24

Table 2.1: Parameters used in the simulation of the semiconductor laser diode.

2.3 A BA laser for high power operation

The simulation tool presented in the previous section is used to assess the output power levels of different laser structures, and the one tested in the example is also chosen to be implemented in the ECL. In fact, with the chosen facet reflectivities and mounting scheme, it fulfills the requirements in terms of output power, in that it emits several Watts (in QCW operation). The technical aspects of its epitaxial structure, chip layout, facet coating and packaging are briefly described in the present section.

2.3.1 Epitaxial structure and layout

Epitaxial structure

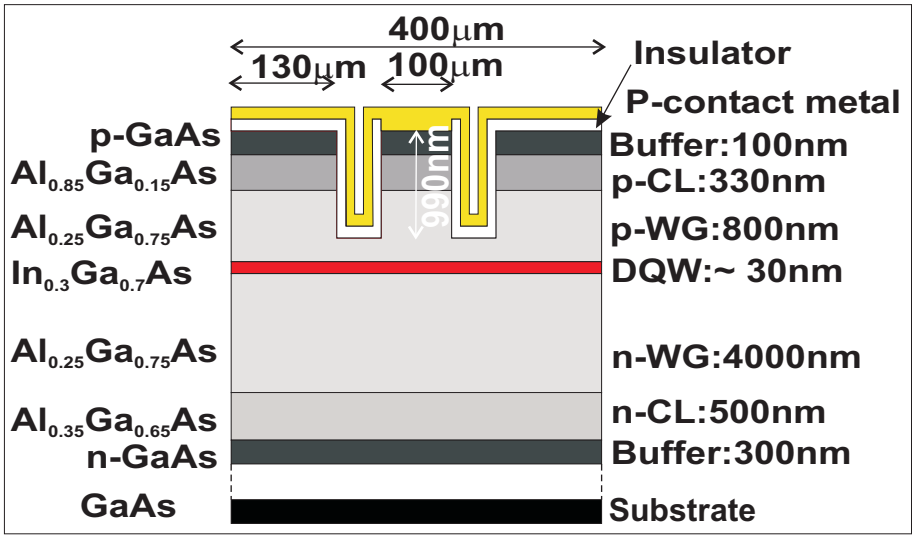

Figure 2.3: Schematic of the geometry and the vertical structure of the broad area semiconductor laser diode. The figure is not to scale, and the substrate($\backsim 120\,\mu m$) is depicted by a layer under broken lines in order to suggest that it is much thicker than the rest of the layers.(WG:Waveguide, CL:Cladding, DQW: Double quantum well).

The epitaxial structure of the semiconductor chip shown in figure 2.3 is grown by metal oxide vapor phase epitaxy (MOVPE) [19, 33] on a $GaAs$ substrate with a thickness of approximately $120\,\mu m$. The undoped active region, with a total thickness of around $30\,nm$, consists of two strained $In_{0.3}Ga_{0.7}As$ quantum wells separated by $GaAsP$ spacers (not shown on the figure). The waveguide layer, a so-called asymmetric super large optical cavity (ASLOC) structure [5], is composed of n-doped and p-doped $Al_{0.25}Ga_{0.75}As$ layers with respective thicknesses of $4000\,nm$ and $800\,nm$. The cladding layer is made of $Al_{0.85}Ga_{0.15}As$ on the n-doped side and of $Al_{0.35}Ga_{0.65}As$ on the p-doped side. The structure is completed by a highly doped $GaAs$ buffer layer on the p-side and a moderately doped buffer layer of the same material on the n-side. All heterojunctions are graded in order to reduce the series resistance of the diode structure [34].

This particular design of the vertical structure of the semiconductor chip is a fine tuning between the optical, electrical and thermal properties of the device that ensure high power operation [2, 21].

With the thickness, the composition and the doping of the different layers forming the laser structure known, the mode guiding inside the vertical waveguide is simulated with the QIP software (internally developed at the Ferdinand-Braun-Institute. Simulation results courtesy of Ms. Agnieszka Pietrzak). In a first step, the respective refractive indices of the layers constituting the laser structure are calculated using a modified single-effective-oscillator model [35]. The refractive index profile of the laser structure is shown in figure 2.4(a). In a second step, a one-dimensional waveguide equation [36] is used to determine the near-field and far-field intensity profiles of the guided mode. They are presented in figure 2.4(b) and 2.4(c), respectively. The simulation results are validated by the comparison with the measured far-field intensity profile (also shown in figure 2.4(c)) of a laser diode with the vertical structure described in this section. The details of the measurement process for laser beam profiles are given in chapter four. From the graph, it can be seen that the two distributions are in good agreement with each other.

In the present work, the beam profile in the vertical direction is only subsequently used in order to estimate the back coupling efficiency into the waveguide of the vertical mode in an external resonator. For this purpose, it is only important to have an estimate of the M^2 value of the beam. The divergence angle of the far-field is measured to be 14° at full-width-half-maximum (FWHM), or 35.2° according to the second moments definition of the spread of the beam. The second moments diameter of the intensity profile in the near-field is taken from the simulation results, and is found to be $3.36\,\mu m$. As a result, the M^2 value of the beam is found to be 1.5, indicating that the emission in the vertical direction is close to a Gaussian distribution.

Lateral layout

Referring back to figure 2.3, the build of the laser diode is now considered in the lateral direction. The chip has a total width of $400\,\mu m$, and a trench of $20\,\mu m$ in width and $990\,nm$ in depth is etched at a distance of $130\,\mu m$ on either side of the outer border on the p-side. An isolating layer is placed at the top of the epitaxial structure, with an opening of $100\,\mu m$ over to the mesa of identical width between the two trenches. A metal contact layer that extends over the full width of the chip is deposited, on the p-side, above the isolator and on the n-side, below the $GaAs$ substrate. The layout on the p-side defines the current injection window of the diode. The current is injected via the metal contact and flows into the semiconductor across the opening in the isolator. The mesa structure enhances the confinement of the current through to the active zone of the diode.

Both the current injection window and the mesa structure will define the lateral mode guiding inside the laser diode, via gain guiding and a weak index guiding, respectively. In the latter case, the mesa structure etched in the center of the chip induces a refractive index step of approximately 0.002 in the lateral refractive index profile. This results in an enhanced confinement of the lateral optical modes. The implications of the optical

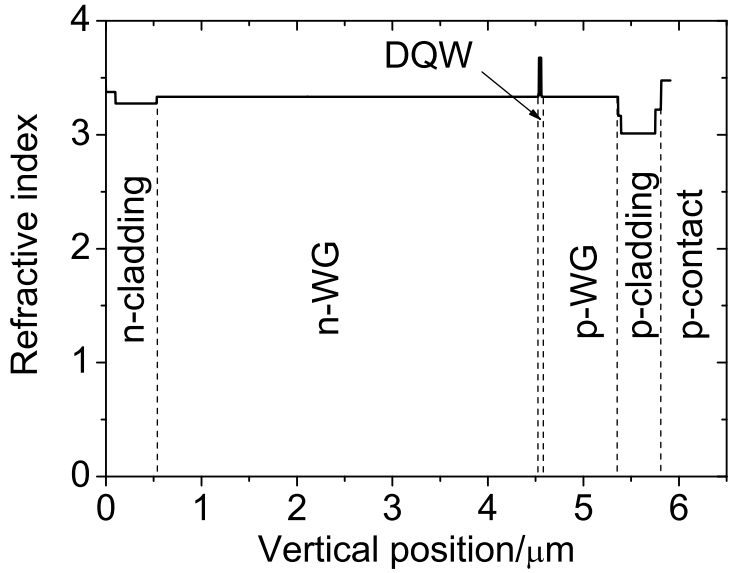

(a)

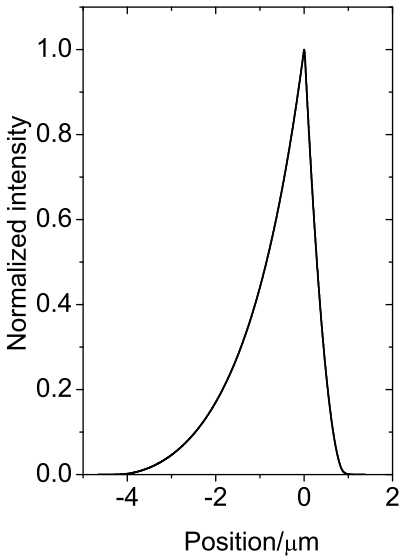

(b)

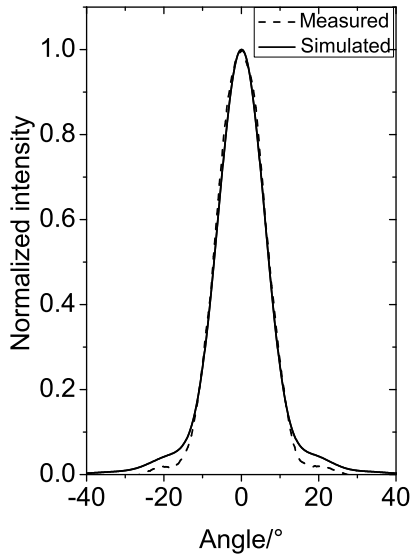

(c)

Figure 2.4: (a) Refractive index profile of the laser structure, (b) Simulated near-field intensity profile of the guided mode, (c) Simulated(full lines) and measured (dotted lines) far-field intensity profile of the guided mode. Graphic courtesy of Ms. Agnieszka Pietrzak

confinement mechanisms on the lateral mode structure of the free running laser diode shall be considered in a subsequent section.

2.3.2 Preparation of the BA laser chips for operation

The semiconductor diode structure described above is grown in several rows over part of a 3 inch GaAs wafer. After the epitaxial growth, etching of the mesa structure, and deposition of the insulating layer and metal contacts, the rows of diode chips, with a resonator length of 1.3 mm, are cleaved off the wafer. Both facets of the chips have a reflectivity of approximately 30 $\%$.

Mirror coating

Depending on the application, the reflectivity of the facets of the semiconductor chips is altered by the deposition of a thin film coating. For amplifiers, as used in the determination of the thermal lens in the laser structure (refer to chapter 5), both facets are anti-reflection (AR) coated to approximately 0.01 $\%$. The free running lasers are, on their part, coated with 5 $\%$ on the facet of light output (front facet) and with 95 $\%$ on the other facet (rear facet). The diodes that are to be used in the external resonator are, as a result, also made to have a reflectivity of 5 $\%$ on the front facet. The rear facet is AR-coated, since the laser resonator is extended outside the diode by an external mirror.

Prior to the reflectivity coating, the facets of the 1.3 mm long chips are passivated with the deposition of ZnSe [25]. Then, depending on the reflectivity to be achieved, thin film layers in the order 10 nm to 200 nm of either one, or a combination of Si, TiO_2 and Al_2O_3 are applied on the facets by the process of reactive ion beam etching (RIBE).

Packaging

After facet coating, individual laser chips are detached from the rows, yielding single emitters with a length of 1.3 mm and a width of 400 μm. During operation, the laser diode emits, in addition to laser light, a certain quantity of heat produced mainly in the active region, but also in the individual epitaxial layers. The heat produced is detrimental to both the efficiency of the laser and its lifetime. Therefore, an effective process is to be adopted in order to effectively channel the heat out of the diode. At the same time, the electrical contacting of the latter to an external current source should be set up.

Heat removal from laser diodes usually follows through three components. In this case, they are the sub-mount, the C-mount and the heat sink. The chips are soldered p-side up, that is, their n-side is soldered with $AuSn$ solder to a CuW sub-mount, which is, in turn, soldered with $PbSn$ to the C-mount made of copper. The sub-mounts acts as a material with a high heat conductivity that effectively extracts heat from the chip, and at the same time it compensates to a certain extent the high mismatch in the coefficient of thermal expansion (CTE) between the $GaAs$ bottom layer of the chip and the C-mount. Every laser diode is individually soldered onto a C-mount in this way. The latter is then fastened to a heat sink made of copper, and that is kept at a constant temperature (here 25 $^\circ C$) by circulating water. The C-mount allows the easy interchange between laser chips that are to be measured on the experimental bench equipped with the heat sink.

The components used for the thermal management of the laser diode also fulfill the purpose of electrical contacts between the chips and an external current source. Usually, one electrode of the external current source is connected to the heat sink, while the other is connected, via a gold stripe, to a support on the C-mount. A series of gold wires originating from the support are then bonded to the metal contact on the p-side of the chip. A packaged laser diode is shown on figure 2.5 below (the heat sink is not shown).

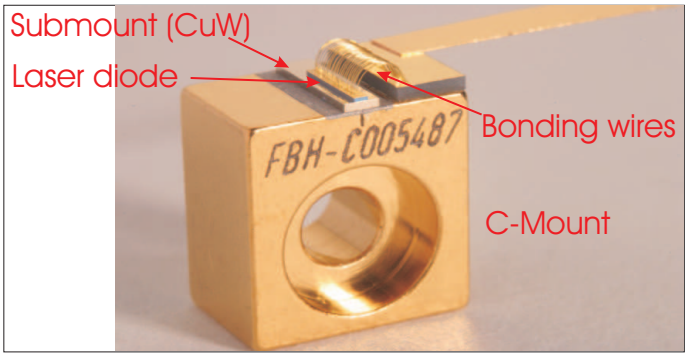

Figure 2.5: Photo of a laser chip after packaging. Photo courtesy of Ferdinand-Braun-Institute/Schurian

2.4 Characterization of the free running BA laser

The free running laser diodes, coated with 5 % reflectivity on the front facet and 95 % reflectivity on the rear facet, are operated in QCW regime with pulse widths of 100 μs at a repetition rate of 25 Hz. The heat sink temperature is held at 25 °C. The power-current-voltage characteristics, the spectrum and the beam profile lateral direction are measured. The values of the output power and of the lateral beam quality are of prime importance, since they are the reference values against which the performance of the ECL will be judged. The spectrum is, on the contrary, marginal to the study since it will not be directly acted upon by the ECL. However, the emission wavelength appears in several calculations and its value needs to be accounted for. Therefore, it is also presented. It should be noted that the experimental processes used in the characterization of the BA laser diode are detailed in chapter four.

2.4.1 Power-current characteristics and spectrum

The power-current-voltage characteristics of the free running BA laser are shown in figure 2.6(a) below. They are practically a reproduction of figure 2.2, where the measured and simulated power-current characteristics of such a laser were compared. Figure 2.6(b) represents the emission spectrum at an injection current of 1 A. The peak wavelength lies at 1053 nm, and this value of the emission wavelength is used in calculations throughout.

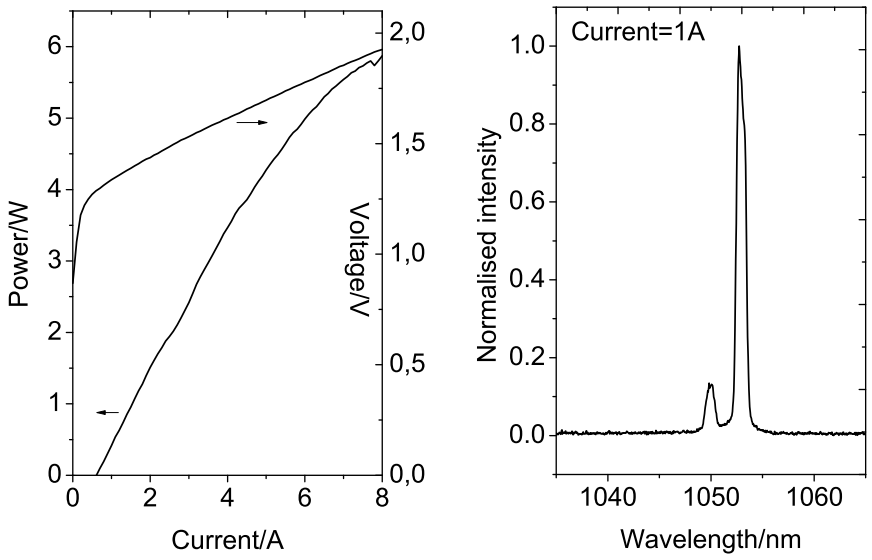

(a) (b)

Figure 2.6: (a) Measured Power-Current-Voltage characteristics of the mirror-coated and mounted laser diode, (b) Emission wavelength at a current of $1\,A$

2.4.2 Beam quality in the lateral direction

The lateral beam formation of the laser diode is governed by both gain guiding due to the extended width of the active zone and a light index guiding due to the refractive index difference induced by the etched trenches on either side of the current injection stripe. The broadened active zone accomodates several higher order modes. As the current injection is increased, the lateral beam profile suffers degradations and/or more higher order modes are allowed to oscillate as a result of non-linear effects such as thermal lensing, carrier-induced index suppression or spatial hole burning [37–40]. These effects impact on the beam quality, as testified in figure 2.7 by the increase in the M^2 value (according to the second moments definition) of the beam as the injection current is increased from $1\,A$ to $8\,A$. It is to be seen that, even at a current of $1\,A$ ($1.7\,I_{th}$), the M^2 value is around 9 and it increases to a maximal value of approximately 25 at a current of $8\,A$ ($13.3\,I_{th}$).

Figure 2.8 shows the near-field and far-field intensity profiles at injection currents of $1\,A$ and $8\,A$. At both currents, the beams have approximately the same widths on the facet, but the far-field is significantly broadened at higher injection current, which is inherent to the oscillation of higher order modes. From the figure, it can be clearly seen that the far-field profile of the emission is centered on the optical axis.

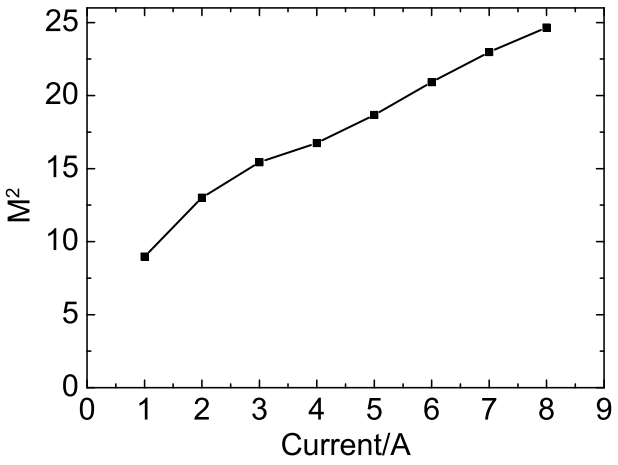

Figure 2.7: Experimental M^2 value of the lateral modes as a function of injection current.

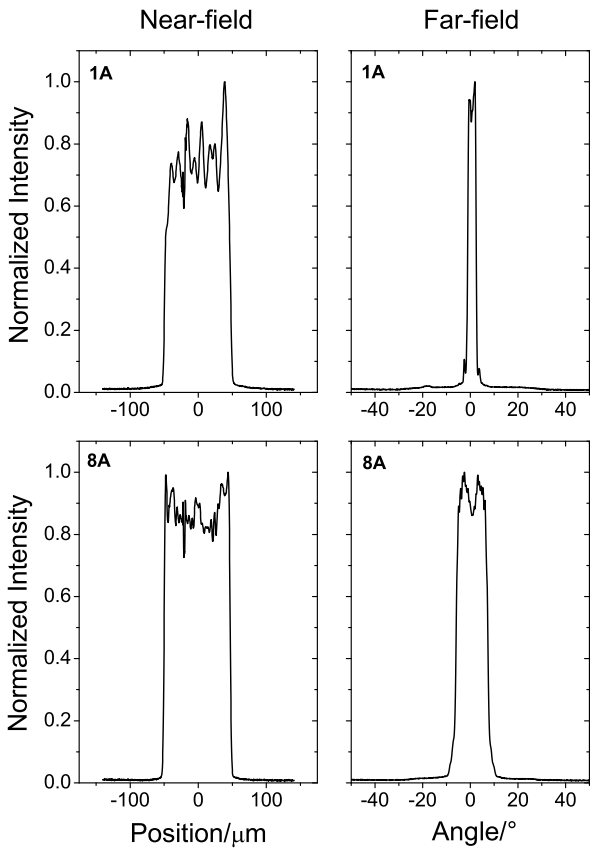

Figure 2.8: Near-field (left) and far-field (right) profiles of the beam of the BA free running laser at currents of 1 A (top) and 8 A (bottom).

2.5 Means of improving the lateral beam quality of BA lasers

A crucial performance target of semiconductor laser diodes is the combination of high power and good beam quality. The simplest of all to produce, the BA laser, achieves the highest output powers for single emitters, but is severely limited by the poor lateral beam quality. To overcome this deficiency, numerous designs have been proposed. They include lasers with an unstable resonator [41], tailored-gain devices [42], ridge-waveguide lasers [5], anti-resonant reflecting optical waveguide (ARROW) lasers [43, 44], slab-coupled optical waveguide lasers (SCOWL) [45], α-DFB lasers [46,47], photonic bandgap crystal (PBC) lasers [48] and monolithically integrated master oscillator power amplifiers with a BA laser diode as power amplifier (MBA-MOPA) [49]. Although they have all demonstrated an improvement in the lateral beam quality with respect to the BA laser, single emitters from the laser designs cited above have, until now, not been able to emit above $3\,W$ in continuous wave (CW) operation at room temperature.

One laser type that achieves output powers in the region of $10\,W$ while maintaining a very good beam quality are tapered lasers. They consist of a ridge-waveguide (RW) section that supports only the fundamental lateral mode, which then expands into a taper section where it is amplified. State-of-the-art versions of tapered lasers have a distributed Bragg reflector (DBR) integrated in the RW section as well as beam spoilers on either side of it. Such a device, emitting at a wavelength of $980\,nm$, has demonstrated $12\,W$ of CW output power with a lateral M^2 value of 5.5 (measured at the $\frac{1}{e^2}$ of the maximum intensity) [50]. At a wavelength of $1060\,nm$, a device with similar design achieves $9\,W$ of CW output power with a lateral M^2 value of 1.3 (measured at the $\frac{1}{e^2}$ of the maximum intensity) [51]. Tapered lasers currently offer the best performances when it comes to the combination of high power and good beam quality. However, their output beam has a high astigmatism (different locations for the vertical and lateral beam waist) in the millimeter range, and it can be very sensitive to the injection current. Therefore, in applications such as fiber coupling, additional optics are required in order to compensate for the astigmatism of the tapered laser diode.

An additional means of improving the beam quality of high power laser diodes is the operation in an external cavity. Such an external cavity laser, with a BA laser diode as gain medium, has reported $2.46\,W$ of output power with a near-diffraction-limited lateral beam profile at an emission wavelength around $976\,nm$ [10]. However, the design is suited to BA laser diodes that emit a double-lobed far-field, and therefore does not apply to the lasers studied here. In the following chapters, a simple concept for an 'on-axis' external resonator laser with a BA laser diode as gain medium is investigated.

Chapter 3

Broad area semiconductor laser with an external resonator

Among the several schemes that have been proposed to improve the lateral beam quality of high power broad area (BA) semiconductor lasers, the external cavity laser (ECL) is an interesting prospect since it is relatively simple to fabricate and versatile. In fact, it allows the interchange of intra-cavity elements and the modification of the resonator geometry without having to revert to additional wafer processing. Owing to its simplicity, the external cavity laser has been extensively experimented. Demonstration of the lateral mode control exercised by external resonators on BA lasers has been mainly carried out on BA diode arrays [52–61], who characteristically emit a double-lobed far-field. The resonator is, as a result, designed with off-axis filtering elements. Generally, one lobe of the far-field is propagated in the external cavity containing spatial filters, while the other lobe is used as output beam. This concept has also been extended to single current stripe BA laser diodes that also emit a double-lobed far-field [10, 62–68]. When it comes to BA laser diodes that emit a single-lobed far-field, as it is the case in this work, the intra-cavity filtering elements of the external resonator are of the same nature as with off-axis resonators, but they are centered on the optical axis. For instance, they can be in the form of apertured mirrors [69], mirrors with non-uniform phase profiles [70–72], or it can be the BA semiconductor laser that itself acts as spatial filter [11, 73, 74].

The latter scheme, as first proposed by Sharfin et al. [11], is of particular interest since it requires only a lens and an external mirror in addition to the laser diode. Thus, it offers the possibility for a simple-to-assemble, high efficiency (reduced losses in intra-cavity elements) and compact ECL. However, it has shown a diffraction-limited lateral emission only at powers no higher than $100\,mW$. The adaptation of this ECL concept to the BA laser used in this work and its extension in the Watt range are investigated.

The present chapter deals with the theoretical principles underlying the concept. In a first step, a passive (gain is neglected) resonator model is used in order to study the lateral mode formation. To the exception of the back coupling efficiency of the vertical mode and some qualitative considerations, the issue of output power is ignored. In a second step, non-linearities arising in the BA laser diode, as under high power operation, are discussed. A refined model of the passive resonator where the diode is under the influence of a thermal lens is then studied. In the light of the findings, an improved external cavity configuration is proposed.

3.1 Model for a passive resonator

The basics of the lateral mode filtering operated by the proposed ECL are explained by a simple model making use of a passive resonator. The planes of the ECL are considered to be mutually orthogonal (also true in practice) such that the emission in the lateral and vertical axis can be decoupled (figure 3.1(a) and figure 3.1(b), respectively). Moreover, during the theoretical study of the mode formation inside the resonator, the paraxial approximation shall be considered as valid throughout. This is, in fact, not always true, but it provides the basis for the application of the ABCD-matrix [26] treatment of the optical system, which is sufficient for the design of the external cavity laser and the understanding of its operating principles.

The main topic of discussion in this chapter pertains to the spatial filtering of higher order modes inside the lateral resonator. Generally, a mode decays inside the resonator when the losses it incurs during one round trip cannot be compensated by the gain it experiences while propagating through the gain medium. It is conceivable, especially in high gain media such as the high power laser diode used here, that residual fractions of a mode that is supposed to decay after a given propagation time still experience enough gain such that it continues oscillating inside the resonator. However, when dealing with a passive model, such a phenomenon cannot be accounted for since the gain is neglected. The approach is binary, such that only modes that suffer no loss at all during a round trip will oscillate in the steady state. Despite its evident limitations, the model of a passive resonator still offers enough insight inside the operating principles of an external resonator laser in order to warrant its application to the design and understanding of the present external cavity laser.

For the sake of clarity and consistency, the notions of 'front' and 'rear' for the facets of the diode, or 'front' and 'back' for the focal planes of lenses, shall be set in accordance with the direction of travel of the beam going through the elements. 'Back' or 'rear' describes the plane facing the region where the light source originates, and 'front' describes the plane facing the region into which it is directing. When it comes to resonators, where the beam travels in round-trips, an arbitrary definition of the direction of propagation is defined. The wave traveling towards the external mirror is considered as forth propagating. Therefore, the front focal plane of a lens in the system will face the external mirror. As for the facets of the diode, the nomenclature is set by the output mirror of the external cavity laser. In this case, the mirror on the facet of the diode is chosen as output coupler, such that it is referred to as front facet, while the one pointing towards the external mirror is the rear facet.

3.1.1 Vertical axis

The mode formation in the vertical axis is completely defined by the waveguide structure in that direction and does not depend on the external resonator. As seen in chapter two, the emission is close to a Gaussian fundamental mode, with a beam waist situated on the rear facet of the diode and a divergence angle of 14° at full width half maximum (FWHM). When studying the mode formation by the external resonator, the intricacies of the vertical waveguide mode are not of importance. Instead, it can be considered as a Gaussian beam with its origin on the rear facet of the diode and propagating through the external cavity and back onto the facet. However, when it comes to power efficiency

considerations of the resonator, it is important that the vertical mode reproduces itself after one round trip, such that its back coupling into the waveguide is optimized. This is best achieved by collimating the emission in the fast axis [75] with the intra-cavity lens, hence its common name of Fast Axis Collimator (FAC).

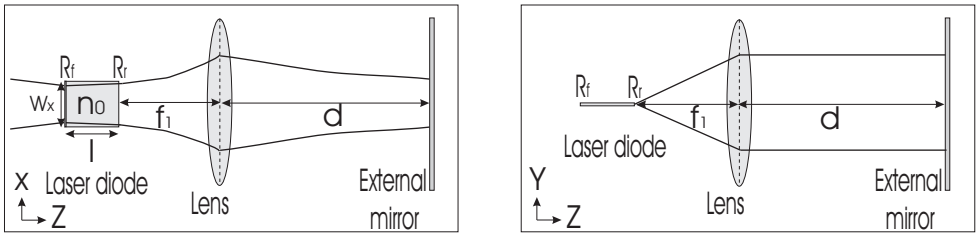

Figure 3.1: Sketch of a simple external resonator laser concept in (a) the lateral direction [x] and (b) the vertical direction [y]

Back coupling efficiency of the vertical mode into the waveguide

The power efficiency of the external cavity laser will be directly dependent on the quality of the back coupling of the vertical mode. Therefore, it is important to get an appreciation of how much of the mode is coupled back into the waveguide. The complete overlap of the vertical mode reflected from the external with the one emitted on the facet of the diode will be hindered by:

- The axial displacement of the external mirror.
- The axial position of the FAC.
- The vertical and angular position of the FAC.

Estimations of the back coupling efficiency are carried out for each of the three cases mentioned above.

Axial displacement of the external mirror

The beam is considered to be a Gaussian fundamental mode, whose beam waist is situated on the rear facet of the diode (origin of the z-axis) and has a radius w. With the knowledge of the above parameters and of the emission wavelength λ, its Rayleigh length (z_R) and thus, its q-parameter are known [76]:

$$z_R = \frac{\pi w^2}{\lambda} \tag{3.1}$$

$$q_0 = i z_R \tag{3.2}$$

For the calculation of the propagation of the Gaussian beam within the paraxial approximation, the external cavity is fully defined by its ABCD matrix. In deriving the latter, the FAC is modeled as a thin lens with a focal length f_1, placed at a distance f_1 away from the waist of the beam. When the distance between the lens and the end mirror is also f_1, the beam waist at the facet is imaged on the mirror, and the subsequent

back coupling into the waveguide after a round-trip is 100 %. Deviations d of the mirror position from this optimal value are studied. In such a configuration of the cavity, the q-parameter after a round trip of the Gaussian beam reads:

$$q_{rt} = \frac{\frac{-2d}{{f_1}^2}{z_R}^2}{1+(\frac{2d}{{f_1}^2}z_R)^2} + i\frac{z_R}{1+(\frac{2d}{{f_1}^2}z_R)^2} \tag{3.3}$$

The real part of q_{rt} gives the position of the beam waist with respect to the facet, while the imaginary part gives its Rayleigh length. Both the waist position and the Rayleigh length, and thus the waist radius, are altered after one round trip. These changes in the beam parameters are at the origin of the back coupling losses.
The coupling efficiency (η) of the two beams is given, as a function of their respective electric fields (E_0 for the emitted beam and E_{rt} after the round trip) in the vertical direction (y), by [77]:

$$\eta = \frac{\int E_0(y)\overline{E_{rt}(y)}dy \int E_{rt}(y)\overline{E_0(y)}dy}{\int E_0(y)\overline{E_0(y)}dy \int E_{rt}(y)\overline{E_{rt}(y)}dy} \tag{3.4}$$

The electric field (with normalized amplitude) of a Gaussian beam at a distance z from its waist can be written as [26]:

$$E(y) = \frac{1}{1-i\frac{z}{z_R}} \exp\left[\frac{-y^2}{w^2(1-i\frac{z}{z_R})}\right] \tag{3.5}$$

By injecting the real and imaginary parts of q_0 and q_{rt} in the above equation, the respective electric fields on the facet can be expressed as:

$$E_0(y) = \exp\left[\frac{-y^2}{w^2}\right] \tag{3.6}$$

$$E_{rt}(y) = \frac{1}{1+i\frac{2dz_R}{{f_1}^2}} \exp\left[\frac{-y^2}{w^2(1+i\frac{2dz_R}{{f_1}^2})}\right] \tag{3.7}$$

Finally, by injecting equations 3.6 and 3.7 in equation 3.4, the fast axis back coupling efficiency reads:

$$\eta = \frac{1}{\sqrt{1+\left(\frac{dz_R}{{f_1}^2}\right)^2}} \tag{3.8}$$

It should be noted that the form of equation 3.8 presented above is, strictly speaking, not complete. In fact, the integration of the electric fields generates an additional term consisting of a quotient of error functions [78]. However, with the present resonator, the operands of these functions are in absolute value much greater than one, such that the quotient always yields a value of unity. Hence, this additional term can be neglected. From equation 3.8, it is deduced that the longer the focal length of the FAC, the better is the back coupling efficiency into the vertical waveguide. However, the high divergence of the beam (14 ° FWHM) restricts the choice of the focal length, such that a compromise value of 8 mm is chosen for the FAC. For the vertical beam of the laser structures

to be investigated, $z_R \approx 0.0084\,mm$. Given the geometry of this external cavity laser, the maximal range for d is around $200\,mm$. In such a case, $\eta = 0.999$. In the light of this estimation, the influence of the mirror displacement on the fast axis back coupling efficiency is negligible.

Axial position of the FAC

When perfectly collimated, the beam waist of the vertical mode on the facet of the diode is placed exactly in the back focal plane of the FAC. Positioning uncertainty will make that the distance between the facet of the diode and the lens will deviate by a small amount δ from the optimal distance f_1. By using the same mathematical treatment as for the displacement of the external mirror, the influence of the value of δ on the back coupling efficiency is inferred as:

$$\eta = \frac{1}{\sqrt{1 + \left(\frac{\delta}{z_R}\right)^2}} \tag{3.9}$$

From the above equation, it can be seen that values of δ in the same order of magnitude as the Rayleigh length z_R will have a telling effect on the fast axis back coupling efficiency. Actually, z_R has already been calculated to be around $0.0084\,mm$. Hence, in order to keep the losses under, say, $5\,\%$, the FAC will have to be positioned with an accuracy within the micrometer range, as shown in figure 3.2(a) below.

Vertical and angular position of the FAC

If the center of the FAC is vertically displaced, or if it is tilted about the lateral axis, then the beam will fall on the external mirror with a given angle. The latter can be correspondingly tilted in order to correct the angular displacement of the beam, and therefore enable a complete overlap of the backwards propagating mode with its emitted counterpart on the facet of the diode. Hence, the angular resolution of the external mirror will act as limiting factor in the back coupling efficiency with regards to vertical displacement and tilt of the FAC. Let α be the angular resolution of the external mirror, such that the angle of reflection of the beam falling on the latter cannot be set better than 2α. For small values of the vertical displacement and of the tilt of the FAC, in the order of magnitude of tens of micrometer and microradian respectively, the approximation of the thin lens for the FAC can still be applied, and the situation can be assimilated to the FAC being optimally positioned and the mirror having a tilt of α. The ray transfer matrix [26] of a beam leaving the surface of the external mirror at a vertical position y will then read:

$$\begin{bmatrix} y \\ 2\alpha \end{bmatrix} \tag{3.10}$$

The ABCD-matrix of the propagation from the external mirror, placed at a distance d from the lens, to the facet of the diode is given by:

$$\begin{pmatrix} 0 & f_1 \\ -\frac{1}{f_1} & 1 - \frac{d}{f_1} \end{pmatrix} \tag{3.11}$$

From the two above equations, the vertical position of the back coupled mode on the facet of the diode is found to be $2f_1\alpha$. As a result, its electric field after the round trip

(E_{rt}) is given by:

$$E_{rt}(y) = \exp\left[\frac{-(y + 2f_1\alpha)^2}{w^2}\right] \tag{3.12}$$

By injecting this result in equation 3.4, the back coupling efficiency is found to be:

$$\eta = \exp\left[\frac{-(2f_1\alpha)^2}{w^2}\right] \tag{3.13}$$

Figure 3.2(b) shows the back coupling efficiency (η) of the vertical mode as a function of the adjustment accuracy in the tilt (α) of the external mirror.

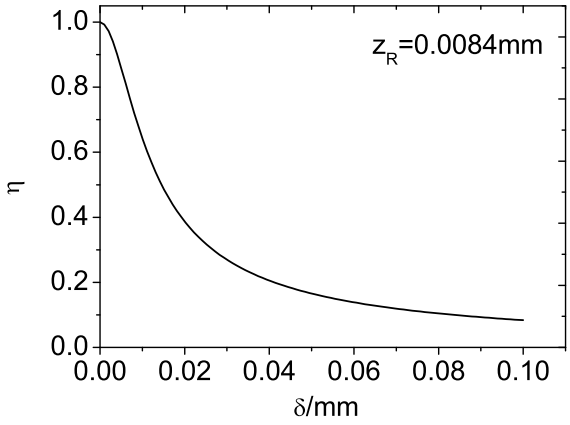

(a)

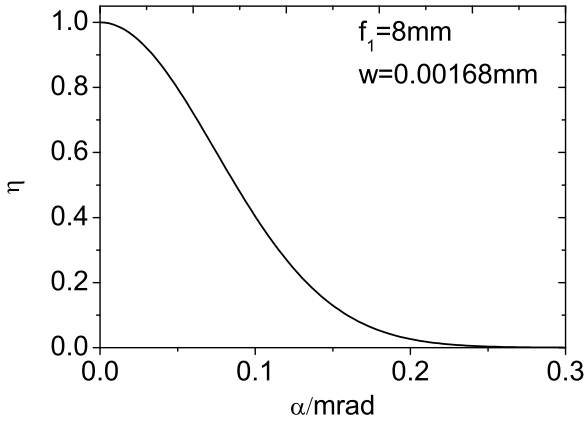

(b)

Figure 3.2: Back coupling efficiency of the vertical mode as a function of (a) the axial displacement of the FAC, and (b) the tilt in the external mirror.

From the estimation of the back coupling of the mode in the vertical axis, it can be concluded that the influence of an axial displacement of the external mirror can be neglected, whereas the axial position of the FAC has to be set with micrometer precision. Vertical misalignment and tilt of the latter is compensated by correspondingly tilting the external mirror. The precision with which the angle of the latter can be set must be in the range of $24\,\mu rad$ in order to ensure a back coupling efficiency above $95\,\%$. As long as the above conditions are fulfilled, the vertical axis can be neglected while the emphasis is put on the lateral resonator. In what follows, the denomination FAC will be

dropped in favour of intra-cavity lens so as to highlight the purpose of the lens in the lateral axis.

3.1.2 Lateral axis

In the passive resonator model, the gain region of the BA laser diode is considered as a fully transmissive homogeneous medium. It has the length of the diode (l), the width of the current injection stripe (W_x), and a refractive index that is equal to the effective refractive index of the laser structure (n_0). Along the length of the diode, the regions falling outside the gain region are considered to be fully absorptive. The resonator is formed by the HR-coated front facet of the diode and the external mirror. The intra-cavity lens, modeled as a thin lens of focal length f_1, is fixed at one focal length (f_1) from the AR-coated rear facet of the diode. The distance d between the lens and the external mirror is varied by moving the latter along the optical axis. The widths of the lens and external mirror are taken to be much larger than the width of the beam falling on them, such that electric fields propagating in the resonator suffer losses only when they spread beyond the lateral boundaries of the homogeneous medium of the diode.

3.2 Modes of the lateral resonator

In steady-state operation, the lateral external cavity can be assimilated to an unconfined resonator that only allows those modes to oscillate which completely fit into the homogeneous medium of the laser diode. The mathematical description of these modes ensues from the eigenvalue equation of the Fresnel-Kirchoff integral, in which the resonator elements are commonly described by their ABCD-matrix [76, 79]. If the study is restricted to the case of a stable resonator, the Gaussian beam is obtained as a solution of the eigenvalue equation and the integrals can be replaced by the q-parameter of the beam. As a result, the ABCD-law can be applied for the calculation of the Gaussian mode [26, 76]. The latter is referred to as the fundamental mode.

3.2.1 The fundamental mode

By assuming stable operation, the q-parameter of the fundamental mode after one round trip (q_{rt}) can be written as a function of the q-parameter at the start point (q_0) and the ABCD-matrix of the propagation as [26, 76]:

$$q_{rt} = \frac{Aq_0 + B}{Cq_0 + D} \tag{3.14}$$

A condition of steady-state operation is that the beam reproduces itself after the round trip, meaning that $q_{rt} = q_0$. This leads to a quadratic equation in q_0, whose solutions can be written as:

$$q_0 = \frac{(A - D) \pm i\sqrt{-(D - A)^2 - 4BC}}{2C} \tag{3.15}$$

The q-parameter of a Gaussian beam at a point z on the optical axis can be written as a function of its radius of curvature ($R(z)$), beam diameter ($W(z)$) and the wavelength (λ) as:

$$\frac{1}{q(z)} = \frac{1}{R(z)} - \frac{i4\lambda}{\pi W^2(z)} \tag{3.16}$$

By equating 3.15 and 3.16, and using the relationship $AD - BC = 1$ (the start and end planes of the propagation find themselves in the same medium), R and W at the starting point of the round trip read:

$$R = \frac{2B}{D - A} \tag{3.17}$$

$$W^2 = \frac{4\lambda}{\pi} \frac{\pm 2B}{\sqrt{4 - (A + D)^2}} \tag{3.18}$$

Equation 3.18 is used to infer both the beam diameter in a given plane and the stability range of the resonator. In fact, a necessary and sufficient condition for a resonator to be stable is that the value of W given by the equation is real [76]. This is only possible when $|A + D| < 2$. Moreover, when the reference plane for the round trip is one of the resonator mirrors, the symmetry of the propagation in the opposite directions makes that the A and D terms of the ABCD-matrix are equal [12]. By injecting this condition in equation 3.17, it is inferred that the radius of curvature of the beam is infinite on both plane mirrors, which means that a beam waist is situated there. A consequence of stable operation is that the radius of curvature of the beam at the mirrors matches the radius of curvature of the latter. Hence, when both resonator mirrors are plane, a beam waist is situated on their surface.

The equations derived above can now be applied to the external resonator under study. For a given length of the resonator, which is set by varying the distance d between the lens and the external mirror, the stability condition can be verified and the beam diameter in any plane can be eventually derived. The ABCD-matrix for a round trip starting, for instance, on the front facet of the diode is derived and its A and D elements are injected in the criterion for stable operation. The range of the distance d over which the resonator is stable is found to be:

$$f_1 < d < f_1 \left(1 + \frac{n_0 f_1}{l} \right) \tag{3.19}$$

At the same time, the elements of the ABCD-matrix are injected in equation 3.18 in order to derive the beam diameter. This process can be applied to derive the beam diameter in any plane inside the stable resonator.

3.2.2 Higher order modes

The Gaussian fundamental mode is the lowest order solution of the eigenvalue equation for the stable resonator. Among a generally infinite number of solutions, those higher order modes that will oscillate depend on the geometry of the resonator. In the present model, the finite rectangular shape of the mirror on the front facet of the diode favors a set of Hermite-Gauss modes [26]. Their propagation in the resonator is similar to that of the Gaussian beam (same beam waist position and Rayleigh length), but the width of a mode with a given M^2 value will be $\sqrt{M^2}$ times larger that that of the fundamental mode. Therefore, the equations used for the calculation of the beam widths of the fundamental mode can be extrapolated to the higher order modes. The mode with the highest M^2 value will have the largest width, such that the M^2 value of the whole beam in the resonator can be taken to be equal to that of the highest order mode oscillating. An example of a stable resonator is shown in figure 3.3(a), where the propagation of the fundamental mode and two higher order modes is sketched.

The higher order modes that are allowed to oscillate in the resonator are those whose beam widths fit completely inside the diode (homogeneous medium) of width W_x. Thus, the highest order mode will have a diameter that is equal to, or slightly smaller than W_x at a given point inside the diode. By using the width of the fundamental mode (W) at this point, an approximation of the M^2 value of the beam inside the resonator is obtained:

$$M^2 \approx \left(\frac{W_x}{W}\right)^2 \tag{3.20}$$

3.3 Spatial mode filtering

Equations 3.17-3.20 are used to predict the operation of the lateral external resonator as a function of the lens-mirror distance d. The principle of the spatial filtering of higher order modes is highlighted by the behavior of the beam widths on the respective facets of the diode. It has been deduced that a beam waist is situated on the mirror-coated facet, implying that the beam is convergent inside the diode (or collimated, as at the lower stability limit). So, a mode that fits into the rear facet will not suffer losses at any point of its trip inside the diode, such that the former can be considered as the only effective aperture in the system. The beam diameter of each mode at this point determines whether it is filtered out or not. An operation diagram, with the beam diameters on the front and rear facet of the diode, its M^2 value and the stability limits as a function of d is drawn in figure 3.3(b).

For fundamental mode operation, the beam diameter on the rear facet of the diode (W_R) must be equal to the width of the latter (W_x). There are two distances d for which this is the case, close to either stability limit. By solving for d in equation 3.18, they are found to be:

$$d = f_1\left\{1 + \frac{n_0 f_1}{2l}\left[1 \pm \sqrt{1 - 4\left(\frac{4l\lambda}{\pi n_0 {W_x}^2}\right)^2}\right]\right\} \tag{3.21}$$

However, in practice, the situation with the higher value of d is not desired, since it produces a big difference in the diameter on the front and rear facets of the diode, and thus implies that the fundamental mode does not take advantage of the full gain area available to it in the active medium. Therefore, the optimal operation of the external resonator takes place when the external mirror is placed at a small distance away from the front focal plane of the lens. For the numerical example in figure 3.3(b), the condition $W_R = W_x$ on the rear facet of the diode is fulfilled when the external mirror is placed $0.5\,mm$ away from the front focal plane of the lens. The beam entering the diode is near-collimated and the fundamental modes occupies almost the whole area of the active zone. No higher order mode is allowed to oscillate since its width would necessarily be larger than W_x. The M^2 value of the beam is correspondingly very close to 1.

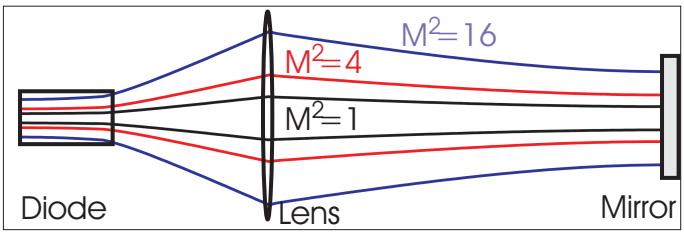

(a)

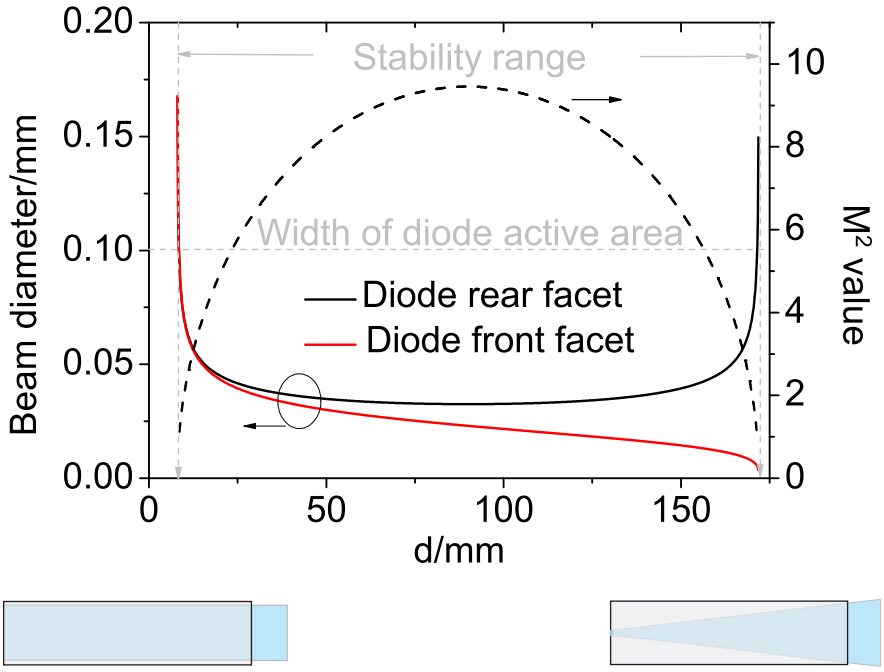

(b)

Figure 3.3: Calculation of the characteristics of the eigenmodes of a simple external resonator concept: (a) Sketch of the appearance of the fundamental mode and two higher order modes in a stable resonator configuration, (b) Beam widths of the fundamental mode on the facets of the diode and M^2 value of the beam in the resonator as a function of the distance d.Parameters used for the calculation:n_0=3.33; l=1.3 mm; W_x=0.1 mm; f_1=8 mm. The area of the beam (blue) inside the active zone of the diode (gray) at the lower (left) and upper (right) stability limits is also shown below the graph

3.4 The passive resonator with a non-uniform refractive index profile

So far, a model of the external resonator that approximates the laser diode with a homogeneous medium has been studied. Its basic principle of operation has indicated how fundamental mode operation can be theoretically achieved by such a laser. The approximation of a uniform refractive index inside the laser diode is very instructive as to the principle of spatial filtering inside the resonator, but it is, especially pertaining to high power operation, an unrealistic model. In fact, it has been shown that nonlinearities in the gain medium of InGaAs/AlGaAs quantum well lasers are detected as early as operation at $\sim$10 % above threshold [80]. Their origin and the effects they induce on the external resonator are going to be looked into.

3.4.1 Nonlinearities in the laser diode

At high powers, the refractive index distribution inside the active medium of the laser diode suffers distortions through the interaction of injected carriers, optical intensity and temperature, giving rise to nonlinear effects such as carrier-induced index suppression, spatial hole burning and thermal lensing [37–40]. The former two effects find their origin in the carrier distribution inside the diode while the latter is a consequence of the heat produced during operation.

A measure of the influence of the carriers on the refractive index is given by the carrier-induced refractive index change (Δn_N). It is given as a function of the confinement factor (Γ), the material differential refractive index ($\frac{\partial n}{\partial N}$) and the carrier density (N) as [81]:

$$\Delta n_N = \Gamma \frac{\partial n}{\partial N} N \tag{3.22}$$

The BA laser used here has a very small value of Γ which is around $2\,\%$ and the typical order of magnitude of $\frac{\partial n}{\partial N}$ for such a structure is $10^{-20}\,cm^3$ and decreases with increasing carrier density [82, 83]. The value of N is calculated by using the rate equation for the carriers above threshold [2]. It is obtained to be in the order of $10^{18}\,cm^{-3}$ for injection currents going up to $8\,A$. The maximal value of Δn_N lies then in the order of 10^{-4}.

In the same way, an estimation of the refractive index change with temperature (Δn_T) is made for an injection current of $5\,A$ (pulse width of $100\,\mu s$ and repetition rate of $25\,Hz$) inside the diode. From the power-voltage-current characteristics, the heat power (P_{th}) is obtained as a function of the current (I), the voltage across the diode (V) and the optical power (P) as (refer to Chapter 2):

$$P_{th} = IV - P \tag{3.23}$$

The temperature change in the active zone of the diode (ΔT) is then derived from P_{th} and the thermal resistance (R_{th}) as:

$$\Delta T = P_{th} R_{th} \tag{3.24}$$

Δn_T is then calculated as a function of the temperature dependence of the refractive index change ($\frac{dn}{dT}$) and ΔT :

$$\Delta n_T = \frac{dn}{dT} \Delta T \tag{3.25}$$

At an injection current of $5\,A$, approximately $4.5\,W$ of heat power is generated. R_{th} is given as $4.3\,KW^{-1}$, leading to a ΔT of approximately $20\,K$ in the active zone of the diode. $\frac{dn}{dT}$ has been calculated to be 2.5 x $10^{-4}\,K^{-1}$, leading to a value of Δn_T in the range of 4.8 x 10^{-3}.

It can be concluded that the thermal effects on the refractive index are one order of magnitude higher than the carrier-induced ones. The latter can thus be neglected in the study of the influence of the refractive index change on the external resonator.

The thermal lens

The perturbation of the local refractive index inside the diode is considered to be purely of thermal origin. During current injection, three principal processes contribute to the heating of the device, namely Ohmic heating, optical absorption and non-radiative recombination [37]. Temperature gradients arising from the diffusion of the heat induce a modulation of the refractive index distribution and contribute to the formation of a positive lens in the lateral dimension of the active area (the effects induced in the vertical direction are irrelevant to the study) [84, 85]. The BA laser diode, formerly represented by a homogeneous medium, is now modeled as a thick lens, with the approximation of a quadratic dependence of its refractive index on the lateral position (x):

$$n(x) = n_0\left(1 - \frac{\gamma^2 x^2}{2}\right) \tag{3.26}$$

The thermal lens coefficient, γ, is for the time being considered as a qualitative coefficient that depends on the temperature gradient in the active zone of the diode. A sketch of the parabolic form of the refractive index distribution is shown in figure 3.4.

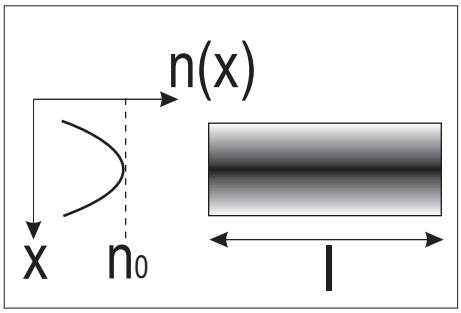

Figure 3.4: Sketch of the approximated parabolic form of the refractive index distribution ($n(x)$) along the lateral dimension (x) of a diode of length l. n_0 is the effective index of the unperturbed medium.

3.4.2 Influence of the thermal lens on the passive resonator

The creation of a lens medium inside the laser diode is set to alter the behavior of the external cavity, but the mode structure (Gaussian fundamental mode and Hermite-Gauss higher order modes) of the stable resonator still holds [76, 86]. The ABCD-matrix for a medium of length l possessing a quadratic refractive index profile as described in equation 3.26 is given by :

$$\begin{pmatrix} \cos(\gamma l) & \frac{\sin(\gamma l)}{\gamma n_0} \\ -\gamma n_0 \sin(\gamma l) & \cos(\gamma l) \end{pmatrix} \tag{3.27}$$

The focal length of the thermal lens (f_γ) and the principal planes (h_γ) are obtained by identifying the elements of the above matrix with that of a thick lens [26]:

$$f_\gamma = \frac{1}{\gamma n_0 \sin(\gamma l)} \tag{3.28}$$

$$h_\gamma = 2 f_\gamma \sin^2\left(\frac{\gamma l}{2}\right) \tag{3.29}$$

The study of the spatial filtering properties of the resonator is repeated with the new ABCD-matrix representation of the laser diode, but this time with γ as additional parameter. The stability range of the resonator and the beam diameter of the fundamental mode on the rear facet of the diode (W_R), with the substitution $\kappa = 2l\gamma$, read respectively:

$$f_1\left[1 + \frac{(\cos(\kappa)-1)n_0 f_1 \kappa}{2l\sin(\kappa)}\right] < d < f_1\left[1 + \frac{(\cos(\kappa)+1)n_0 f_1 \kappa}{2l\sin(\kappa)}\right] \tag{3.30}$$

$${W_R}^2 = \frac{4\lambda {f_1}^2}{\pi} \frac{1}{\sqrt{\frac{{f_1}^4 {n_0}^2 \kappa^2}{4l^2} + \frac{{f_1}^2 n\kappa(d-f_1)}{l\tan(\kappa)} - (d-f_1)^2}} \tag{3.31}$$

It can be deduced from equation 3.31 that W_R will be highest for extremal values of d, that is, close to the stability limits. Like in the previous model, it can be shown that the mode volume is bigger for values of d in the vicinity of the lower stability limit. Therefore, only this region is considered. Once again, the goal is to find d such that W_R is closest to W_x, thus ensuring near-fundamental mode operation. But this time around, both the stability limits and the behavior of W_R are influenced by the value of γ. In fact, it is inferred from equation 3.30 that for $\gamma > \frac{1}{\sqrt{n_0 l f_1}}$, the resonator remains stable at d=0. If W_R is smaller than W_x at this physical limit, then fundamental mode operation cannot be achieved by this configuration for given values of γ. In order to have a clearer view of the situation, the distance d that yields the maximal value of W_R is plotted as a function of γ. The corresponding M^2 values and the beam diameters on either facet of the diode are also derived, as depicted in figure 3.5. γ is made to vary in the range of 0.2-1 mm^{-1}, which are typical values for this structure in the injection current range 1-10 A (refer to chapter 5). The same diode and lens as previously are used.
In the absence of a thermal lens, the results of the previous model are obtained, namely fundamental mode operation for d∼8.5 mm. However, as γ is increased, d must be made smaller so as to achieve the same result, until the physical limit of the configuration is achieved where the external mirror comes in contact with the lens. Then, with γ still increasing, W_R is made smaller and smaller, thus allowing more and more higher order modes to oscillate. By replacing W_R with W_x in equation 3.31 and by solving numerically for γ, it is found that the highest value of the thermal lens coefficient for which fundamental mode is achieved is approximately 0.175 mm^{-1}. Therefore, it is obvious that such an external cavity laser is not appropriate for simultaneous high power operation and effective spatial mode filtering.

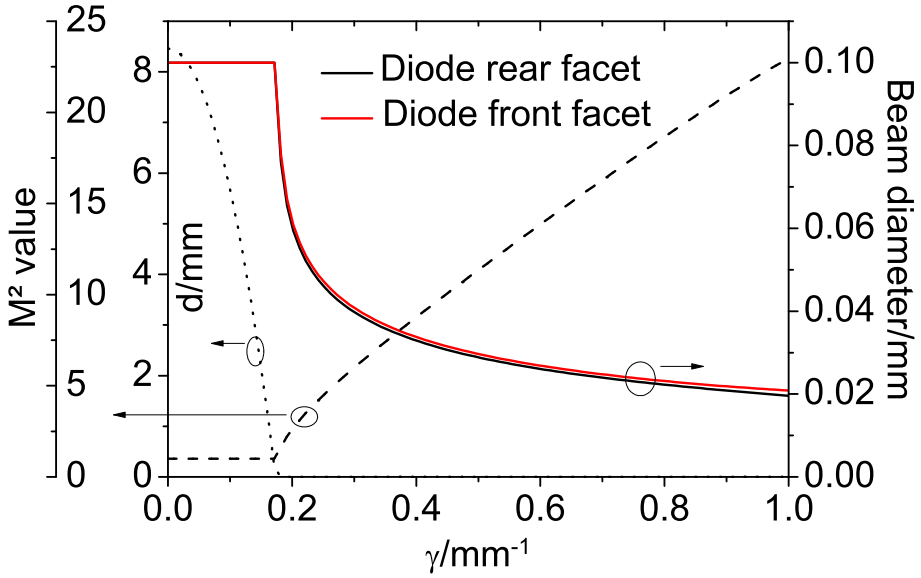

Figure 3.5: Graph of the expected position d giving a minimal M^2 value in the direction of the lower stability limit of the stable resonator, the respective beam widths of the fundamental mode on the diode rear facet and front facet, and the respective M^2 value, as a function of the thermal lens coefficient (γ) in the laser diode. Parameters used for the calculation:$n_0 = 3.33$; l=1.3 mm; f_1=8 mm;

Improved resonator configuration

A new configuration of the resonator is needed in order to achieve fundamental mode operation in the presence of a thermal lens. It must enable the beam width of the fundamental mode (W) at at least one point inside the diode to match its aperture (W_x), preferably in a configuration where the external mirror can be easily traveled along the whole stability range of the resonator, and this even for high values of the thermal lens coefficient (γ) in the region of 1 mm^{-1}. The following alternatives can be considered:

- Reduction of the length (l) of the diode. However, this would lead to the maximum output power being systematically reduced due to the smaller gain region available.
- Reduction of the focal length (f_1) of the lens. This would imply using a lens with a focal length in the sub-millimeter region in order to accommodate the high values of γ. Moreover, the stability range of the resonator would also be reduced to values in the same order of magnitude, making this alternative very difficult to manipulate in practice.
- Use of a modified resonator configuration that allows the free movement of the external mirror over the whole stability range. It may require the use of additional lenses that may make the system less compact and more prone to loss of power in the external cavity. However, this alternative remains practically the most feasible, even if a compromise on size and efficiency is to be made.

A scheme of the latter proposal is considered, whereby only one additional lens is required. In practice, the power lost in the lens should be negligible but an increase in the size of the external cavity laser is however inevitable. Figure 3.6 shows the new configuration for the resonator, where a cylindrical lens ($L2$), with focal length f_2, is inserted between the original cavity lens ($L1$) and the external mirror. They are separated from each other by a distance $d1$. The latter is adjusted such that the two lenses form a telescope ($d_1 = f_1 + f_2$). The rear facet of the diode is imaged ($I(R_r)$) at the front focal plane of $L2$, with a magnification factor (m) given by $\frac{f_2}{f_1}$.

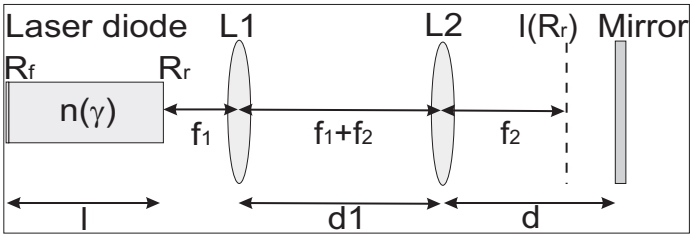

Figure 3.6: Sketch of a resonator scheme designed to accommodate the thermal lens arising in the laser diode.

By injecting the value of m in the stability condition for the resonator ($|A + D| < 2$), the corresponding range of values of d for which stable operation occurs is obtained to be:

$$f_2 - m^2 \frac{\tan(\gamma l)}{n_0 \gamma} < d < f_2 + \frac{m^2}{n_0 \gamma \tan(\gamma l)} \tag{3.32}$$

Moreover, with the help of equations 3.28 and 3.29, the thermal lens is represented in the form of a thick lens with focal length f_γ and principal planes h_γ. Equation 3.32 is then expressed as:

$$f_2 - m^2 \frac{2h_\gamma}{1 - (n_0 \gamma h_\gamma)^2} < d < f_2 + m^2 (f_\gamma - h_\gamma) \tag{3.33}$$

The lower stability limit is the image of the front facet of the diode through the thermal lens and the telescope formed by $L1$ and $L2$, while the upper stability limit is the image of the front focal plane of the thermal lens through the telescope only. Moreover, when $d = f_2$, the beam waist on the external mirror is imaged on the rear facet of the diode, and the resonator is analogous to a free running laser. These three particular positions of d are depicted in figure 3.7 below.

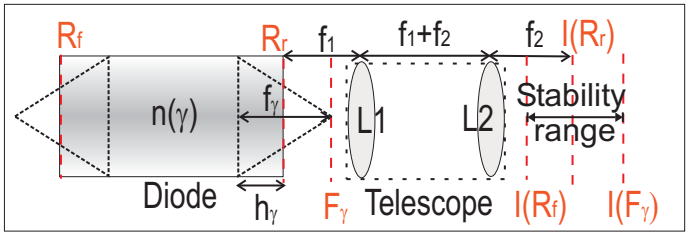

Figure 3.7: Images through the telescope ($I(\star)$) of the front facet (R_f) of the diode, its rear facet (R_r), and the front focal plane of the thermal lens induced in the diode (F_γ). The thermal lens is represented as a thick lens with a focal length f_γ and principal planes h_γ.

From the ABCD-matrix of the round-trip within the stability limits, the beam widths of the fundamental mode (W_F and W_R), respectively on the front and rear facets of the diode, are inferred:

$$W_F{}^2 = \frac{4\lambda}{\pi} \frac{\sqrt{2}\left\{ m^2 \sin(2\gamma l) + n\gamma(d-f_2)\left[\cos(2\gamma l)+1\right]\right\}}{n\gamma\sqrt{(1-\cos(4\gamma l))\left[m^4 - n^2\gamma^2(d-f_2)^2\right] + 2m^2 n\gamma(d-f_2)\sin(4\gamma l)}} \tag{3.34}$$

$$W_R{}^2 = \frac{4\lambda}{\pi} \frac{\sqrt{2}\left[m^2 \sin(2\gamma l) + 2n\gamma(d-f_2)\cos(2\gamma l)\right]}{n\gamma\sqrt{(1-\cos(4\gamma l))\left[m^4 - n^2\gamma^2(d-f_2)^2\right] + 2m^2 n\gamma(d-f_2)\sin(4\gamma l)}} \tag{3.35}$$

A comparison between the beam widths on either facet as a function of the position of the external mirror provides some useful, though not extensive, information about the characteristics of the beam formation inside the diode. By using equations 3.32/3.33, 3.34 and 3.35, three different regions of operation of the external mirror are studied:

- $\boldsymbol{d = f_2}$
  W_F is equal to W_R. The beam waist on the external mirror is imaged on the rear facet of the diode, resulting in a mode formation analogous to a free running laser. The expression for the beam widths of the fundamental mode reduces to:

  $$W_F = W_R = \sqrt{\frac{4\lambda}{\pi n_0 \gamma}} \tag{3.36}$$

  By injecting equation 3.20 in equation 3.36, the M^2 value of the beam, as a function of the aperture of the diode (W_x), is estimated:

  $$M^2 \approx \frac{\pi n_0 \gamma W_x{}^2}{4\lambda} \tag{3.37}$$

  As the thermal lens coefficient increases, the M^2 value also increases, as expected. For instance, at γ=1 mm^{-1}, the M^2 value is around 25 for the diode used in this case. Fundamental mode operation cannot be achieved in this configuration.

- $\boldsymbol{d < f_2}$
  Within the range of γ that is considered here, that is, between 0.2 mm^{-1} and 1 mm^{-1}, the values of $\cos(\gamma l)$ and $\sin(\gamma l)$ always remain positive. Therefore, from equations 3.34 and 3.35, an inequality between W_F and W_R can be solved, and it shows that as long as d is smaller than f_2, then W_R is larger than W_F. Moreover, at the lower stability limit, W_F tends towards zero whereas W_R tends towards infinity. In the vicinity of the stability limit, there is one point where W_R matches the width of the aperture of the diode (W_x), enabling the filtering of higher order modes. However, W_F is very small at that point, suggesting that the overlap of the fundamental mode with the gain medium of the diode is not going to be optimal.

- $\boldsymbol{d > f_2}$
  The same comparison as above is made between the beam widths on the respective facets of the diode. In this case, it is found that W_F is always larger than W_R, and that both beam widths tend monotonically towards infinity at the upper stability limit. Here, the front facet of the diode is susceptible to act as limiting aperture in the system. Moreover, since the beam width on both facets increases when the external mirror is moved towards the stability limit, it is expected that the overlap between the fundamental mode and the gain medium of the diode will be higher than in the previous case.

The qualitative study of the beam widths on the facets of the diode tend to indicate that operation in the vicinity of the upper stability limit will enable both fundamental mode operation and maximal overlap between the beam and the gain medium of the diode. Therefore, as from now on, for the quantitative study of the resonator, only the range of operation $d \geq f_2$ will be considered.

The equivalent resonator

In the stable resonator, a beam waist always lies at the position of the external mirror. It can be considered as a source beam, with a Rayleigh length z_R, that is placed at a distance d from the intra-cavity telescope. The propagation of this source to the rear facet of the diode is readily known by calculating the ABCD-matrix of the propagation and applying it to its q-parameter. q_R, the q-parameter on the rear facet of the diode, then reads:

$$q_R = \frac{1}{m^2}(d - f_2 + iz_R) \tag{3.38}$$

Since only values of $d \geq f_2$ are considered, the beam waist generated by the propagation always lies in the free space between the diode and the telescope. Moreover, its position and its Rayleigh length are, by a factor $\frac{1}{m^2}$, directly proportional to those of the beam waist lying on the external mirror, as it can be seen in equation 3.38. It is as if the lateral resonator were replaced by an equivalent one consisting of only the diode and a virtual external mirror that lies at the position of the generated beam waist. The bounds of operation of the equivalent resonator are deduced by injecting equation 3.33 into equation 3.38. For $d = f_2$, the virtual mirror lies on the rear facet of the diode, yielding, as already mentioned before, a situation analogous to the free running laser. When d is positioned at the upper stability limit, the virtual mirror lies correspondingly at the front focal plane of the thermal lens. The correspondence between the planes on either side of the telescope has already been depicted in figure 3.7. It should be noted that this conception of the equivalent resonator is not valid for $d < f_2$ since the generated beam waist is situated inside the diode consisting of an inhomogeneous medium, and the linear relationship in the displacement and beam widths is no more ensured. Since a direct proportionality exists between the actual external resonator and the equivalent resonator, the latter can be used in the study of the mode formation (calculations are simplified) and the results can be subsequently transposed to the former concept.

From the qualitative study of the resonator, it came out that by moving the external mirror in the vicinity of the upper stability limit, fundamental mode operation could be achieved, with the front facet of the diode acting as limiting aperture in the system. Moreover, the overlap between the beam and the gain medium of the diode should also be maximal at this point. These conclusions were based on the tacit approximations that, firstly, the beam remains confined inside the diode, and secondly, no intermediate beam waists are generated inside. The former approximation ensures that the front facet of the diode is effectively the limiting aperture, while the latter justifies the supposition that overlap between beam and gain medium is optimal. However, in the inhomogeneous medium of the thermal lens, there is no guarantee that these approximations hold. Therefore, their validity has to be checked in the present case, where the thermal lens coefficient (γ) lies between 0.2 mm^{-1} and 1 mm^{-1}.

With the help of the equivalent resonator model, it shall be shown that, for $\gamma \in$ [0.2,1], the beam remains confined inside the diode and no intermediate beam waists are generated within. The resonator is bound by a mirror on the front facet of the diode and an external mirror situated, in free space, at some distance to its rear facet. Since stable operation is considered, a beam waist is situated on either mirror. For the sake of the demonstration, it is sufficient to consider the beam waist on the front facet of the diode as a source that propagates through the medium of the thermal lens. The ABCD-matrix of the propagation is given by equation 3.27. For simplicity, only the half-width of the diode and the beam radii are going to be used. The q-parameter at any axial point z during the propagation through the thermal lens is given by:

$$q = \frac{\sin(2\gamma z)\left[1 - {n_0}^2\gamma^2{z_R}^2\right] + iz_R}{2n_0\gamma\left[{n_0}^2\gamma^2{z_R}^2\sin^2(\gamma z) + \cos^2(\gamma z)\right]}, \tag{3.39}$$

where z_R is the Rayleigh length on the front facet of the diode. For a beam waist to appear inside the diode, the real part of equation 3.39 has to be negative. Knowing that both $\cos(\gamma l)$ and $\sin(\gamma l)$ remain positive over the range of $\gamma\in$[0.2,1], the condition for a beam waist to appear inside the diode reads:

$$z_R < \frac{1}{n_0\gamma} \tag{3.40}$$

This is not possible since the minimum value of z_R in the stable resonator is $\frac{1}{n_0\gamma}$.

The beam radius $w(z)$ at any axial point z inside the diode is also inferred by comparing equation 3.39 to equation 3.16:

$$w(z) = \frac{1}{n_0\gamma}\sqrt{\frac{\lambda}{\pi z_R}}\sqrt{{n_0}^2\gamma^2{z_R}^2\cos^2(\gamma z) + \sin^2(\gamma z)} \tag{3.41}$$

where λ is the operating wavelength of the emission. The first derivative of $w(z)$ with respect to z yields three extrema, namely $z = [0, \frac{\pi}{2\gamma}, -\frac{\pi}{2\gamma}]$. The second derivative yields a positive value for $z = 0$ and negative values for the two other solutions, as long as z_R is larger than $\frac{1}{n_0\gamma}$. For the latter value, the second derivative yields zero for all three values

of z. As expected, the beam has no extrema inside the diode since it corresponds to the situation where $d = f_2$. As d increases, the Rayleigh length also increases. Therefore, the derivatives show that the beam width always has a maximum at z=0, the position of the beam waist on the front facet of the diode. Hence, for $d \geq f_2$, the fundamental mode always remains confined inside the diode, irrespective of the value of γ, as long as the resonator is stable. Therefore, the supposition that the front facet of the diode is the limiting aperture in the system holds, as well as the supposition that the beam at the rear facet diverges to the front facet, thus enabling maximal overlap with the gain medium of the diode.

It now remains to find the value of d that produces the beam on the front facet of the diode to match the aperture width (W_x), such that fundamental mode operation is made possible. The calculation can be carried out on the equivalent resonator and then transposed to the actual resonator or it can be inferred directly from equation 3.34. By using either method, and by replacing the values of equations 3.28 and 3.29, the optimal position of the external mirror (d_{opt}) reads:

$$d_{opt} = f_2 + m^2(f_\gamma - h_\gamma)\left(\frac{\xi}{1+\xi}\right) \tag{3.42}$$

$$\xi = \left[\left(\frac{\pi {W_x}^2}{4\lambda}\right)^2 {n_0}^2\gamma^2 - 1\right]\sin^2(\gamma l) \tag{3.43}$$

It has been shown that the position d of the external mirror that ensures fundamental mode operation, as given in equation 3.42 above, also corresponds to a maximal area of the mode inside the diode. However, the mode area in question is always smaller than the area of the diode. Moreover, it can be deduced from equation 3.41 that as γ increases, the mode area inside the diode at $d = d_{opt}$ decreases. For γ=1 mm^{-1}, the mode area is found to be approximately 73 % of the gain area available in the medium.

The only remaining unknown quantity in the equations is the value of m, which is the ratio $\frac{f_2}{f_1}$. f_1 has already been set to the value 8 mm, and it remains to set the value of f_2. The latter should preferably have a large value, since it increases both the travel distance of the external mirror and the Rayleigh length of the beam falling on it. Hence, the sensitivity of the positioning of the external mirror is reduced. However, it should also be taken into account that large values of f_2 would result in having very large values of d, especially when γ is small. Given that the study of the external resonator will principally be made on values of γ above 0.5 mm^{-1}, a compromise value of f_2 of 50 mm is chosen. For fundamental mode operation, it results in positions of the external mirror of approximately 30 mm and 3 mm away from the point $d = f_2$ for γ worth 0.5 mm^{-1} and 1 mm^{-1}, respectively.

The new configuration of the external resonator designed to accommodate the effects of the thermal lens has been theoretically studied and its different ranges of operation have been qualitatively appreciated. It has been found that in the vicinity of the upper stability limit, fundamental mode operation, together with maximal overlap of the mode with the gain area is possible. Figure 3.8 below shows an example of an operation diagram similar to that in figure 3.3(b), but under the influence of a thermal lens with γ=0.7 mm^{-1}. In this case, d_{opt} is calculated to be approximately 63 mm and the overlap between the fundamental mode and the gain medium of the diode is around 74 %.

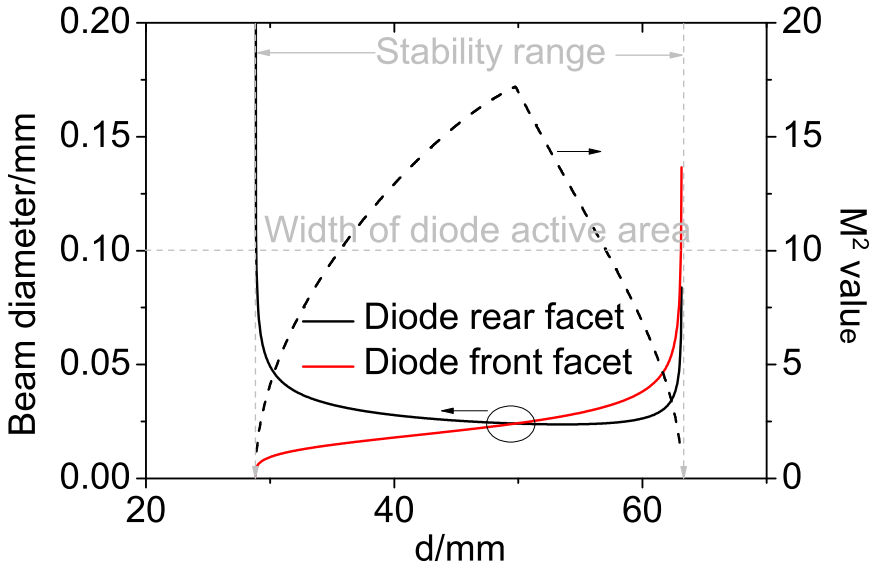

Figure 3.8: Adjustment of the stability range with the help of an additional lens: Determination of the beam widths of the fundamental mode on the diode facets and of the M^2 value as a function of d. Parameters used for the calculation:n_0=3.33; γ=0.7 mm^{-1}; l=1.3 mm; f_1=8 mm; f_2=50 mm.

Chapter 4

Definition and measurement of laser beam characteristics

In the course of this work, semiconductor laser systems have been assembled in various configurations, depending on the nature of the investigations. The complexity of the systems varies from the free running laser diode, where the resonator mirrors are deposited on the chip facets, to a fairly complex master oscillator power amplifier (MOPA), including a seed laser, an amplifier chip and a series of beam forming optics between them. It is not the scope of this chapter to describe the laser systems in detail, instead, the accent will be put on the measurement principle and the instruments involved in the characterization of the lasers. Irrespective of their complexity, the laser systems will be here considered as a monolithic block, with an output beam to be measured. The detailed description of each system will be done in subsequent chapters. The laser systems, with an emission wavelength around 1.06 μm, have been driven in quasi continuous wave mode with a current pulse width of 100 μs at a repetition rate of 25 Hz. In the case where more than one laser diode is involved (seed laser + amplifier), the current injection between the two chips is synchronized. All the lasers have their heat sink kept at a temperature of 25 $^{\circ}C$. These operating conditions hold for every laser system under test, unless otherwise specified. The parameters used to characterize and monitor the output beams have been:

- The power-current characteristics
- The emission spectrum
- The spatial distribution of the optical field (beam quality)

A special emphasis will be put on the characterization of the beam quality. In fact, it is the parameter that lies at the center of the investigations. Its improvement has been the driving theme of this work. Moreover, its measurement has also been the most challenging technical aspect of the experiments. Therefore, after a short description of the measurement of power and spectrum, a detailed discussion on the beam quality is made. A schematic representation of the measurement setup used to simultaneously characterize the three above-named parameters is shown in figure 4.1 below.

The laser diode is forward biased using a current source whose modulation profile is given by a function generator. The laser heat sink is kept at constant temperature using a water circulator that can optionally cool or heat the running water with respect to ambient temperature. The water circulator can be adjusted with a precision of $\pm 1\,^{\circ}C$.

The output beam of the laser is collimated with the help of an aspheric lens ($L1$) having a focal length of $8\,mm$ and a numerical aperture of 0.5. The aspheric form of the lens ensures the minimization of optical aberrations. The collimated beam is then separated into two equal parts in a 50/50 beam splitter. One part is reflected in the lateral direction (path 1), where it is used for the power-current characterization and the spectrum measurement. The transmitted part (path 2) is directed on a camera by a series of lenses (here $L2$ and $L3$) where the beam quality is measured.

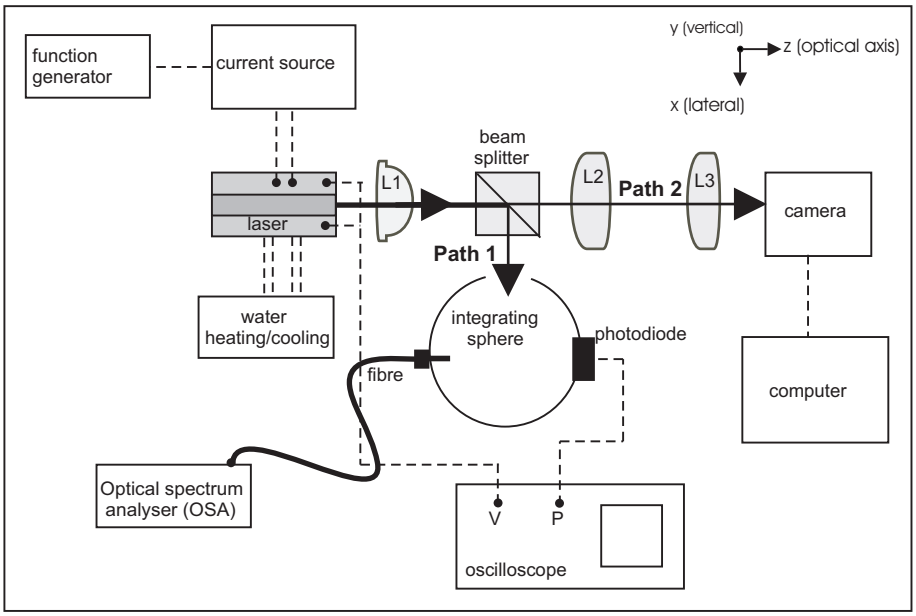

Figure 4.1: Sketch of the experimental setup for the characterization of laser systems

4.1 Measurement of power and spectrum

The part of the output beam following path 1 enters an integrating sphere comprising a photo diode and a fiber termination. The photo current generated in the photo diode upon illumination is fed into a trans-impedance circuit and the corresponding potential difference is read on an oscilloscope, where the voltage across the laser diode is also directly read. The optical flux incident in the integrating sphere undergoes multiple reflections on the highly reflective inner surface. This results in a spatial integration of the light. The direct calculation of the integrating sphere throughput (ratio of the incident power falling on the detector surface) is cumbersome and can lead to high calculation uncertainty. Therefore, the detector output is calibrated with respect to the incident power behind the collimation lens using a calibrated thermoelectric power meter. In our case, the optical power behind the collimation lens per unit voltage drop across the detector trans-impedance circuit is determined. At the operating wavelength of $1060\,nm$, it is found to be $58\,WV^{-1}$, with a standard error of approximately $10\,\%$. The measured conversion ratio takes into account several uncertainty sources such as absorption in the beam splitter, reflection loss in the integrating sphere, noise and conversion loss in the photo detector, and measurement uncertainty in the calibration power meter and in the oscilloscope.

Part of the laser output is collected by the optical fiber situated at one port of the

integrating sphere. The fiber is multi mode with a core diameter of 50 μm. The light is fed, via a 5 μm entrance slit, into an optical spectrum analyzer (OSA), a HR4000 from Ocean Optics, with a spectral range of 140 nm, going from 950 nm to 1090 nm. The spectrum analyzer, combined with the entrance slit, offers a resolution of 85 pm around the emission wavelength of 1060 nm. A signal to noise ratio of approximately 25 dB and a dynamic range of 30 dB are specified for a full scale illumination of the spectrometer's detector.

4.2 Measurement of the beam quality

The lasers that are to be measured emit a partially coherent, simple astigmatic beam composed of two orthogonal intensity profiles in the plane perpendicular to the optical axis:

- A near single mode emission in the vertical axis due to the waveguide structure in that direction
- A multimode emission in the lateral axis

The emitted beam does not fulfill the conditions of the paraxial approximation, especially in the vertical direction where the divergence angle is in excess of 10 $^\circ$ at full width half maximum. However, via a collimation lens and further optics, the divergence of the beam propagating in the measurement system is reduced to such an extent that the paraxial approximation holds throughout.

The ultimate goal is a laser with a single Gaussian fundamental mode in the lateral direction. So, it is judicious to have a comparison between the actual multimode emission of the lasers and the desired emission. The measurement of the M^2 value is well suited to the task and it reflects the propagation characteristics of the real beam with respect to the fundamental mode. It is defined through a set of parameters that fully characterize the propagation of the beam in an optical system governed by the ABCD rule [26, 87–90]. Practically, the quantity that is readily measurable is the intensity profile along the transversal axes. It, in turn, provides the beam width, which is fundamental in the measurement of the other beam parameters.

4.2.1 Definition of the beam width

However, there exist several different definitions of the beam width, each of which will, in general, give a different value, depending on the profile of the beam to be measured [91]. Two such definitions shall be used here:

Second moments

Considering the intensity distribution $I(x, y)$ in a plane (x, y) normal to the propagation axis (z), the beam diameter (W) in the lateral direction (x) is given by [3]:

$$W^2 = 16\frac{\iint (x-\bar{x})^2 I(x,y)dxdy}{\iint I(x,y)dxdy} \tag{4.1}$$

$$\bar{x} = \frac{\iint xI(x,y)dxdy}{\iint I(x,y)dxdy} \tag{4.2}$$

The second moments beam width is a standard definition set by the ISO-11146 norm [3]. It offers the major advantage that the ABCD propagation laws hold rigorously for higher order mode beams whose widths are defined in such a way [26, 91]. However, it may not be appropriate for the measurement of beams that have fractions of their intensity distributed in the wings on either side of the central lobe [26,89,92]. The quadratic term in the right hand side of equation 4.1 overemphasizes the contribution of small intensity terms far from the beam centroid. Moreover, it is very sensitive to noise and offset in the detection system. The result is then a beam width that may not reflect the width where the majority of the power is enclosed (the central lobe, for instance).

Knife-edge diameter

Whilst the second moment method gives a rigorous measure of the beam width, it does however fail to give an indication of the fraction of the total power contained within the defined beam diameter [89]. When such information is required, the knife-edge definition of the beam diameter is used. It defines a slice (whose extent defines the beam diameter) of the beam where a given percentage of the total power is enclosed. The marginal intensity distribution $I(x, y)$ along the lateral dimension is integrated and the distance between the upper and lower $\frac{100-a}{2}\,\%$ of the curve defines the $a\,\%$ knife-edge beam diameter.
Figure 4.2(a) below shows an example of an arbitrary intensity profile, where the beam width is determined by the second moments and by the knife-edge diameter at $95\,\%$ of the total integrated intensity. The latter is shown in figure 4.2(b).

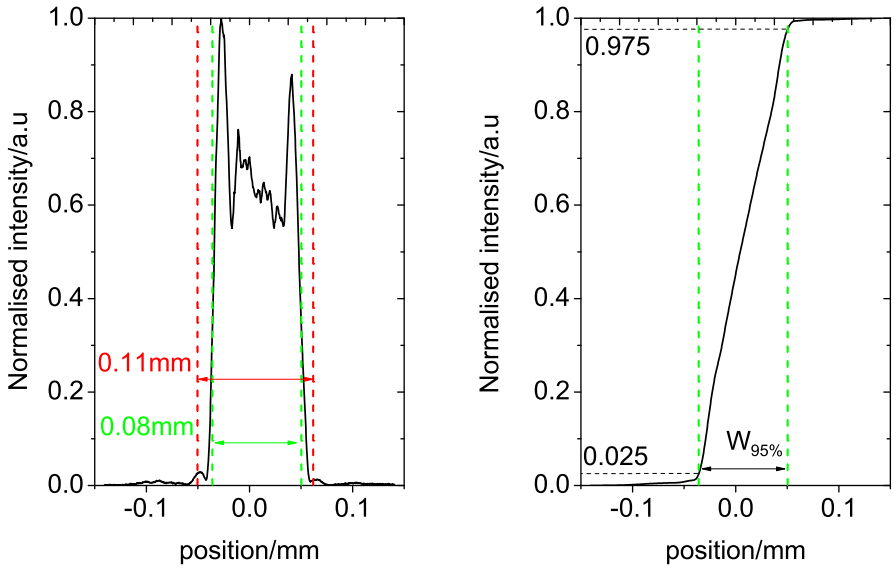

Figure 4.2: (a) Second moments (red) and 95 % knife-edge (green) measurements of the beam diameter, (b) Integral of the marginal distribution of the beam intensity and bounds of the 95 % knife-edge diameter

4.2.2 Extracting the M^2 value from the beam width measurements

Beam caustic

The beam caustic is a measurement of the beam width at different axial positions over a distance of free-space propagation. Following the ABCD rules for the propagation of a Gaussian beam, the successive beam widths ($W(z)$) along the propagation axis (z) are given as a function of the beam waist diameter (W_0), its position on the optical axis (z_0), and the Rayleigh length (z_R):

$$W(z) = W_0\sqrt{1 + (\frac{z - z_0}{z_R})^2} \tag{4.3}$$

The caustic measurements performed in the course of this work have been carried out in compliance with the procedures and recommendations of the ISO-11146 norm [3]. A minimum of 10 intensity profiles are recorded and the subsequent beam diameters are, following equation 4.3, fitted by a hyperbola. The fit coefficients provide the values of W_0, z_0 and z_R. The M^2 value, as a function of the wavelength (λ), is then inferred as:

$$M^2 = \frac{\pi {W_0}^2}{4\lambda z_R} \tag{4.4}$$

This method, due to the large number of data points, enables the statistical minimization of the relative error in the beam width. Furthermore, the beam caustic is a very practical tool for the detection of flawed measurements (excluding systematic errors). Measurement points with a high relative error are readily singled out since they lie far

outside the hyperbola fitted on the data set. However, the caustic measurement gives the real beam parameters according to the ABCD rule only when the second moments definition for the beam width is used. In fact, for an emission with a set of higher order modes that overlap coherently, as it is the case with diode lasers [2], the caustic measured by the knife-edge method will intrinsically deviate from the hyperbolic propagation defined in equation 4.3. An illustration is shown in figure 4.3. The intensity distribution of a noise-free and unclipped arbitrary beam is simulated. The highest order mode, with an M^2 value of 7, is made to overlap coherently with the lower order modes. A beam diameter (second moments) of 0.1 mm, positioned at the origin, is chosen. The beam caustic of this intensity distribution is calculated by using both the second moments and the 95 % knife-edge definitions of the diameter. The respective caustics are then, in each case, fitted by a hyperbola (following the ABCD rule). It is observed that the calculated beam diameter is in perfect agreement with the ABCD propagation rule in the case of the second moments beam definition. On the contrary, when the beam is defined by the 95 % knife-edge method, a clear discrepance between the data points and the fit is observed. Therefore, a caustic performed on the beam of a laser diode using the knife-edge defintion for beam width may give erroneous values for the beam parameters (according to the ABCD rule) and will be generally non-hyperbolic.

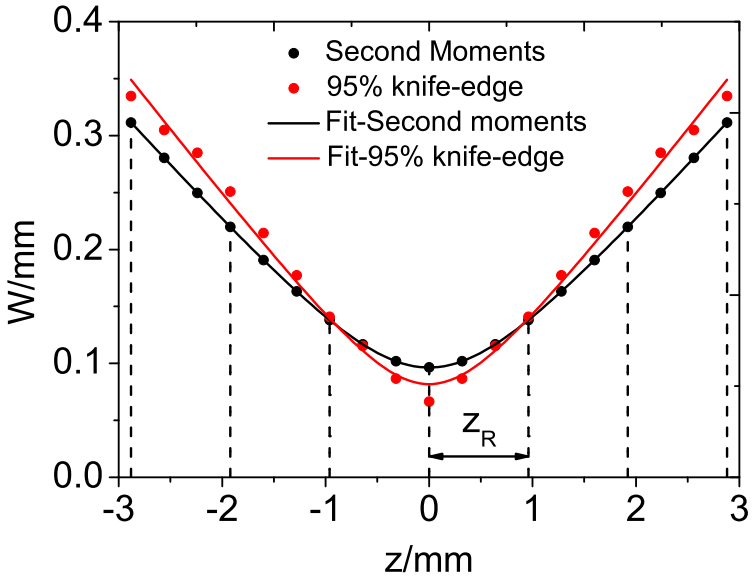

Figure 4.3: Caustic of an artificial beam defined by the second moments method (black dots) and the 95 % knife-edge method (red dots). The corresponding hyperbolic fits are shown in solid lines. The parameters used for the generation of the beam are as follows: W_0(second moment)=0.1 mm, M^2=7, z_0=0 mm, λ=1060 nm

The beam caustic, associated with the second moment definition of the beam width, is the standard method used for the determination of the M^2 value in the present work. However, it can be very time consuming and it can be, in some special cases, bypassed by a quicker measurement method.

From beam waist diameter and divergence angle

In the particular situation where the position of the beam waist is known and its intensity profile is readily accessible for measurement, then the beam waist diameter (W_0) and

the divergence angle (θ), along with the wavelength (λ), are used to infer the beam propagation product [26, 89]:

$$M^2 = \frac{\pi W_0 \theta}{4\lambda} \tag{4.5}$$

θ is readily obtained by measuring the beam width in the focal plane of an aberration-free lens [3]. The ratio of the beam width to the focal length of the lens gives to a good approximation the divergence angle. The M^2 value is then extracted following equation 4.5 above. This method is quick and practical in that only two measurements are required in order to extract the beam parameters. However, the small number of measurements makes it very prone to errors.

This method is particularly adapted to the measurement of the beam quality of broad area semiconductor laser resonators. The lateral beam waist of the latter is known to be situated at the facet, making it easily accessible for measurement. In this particular case, it is common to refer to the beam waist as the near-field, which is defined as the intensity profile on the laser facet. In the same manner, when inferring the divergence angle, the measured intensity pattern (in the focal plane of a lens) is referred to as the far-field. Figure 4.4 illustrates the notions of beam waist, near-field and far-field in two different situations: (a) in a laser amplifier with a beam waist situated at an arbitrary position inside the diode, and (b) a free running laser diode where, due to the position of the beam waist on the facet, only the denominations "near-field" and "far-field" appear. In both cases, the latter is generated in the focal plane of a thin lens, with focal length "f". When the beam waist inside the diode is situated exactly one focal length away from the lens (as in case (b)), then the position of the waist generated by the lens corresponds with the far-field. In practice, this configuration minimizes the positional error on the measurement of the divergence angle.

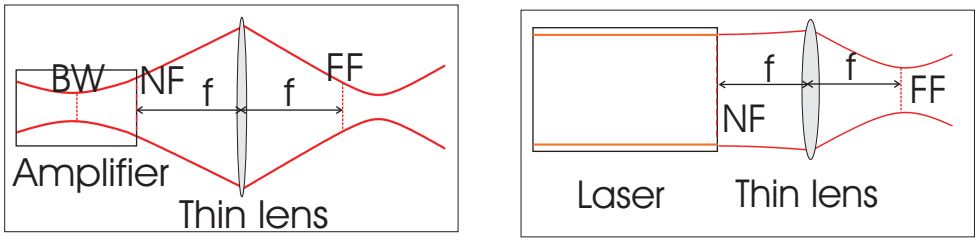

(a) (b)

Figure 4.4: Sketch representing the beam waist (BW), near-field (NF), and far-field (FF) as it generally is for (a) an amplifier, and (b) a laser diode. The far-field is here shown to be measured in the focal plane of a thin lens with focal length "f"

4.2.3 Experimental setup for the characterization of beam quality

The measurements involved in the characterization of the beam quality are the recording of the intensity profile of a given laser beam with the help of a CCD camera in this case. For the precision of the measurement, it is important that as little as possible light is lost through clipping on the path to the CCD chip, and that the former be resolved by at least a certain number of pixels, for instance 20, as recommended by the ISO-11146 norm [3]. Hence, a certain number of properties of both the lasers to be measured and the CCD camera are to be taken into account in the setup of an experimental bench:

- Due to the waveguide structure in the vertical direction, the emission is not affected whether the semiconductor chip is used as free running laser, a gain medium in an external resonator laser, or as an amplifier. The emission is a near-fundamental mode, with a M^2 value around 1.5 or less. The beam waist is situated near the output facet, and is approximately 5 μm in diameter. The divergence angle reads 14 $^\circ$ at full width half maximum (FWHM). Due to the high divergence, the output beam has to be collimated, preferentially by a lens with a small working distance. As a result, an aspheric lens with a back focal length of 5.9 mm and a numerical aperture of 0.5 is used.

- The measurements of interest pertain to the lateral direction of the output laser beam. Depending on the configuration of the laser chip, the Gaussian beam characteristics will be very different and the method used to characterize them also differs. Below is a description of the expected beam characteristics of the three different laser configurations that are to be measured:

  - A free running laser diode will have a beam waist of approximately 100 μm lying near the output facet, and an M^2 value of up to 30, depending on the injection current. The beam waist position will not be sensibly affected by the operating conditions. The determination of the M^2 value through beam waist (near-field) and far-field measurement is easily applied.
  - Just in the same way, in an external resonator laser under stable resonator operation, the beam waist will essentially lie on the output facet. However, the beam width may vary depending on the operating conditions, as is the case when slits are used inside the resonator as modal filters. M^2 values vary according to resonator length, slit width and injection current and typically lie between 5 and 30. The same measurement procedure as above applies.
  - Behaving totally differently is an amplifier seeded with a probe beam (from a ridge waveguide laser in the present work). It may have a lateral beam waist of some 5-10 μm lying halfway between the facets of a 1.3 mm long chip whereas the vertical beam waist lies on the output facet. This astigmatism may also vary drastically under different injection currents. The lateral M^2 remains essentially lower than 5. Locating and accessing the beam waist at every operating point may not always be possible. A caustic measurement is certainly more appropriate for the determination of the M^2 value.

- The CCD chip has, in its basic configuration, a square pixel size of 4.4 μm arranged in an array of 1600 (H) x 1200 (V). In order to reduce the size of the output data of the camera, the effective pixel size is changed to 8.8 μm, with a resolution of

800 x 600, via 2 x 2 pixel binning. The beam size falling on the CCD chip should be between 200 μm and 5 mm.

Taking the points above into consideration, the measurement bench sketched in figure 4.5, itself a more detailed reproduction of 'path 2' followed by the laser diode in figure 4.1, has been implemented. The technical details of the optics, pertaining to the beam path, are shown in table 4.1. The aspheric lens used as fast axis collimator is depicted as $L1$, with back focal length f_{1b} and focal length f_1. It is followed by a beam splitter whose function is to enable the simultaneous measurement of power (as well as spectrum) and beam quality. Its effect on the beam propagation to the camera is negligible, except for a small optical path difference (e) arising from the higher refractive index along its length. $L2$ is a spherical lens which is placed one back focal length (f_{2b}) away from the front focus of $L1$. In this configuration, they from a spherical telescope, which images the laser facet at the front focal plane (f_2) of $L2$ with a magnification of $\frac{f_2}{f_1}$. The telescope offers the advantage of simultaneously magnifying the near-field and reducing the beam divergence, both by the same factor. $L2$ is chosen such that its focal length f_2 is equal to 200 mm, which gives a factor of 25. Bearing in mind that the near-field intensity of the laser chips extends at most over around 100 μm, then the beam width on the camera chip placed in the front focal plane of $L2$ (f_2) is approximately 2.5 mm, well under the maximum set at 5 mm.
As for the far-field measurement, an additional lens $L3$, with a focal length of approximately 100 mm is placed in between $L2$ and the camera. The beam diameter recorded in its front focal plane (f_3) is then used to derive the divergence angle. Measurement uncertainty arising from the positioning error of the camera is minimized when $L2$ and $L3$ are confocal. In this case, the measurement of the intensity profile is carried out at the position of the beam waist generated by $L3$. The setup used for caustic measurements is identical, except that $L3$ is removed. The camera is traveled on either side of the beam waist generated in the focal plane of $L2$ and the respective beam diameters are recorded. However, when an amplifier is seeded with a beam having a Rayleigh length (inside the diode) in the order of half a millimeter and above, the setup is no more appropriate for a caustic measurement. This is because the Rayleigh length of the beam behind $L2$ is then in the order of hundreds of millimeter. In this case, an additional lens is required between $L2$ and the CCD camera.

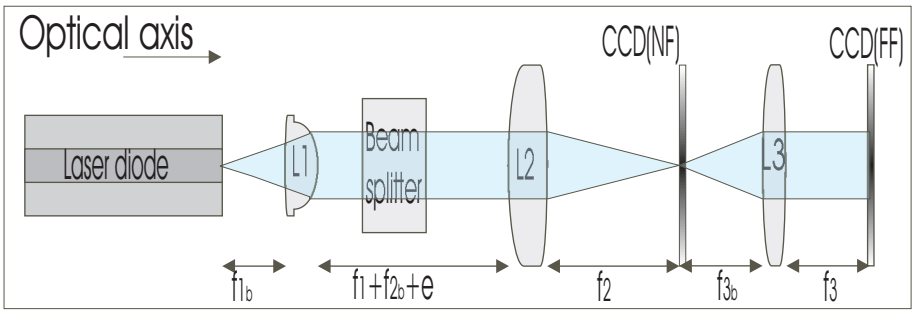

Figure 4.5: Experimental setup for the determination of the beam quality. An eye-guide for the vertical beam path is shown (light blue)

	$L1$	$L2$	$L3$	Beam splitter
Back focal length/mm	5.9	195.6	97.1	-
Focal length/mm	8	200	100	-
Thickness/mm	3.7	8.0	5.5	20.0
Refractive index	-	-	-	1.51

Table 4.1: Parameters of the optical elements relevant to the arrangement of the experimental setup for the measurement of the beam quality

The CCD camera

A camera of the scorpion series from Pointgrey research is used. It consists of a Sony ICX274 CCD chip with 4.4 μm square pixels arranged in an 1600 x 1200 array. The specified signal to noise ratio is 57 dB. The camera is driven by the ProfileViewer software, which was internally developed at the Ferdinand Braun Institute.For all the experiments, the pixel size is brought to 8.8 μm with a 800 x 600 resolution via a 2 x 2 pixel binning. The image contrast and the exposure time are manually set according to the requirements of the application. The light intensity incident on the CCD array is attenuated using a series of neutral density filters. The signal is averaged over 16 frames. The appearance of the graphic interface of the camera is shown in figure 4.6.

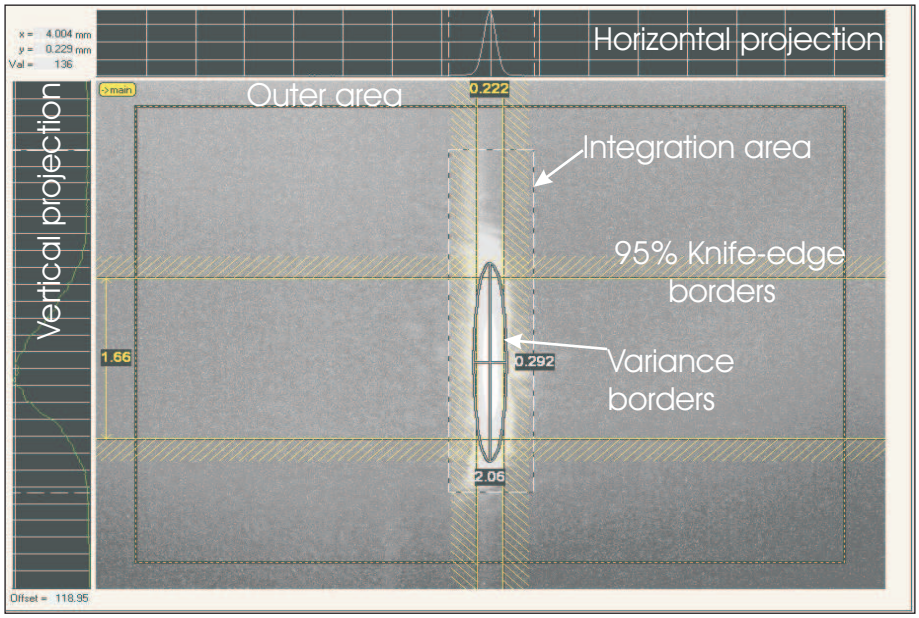

Figure 4.6: Appearance of the CCD camera graphical interface

The CCD array is divided into three sections:

- The outer area is originally composed of the outermost 19 % of the total number of pixels. It is meant to be exposed to none of the signal, and its averaged intensity provides the pixel offset value.

- The integration area is a manually set surface that defines the bounds for the integration of the signal intensity. It excludes the regions of the CCD chip where signal intensity is negligible and therefore act as a pure noise contribution. When some signal intensity is found inside the outer area, it comes to an overlap between the latter and the integration area. In such a case, the pixel offset is determined in only the part of the outer area where no overlapping occurs.

After offset subtraction, the output signal is numerically integrated in order to extract the beam centroid and the beam diameter according to the second moments or knife-edge definitions. An example of the borders of the beam width according to both definitions is shown in the figure.

4.2.4 Estimation of the uncertainty in the measurement of the beam quality

The experimental setup for the measurement of beam quality can be seen as composed of a laser under test, a series of optics and a CCD camera (associated with a series of neutral density filters) for the recording of the beam intensity. The laser can be considered to be free from fluctuations in the present measuring regime. The neutral density filters are, on their part, responsible for two eventual error sources in the system:

- The setting up of a thermal lens. The filters are absorptive and in the case where high intensities are incident on them, the build up of a thermal gradient inside the glass occurs. The beam profile is then distorted through the induced dynamic lens. This effect is in practice minimized by placing a highly reflective mirror in front of the measurement setup. It lets only a small fraction of the incident light through. Therefore, the thermal lens in the neutral density filters can be considered as negligible in the experiments.
- Parasitic reflections. Fresnel reflections on the surface of the filters are captured by the camera. In the worst case, they overlap with the useful signal. In practice, the filters are oriented in such a way that the parasite light falls outside the integration area. However, this is not always possible and the contribution of reflections on the measurement is to be taken into account.

When estimating the uncertainty on the measurements, one has to consider the influence of the lenses and of the camera (including filters) on the intensity profile. As for the former, they are considered aberration free in the bounds of the measuring conditions (lenses well centered and oriented), and their only contribution to error comes from their position on the optical axis. The estimated uncertainty is 1.5 μm on the position of $L1$ and 0.5 mm on the position of $L2$, $L3$ and the camera.Using the ABCD matrix [26] for the propagation of a laser beam with a waist of 100 μm situated on the front facet of the diode and with an M^2 value of 30, the propagation of the relative error [78] through the system is measured to be in the order of 0.05 $\%$ for both the near-field and the far-field. The relative error on the M^2 value is then around 0.1 $\%$. In the case of a caustic measurement, the positional error comes only from the camera and it is averaged over the number of measurement points in the data set. Therefore, the positional uncertainty is even lower in this case.

The other source of error is the recording and processing of the beam intensity by the CCD camera. The uncertainty depends on the noise contribution of the camera, but also very strongly on the beam to be measured. Though a rigorous definition of the relative error is to be made on the case to case basis, it is however interesting to find a generalized estimation of the upper bound of the error in the lateral beam width that can be readily associated to the measurement setup. First of all, some conditions (that have been as far as possible respected in practice) that minimize measurement error are assumed [93]:

- The incident beam on the CCD chip is attenuated such that the maximum beam intensity matches the saturation intensity of the detector
- The lateral beam width covers approximately one third of the total number of pixels and is centered on the CCD chip
- The beam is centered inside the integration area and the latter is as small as possible, but large enough not to clip it, which would induce a systematic error in the measurement of the beam width

Under such circumstances, the relative error on the beam radius shows a cubic dependence on the reduced width of the integration area:

$$\frac{\sigma_{w_x}}{w_x} \propto (\frac{\Delta x N_x}{2w_x})^3, \tag{4.6}$$

where σ_{w_x} is the standard deviation of the beam radius w_x, Δx is the lateral pixel size and N_x the number of pixels in the lateral dimension of the integration area. The latter is the most significant contribution to σ_{w_x}. Therefore, by analyzing the effect of varying the integration area on the beam width, a good estimation of the measurement error can be obtained. This influence is most significant when parasite light, in addition to the noise of the detector, lies in the vicinity of the intensity profile to be measured on the CCD chip. Then, it can be difficult to identify the extremities of the useful signal, and, as a consequence, the bounds of the integration area.

An estimate of the relative error on the beam width is obtained by varying the size of a defined integration area by a number of lateral pixels symmetrically about the centroid and by recording the change in the value of the beam width. Each extremity of the integration area along the lateral dimension is varied over an uncertainty interval $(\frac{\Delta N_x}{2})$ consisting of 20 pixels. The relative error on the beam width ranges from well under $1\,\%$ for beams recorded in the absence of parasite light and rises up to approximately $10\,\%$ for those that overlap with reflections or background spontaneous emission. Figure 4.7 shows the extreme cases used for the estimation of the lower bound (case (a)) and the upper bound (case (b)) of the relative error. In case (a), the signal is free of stray light and a contrast level of the image where the beam extremities are sharply defined is easily achieved. The relative error on the beam width reads $0.4\,\%$ when the integration area is varied by ΔN_x . On the other hand, case (b) is representative of the situation where significant background spontaneous emission intensity and reflections overlap with the useful signal. The image contrast has to be carefully adjusted in order to distinguish between the bounds of the beam and the underlying stray light. Even though, the boundaries are not clearly defined. The relative error on the beam width, while varying the integration area over ΔN_x, sums up to $9.8\,\%$. Following the same procedure, the relative error on the position of the beam centroid is found to be $0.86\,\%$. An upper bound of $1\,\%$ will thus be associated this source of measurement uncertainty.

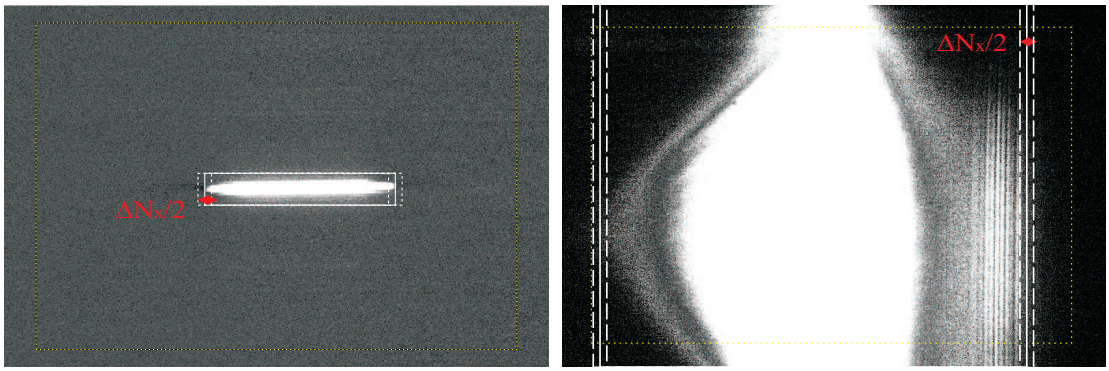

(a) (b)

Figure 4.7: Intensity profiles from two different beams: (a) with clearly defined borders, (b) with a large amount of spontaneous emission, or stray light, making it difficult to find the borders of the beam. The integration areas are represented in white with solid lines, whereas their two uncertainty intervals ($\frac{\Delta N_x}{2}$) are represented in dotted lines.The yellow dotted lines are the demarcation of the outer area.

Within the approximations stated above, the relative error on the beam width coming from the camera is estimated to have an upper bound around $10\,\%$. In comparison to this error source, the uncertainty on the position of the optical elements can be neglected. Thus, for an M^2 value determined via the method of beam waist and far-field, a relative error of approximately $20\,\%$ is associated with the measurements. As for the beam caustic, the relative uncertainty is statistically minimised over the number of data points. The standard error of the hyperbolic fit, which goes as high as $6\,\%$ in this case, may be used as an estimation of the uncertainty. However, it should be noted that in both measurement methods, the systematic error in the measurement processes cannot be determined.

Due to the fact that the measurement error is heavily dependent on the intensity profile to be measured itself, it is not possible to define a general uncertainty value of a beam quality measurement system. Commercial systems, for instance, specify the tolerance on the positioning of optics or give the electrical noise of their detectors, but are not able to give an effective system error since they have no information on the beams that are to be measured. In this work, the gross knowledge of the beam shapes and their optical noise has allowed the formulation of an estimate of the relative error in the 'worst case scenario'. The stated $20\,\%$ uncertainty on the M^2 value is only to be taken as a case-specific estimation.

Chapter 5

Determination of the thermal lens in a BA laser diode

The theoretical study of the external cavity laser concept points out that the knowledge of the thermal lens arising inside the laser diode is necessary for the design of a resonator with effective spatial mode filtering. Back then, the thermal lens coefficient has been arbitrarily chosen, though with hindsight on its typical values for semiconductor laser diodes. However, for the practical implementation of the external resonator, a quantitative knowledge of the thermal lens arising in the lateral direction is a prerequisite.

Several methods for the characterization of the thermal lens in semiconductor laser diodes have been reported in the literature. These include, for instance, the compensation of the thermal lens with variable lenses, and thus the determination of its strength [85], temperature mapping techniques [94] and interferometric measurement techniques [95]. In the present study, a simple experimental method that makes use of the variations in the far-field profile as a function of the induced thermal lens inside a diode amplifier is used. This measurement method is inspired from a well-known technique that is commonly applied to solid-state lasers [96, 97]. The diode amplifier is in all terms identical to the laser diode that is used inside the external resonator, except that both of its facets are anti-reflection coated. The deviation of an injected probe beam by the refractive index gradients characteristic of the thermal lens inside the amplifier is measured in the far-field. The thermal lens coefficient is then deduced from the measured profiles.

After a general presentation of the experimental setup, the measurement principle is detailed, along with the calculations that are required in order to extract the value of the thermal lens. Then, the issue of beam shaping inside the amplifier under test is discussed. The experimental results are presented next. In order to validate the latter, the thermal lens arising inside a similar free running laser diode is deduced, followed by a simulation of the heat distribution inside the amplifier. Measurement results and simulation are compared in order to validate the former and also to get a better understanding on the creation of the thermal lens inside the medium of the diode.

5.1 The experimental setup

A schematic of the optical setup that extends over a distance of approximately $1\,m$ is shown below (figure 5.1), together with the specifications of the optical elements (table 5.1). The probe beam is provided by the emission of the seed laser, a ridge-waveguide (RW) laser in this case. The latter has a vertical structure identical to that of the amplifier, whereas its lateral structure consists of a $6\,\mu m$ wide ridge waveguide. The emission in both axes is near-Gaussian, with M^2 values close to one and both beam waists are situated on the facet of the diode. Since the coupling of the emission of the seed laser into the amplifier is different in the vertical axis and lateral axis, these shall be considered separately. At the exit of the amplifier, the standard setup for the measurement of a far-field profile, as described in chapter 4, is implemented.

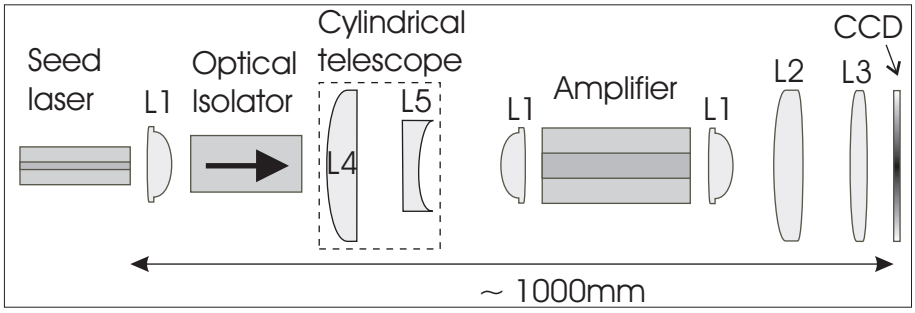

Figure 5.1: Experimental setup for the determination of the thermal lens in a semiconductor amplifier

	L1	L2	L3	L4	L5
Back focal length/mm	5.9	195.6	97.1	96.6	-38.4
Focal length/mm	8	200	100	100	-40
Thickness/mm	3.7	8.0	5.5	5.2	2.0

Table 5.1: Parameters of the lenses relevant to the arrangement of the experimental setup for the measurement of the thermal lens

5.1.1 Vertical axis

Since both the seed laser and the amplifier have the same vertical structure, effective coupling of the beam from the waveguide of the former into that of the latter is achieved by a 1:1 imaging of the facets on each other. This is achieved by collimating the emission of the seed laser with an aspheric lens ($L1$), and by focusing it into the amplifier with an identical lens, except that its orientation is reversed. An optical isolator, with specified isolation of $60\,dB$, is inserted between the two in order to avoid back reflections into the seed laser. Moreover, the vertical beam is unaffected by the cylindrical telescope, which is meant to act exclusively on the lateral beam.

5.1.2 Lateral axis

In this case, the beam emitted from the $6\,\mu m$ wide ridge waveguide has to be injected into the $100\,\mu m$ wide active zone of the amplifier. The challenge does not lie into the effective coupling, but rather more in the shaping of the lateral beam inside the amplifier.

The positions of the two aspheric lenses is set by the vertical beam, so that they cannot be moved in order to tailor the lateral beam. For this reason, a slightly unadjusted lateral telescope consisting of two cylindrical lenses ($L4$ and $L5$) with respective focal lengths of $+100\,mm$ and -40 mm, is used to adjust the position and the size of the lateral beam waist inside the amplifier. The optical isolator fulfills exactly the same purpose in the lateral direction as it does in the vertical direction. The measurements for the characterization of the probe beam are carried out at the output of the optical isolator rather than at the facet of the RW laser. Therefore, any losses and beam distortions that may occur inside the isolator are automatically taken into account. Figure 5.2 shows the characteristics of the probe beam, as measured at the exit of the optical isolator. The measurements have been carried in quasi-continuous-wave (QCW) operation, with current pulses of 100 μs and a repetition rate of 25 Hz. The operating temperature is 25 $°C$.

5.2 The measurement principle

The measurement technique is based on the deviations in the far field position, due to the refractive index gradient arising from thermal lensing in the active medium of the amplifier, of a beam injected at different position on the entry facet of the latter. Figure 5.3(a) shows a schematic of the beam path inside such a medium for different injection points, and figure 5.3(b) shows the deviation of a beam measured in the far field for different values of the lateral position of the injected probe beam. It can be seen from the graphic that injection of the beam at different lateral positions result into the output beam having different exit angles as a result. Moreover, the angle also depends on the strength of the thermal lens, the effective refractive index and the length of the diode. These angular deviations are characterized in the far field by a lateral deviation of the centroid of the beam profile. By measuring these, and by knowing all other parameters except the thermal lens coefficient, the latter can be deduced.

The process described above shall now be put into equations within the approximation of a quadratic dependence of the refractive index of the active medium on the lateral position. The paraxial approximation is considered to be valid, and all lenses are assimilated to thin lenses. The modeling of the thermal lens as a thick lens with a quadratic refractive index profile ensues similarly to the treatment in chapter three. The gain medium of the amplifier is then described by its ABCD-matrix, as a function of the thermal lens coefficient (γ), length of the diode (l), and effective refractive index (n_0). The formulation of equation 3.27 is replicated:

$$\begin{pmatrix} \cos(\gamma l) & \dfrac{\sin(\gamma l)}{\gamma n_0} \\ -\gamma n_0 \sin(\gamma l) & \cos(\gamma l) \end{pmatrix} \tag{5.1}$$

The propagation of a beam from the entry facet of the amplifier to the CCD camera (refer to figure 5.1) is given by its ABCD-matrix, where f_i is the focal length of lens L_i. The matrix (M) reads:

$$M = \begin{bmatrix} \dfrac{f_1 f_3 \gamma n_0 \sin(\gamma l)}{f_2} & \dfrac{-f_1 f_3 \cos(\gamma l)}{f_2} \\ \dfrac{f_2 \cos(\gamma l)}{f_1 f_3} & \dfrac{f_2 \sin(\gamma l)}{f_1 f_3 \gamma n_0} \end{bmatrix} = \begin{bmatrix} A & B \\ C & D \end{bmatrix} \tag{5.2}$$

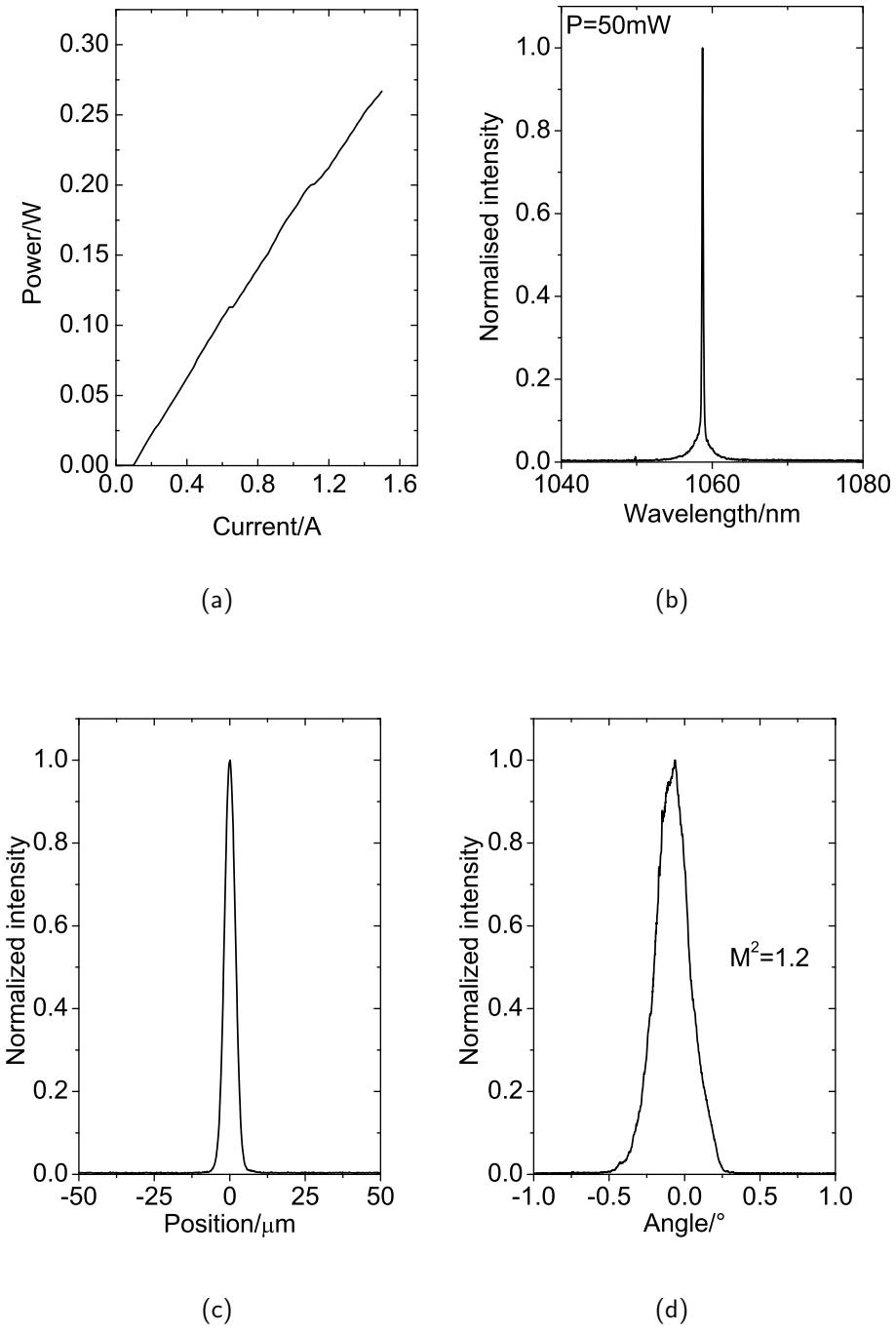

Figure 5.2: Measured: (a) Power-current characteristics, (b) Spectrum, (c) Lateral near-field and (d) lateral far-field of the probe beam system (seed laser+L1+Isolator). The spectrum and beam quality measurements are carried out at a power of 50mW

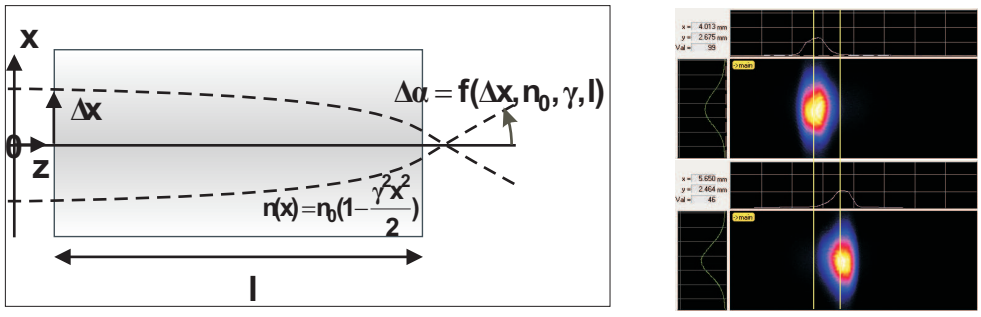

(a) (b)

Figure 5.3: (a)Sketch of the propagation of beams along the optical axis (z) in a laser diode under the influence of a thermal lens. A beam through the center (full line) and beams at a distance Δx from the center (dotted lines)are traced, (b) Measured camera image of the far-field of a beam injected at Δx on either side of the center of a diode under the influence of a thermal lens

Let two beams r_1 and r_2, parallel to each other, that strike the amplifier entry facet at different lateral positions. Their ray transfer matrices read, with x being the position on the facet and α the angle to the normal to the facet:

$$r_1 = \begin{bmatrix} x \\ \alpha \end{bmatrix} \qquad r_2 = \begin{bmatrix} x + \Delta x \\ \alpha \end{bmatrix} \tag{5.3}$$

Using equations 5.2 and 5.3, the respective ray transfer matrices on the CCD chip are given by:

$$r_{1CCD} = \begin{bmatrix} Ax & B\alpha \\ Cx & D\alpha \end{bmatrix} \qquad r_{2CCD} = \begin{bmatrix} A(x + \Delta x) & B\alpha \\ C(x + \Delta x) & D\alpha \end{bmatrix} \tag{5.4}$$

From equations 5.2 and 5.4, it can be deduced that the lateral shift between the two beams on the CCD chip is:

$$\Delta x_{CCD} = A\Delta x = \Delta x \frac{f_1 f_3 \gamma n_0 \sin(\gamma l)}{f_2} \tag{5.5}$$

Equation 5.5 is solved numerically to infer the value of γ. From there on, the refractive power (D_γ), focal length f_γ, and local refractive index modulation $\Delta n(x)$ of the gain medium of the amplifier under the influence of the thermal lens can be calculated [26]:

$$D_\gamma = n_0 \gamma \sin(\gamma l), \qquad f_\gamma = \frac{1}{D_\gamma}, \qquad \Delta n(x) = -\frac{n_0 \gamma^2 x^2}{2} \tag{5.6}$$

5.3 Beam shaping inside the amplifier

The present measurement technique of the thermal lens requires the probe beam to be as thin as possible inside the amplifier. Indeed, the inference of the thermal lens coefficient will depend on the deviation of the probe beam by the refractive index gradient inside the active medium of the amplifier. It is deduced from equation 5.5 that the higher the value of Δx on the entry facet of the amplifier, the higher the value of Δx_{CCD} on the camera, and hence the better the precision of the measurement. However, care must be taken that the beam does not strike the border of the active area, in which

case parasite reflection in the far field are susceptible to corrupt the measurement. An example is given in figure 5.4, where the probe beam, with an M^2 value close to one, is injected in the absence of the cylindrical telescope (figure 5.4(a)) into two different amplifiers with respective lengths of 1.3 mm and 3.9 mm. In the former case, the probe beam propagates through the amplifier without hitting the borders of the active area, whereas it does in the latter case. The respective far field profiles are shown in figures 5.4(b), for the 1.3 mm long device, and 5.4(c) for the 3.9 mm long one. It can be seen that when the probe beam strikes the border of the active zone, the far field profile is severely degraded. Thus, having a thin probe beam allows one to achieve a larger Δx while ensuring that it remains clear of the borders of the active zone. Moreover, a thin probe beam interacts with only a small portion of the refractive index gradient, and thus enhances the spatial resolution of the measurement.

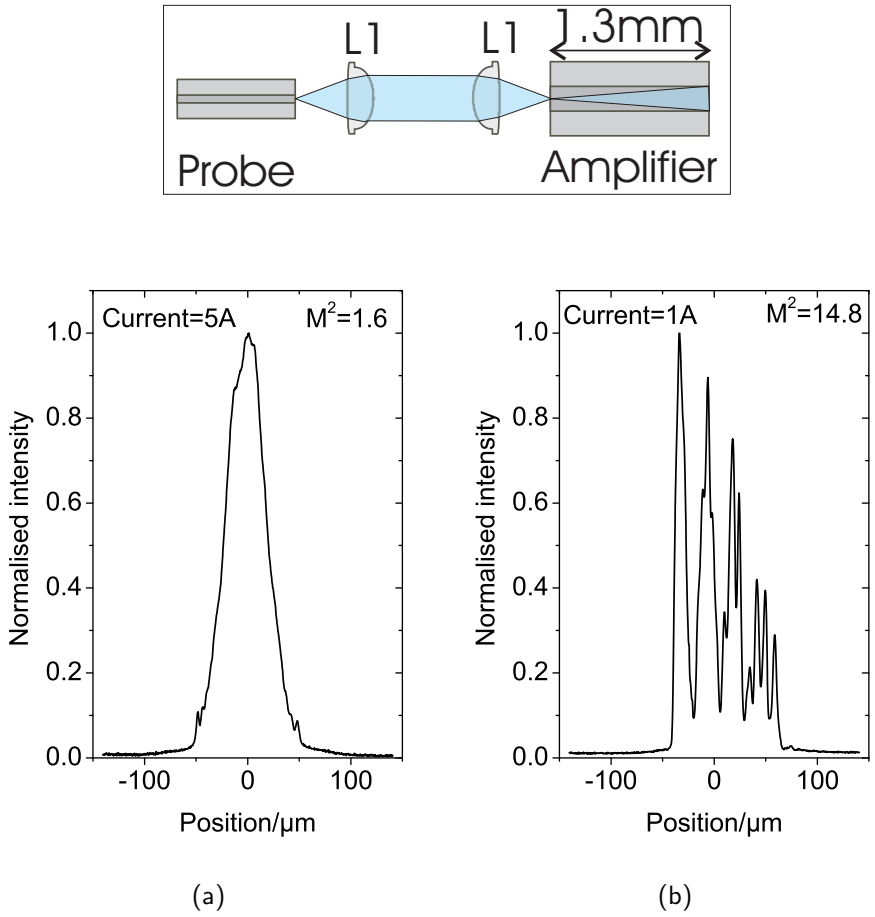

Figure 5.4: (a) Sketch of the setup used to test the influence of reflections of the probe beam in the waveguide of the amplifier, (b) Measured lateral near field of the probe beam on the output facet of a 1.3mm long amplifier. The injection current is 5A and the measured M^2 value is 1.6, (c) Measured lateral near field of the probe beam on the output facet of a 3.9mm long amplifier. The injection current is 1A and the measured M^2 value is 14.8

In the absence of the cylindrical telescope, the beam has a waist on the entry facet of the diode and diverges throughout its propagation. At the output facet, it occupies almost the whole area of active zone, as shown in figure 5.5(a). With such a beam propagation, it is almost impossible to probe the refractive index gradient inside the diode. Therefore, the probe beam has to be made thinner, with the beam waist situated in the middle of the diode, such that the beam width on both facets is equal. The choice of the lenses forming the telescope ($L4$ and $L5$) and their positioning is constrained by the space available inside the setup. By referring back to figure 5.1, it is seen that the only available space is between the optical isolator and the aspheric lens facing the entry facet of the amplifier. With this in hindsight, the lens $L4$ is chosen to be convex and has a focal length of 100 mm. On the contrary, $L5$ is concave, with a focal length of -40 mm.

It remains to derive the position of the telescope, and the distance between its constitutive lenses, such that the desired beam propagation inside the amplifier is obtained. The approach is progressive. First, a rough calculation is made in order to obtain an approximate positioning of the lenses that suits the purpose. It is then practically implemented, and the beam spread inside the amplifier is recorded with the CCD camera. The lenses are then adjusted until a satisfactory beam propagation is obtained.

The calculation is made within several simplifications. All lenses are modeled as thin lenses, the paraxial approximation is taken to be valid, the thermal lens inside the amplifier is neglected and the optical isolator is considered to be a neutral medium (no effect on the beam). The position of the telescope is referenced by two variables, namely the distance k between the facet of the RW laser and $L4$ and the distance δ that separates the two cylindrical lenses ($L4$ and $L5$). All other distances in the setup are known, as well as the beam parameters at the facet of the seed laser and the ABCD-matrix of the propagation through the whole system. In a first step, the q-parameter of the beam at the center of the amplifier is calculated. Since the beam waist is expected to be situated there, the real part of the q-parameter should be equal to zero. This condition provides a first equation in k and δ. In a second step, the q-parameter at the entry facet of the amplifier is calculated, and the beam diameter is subsequently inferred (refer to equation 3.16). At this point, the latter should be minimal. Therefore, its full first derivative with respect to k and δ should be equal zero. The second condition on the variables k and δ is thus obtained. Two limiting conditions also add up to this system of two equations, namely the fact that the second derivative of the beam diameter has to be positive (for a minimum point) and the space available for the positioning of the two lenses without them being hindered by other elements in the setup. The equations are solved numerically and values of k and δ that ensure that the beam waist is centered inside the amplifier and that the beam diameter on the facets is a local minimum are obtained. The lenses are mounted in that respect, the beam inside the amplifier is recorded and adjustments are made until a satisfactory beam propagation is obtained. Figure 5.5(b) shows an example of the tailored probe beam inside the diode. The calculated path (dotted lines) predicts a beam waist diameter of 8 μm exactly in the center and a beam diameter of 35 μm on either facet. In practice (solid lines), the beam waist is situated approximately 80 μm to the left of the center, but the larger beam width on the exit facet of the amplifier is approximately 35 μm.

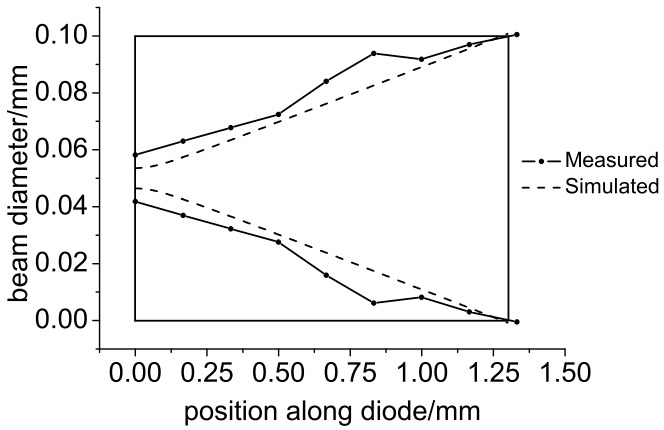

(a)

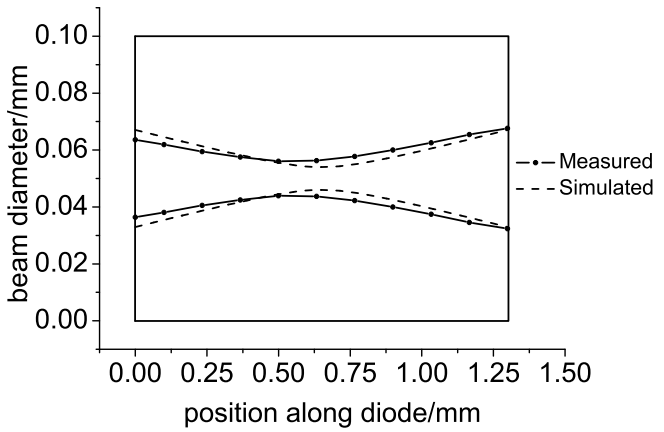

(b)

Figure 5.5: Beam shaping of the probe inside the amplifier for two different configurations: (a) without the cylindrical telescope and (b) with the cylindrical telescope. In both cases, the dotted lines are simulation results and the full lines are measured data. The frame represents the dimensions of the active area of the laser amplifier (aspect ratio not respected).

5.4 Experimental procedure and results

5.4.1 The experimental procedure

Both the seed laser and the amplifier are mounted first on a CuW sub-mount, which is then mounted on a C-mount. The latter is itself mounted on a copper block that is kept at a temperature of 25 $°C$ with the help of a common water circulator. During the measurements, the injection current into the seed laser will be kept constant at 371 mA, which corresponds to an effective power in the probe beam (after the isolator) of 50 mW. The current injection inside the seed laser is synchronized with that in the amplifier.

The probe beam is tailored with the cylindrical telescope and is made to have a beam waist diameter of 8 μm halfway inside the amplifier. The beam diameter on either facet is 35 μm. In a first measurement step, the amplifier is translated to the right, such that the probe beam strikes the entry facet 25 μm to the left. The beam position on the CCD camera is measured. The second measurement step consists in translating the amplifier

$50\,\mu m$ to the left, such that the beam now strikes the facet $25\,\mu m$ to the right. The corresponding beam position on the CCD camera is again measured. From these two measurements, the thermal lens coefficient of the induced thermal lens in the amplifier is calculated, with the knowledge of the effective refractive index of the vertical guided mode, which is calculated separately. In the case of the diode used in the experiments, its value is 3.33. The beam is translated only $50\,\mu m$ along the $100\,\mu m$ broad laser diode active area in order to make sure that the beam does not strike the borders of the active region, in which case parasite reflections would appear on the far-field profile and degrade the measurement. This procedure is carried out for currents ranging from $1\,A$ to $10\,A$, at a constant pulse width of $100\,\mu s$ and repetition rate of $25\,Hz$. The same procedure is then repeated, but this time with a fixed drive current of $10\,A$ and different pulse widths ranging from $50\,\mu s$ to $500\,\mu s$. The repetition rate remains unaltered.

5.4.2 Experimental results

Knowing the thermal lens coefficient, the maximal refractive index difference between the center of the diode active region and its extremity is deduced, as well as the respective refractive power and focal length of the induced thermal lens. The experimental results are depicted in figure 5.6.

With a rise in injection current, the thermal lens coefficient (figure 5.6(a)) increases as a result of a higher amount of heat generated by non-radiative recombination in the active area. In fact, the temperature gradient between the active zone and the regions of the diode lying outside the current injection stripe increases, creating a steeper refractive index gradient along the width of the diode (figure 5.6(c)). With increasing current, the medium develops a lens with higher refractive power (figure 5.6(e)), thus shorter focal length (figure 5.6(g)). However, the slope of the thermal lens coefficient decreases as current is increased. This can be explained by the fact that with increasing heat power, the regions outside the current stripe also start to heat up. Hence, although the net temperature in the active zone increases, the temperature gradient saturates while the temperature outside the current stripe is increasing at the same time. This effect can be clearly seen in figure 5.6(b), where despite an increase in temperature through longer pulse widths, the thermal lens coefficient stays constant. The local refractive index between pulses of different lengths shows little change (figure 5.6(d)). Hence, the refractive power and focal length (figures 5.6(f) and 5.6(h) respectively) remain almost constant.

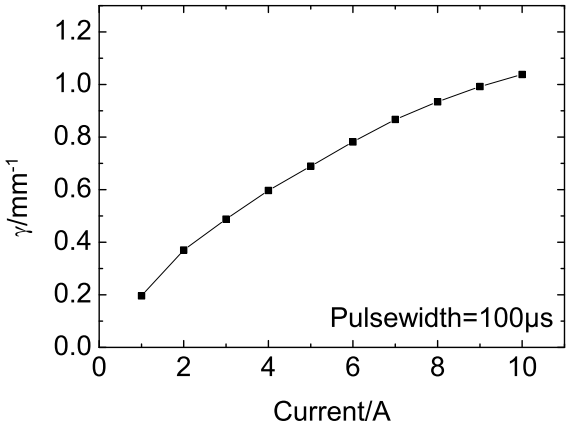
γ/mm-1
Pulsewidth=100µs
Current/A

(a)

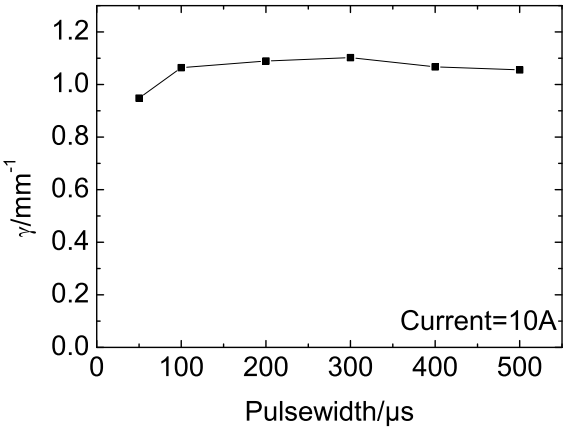
γ/mm-1
Current=10A
Pulsewidth/µs

(b)

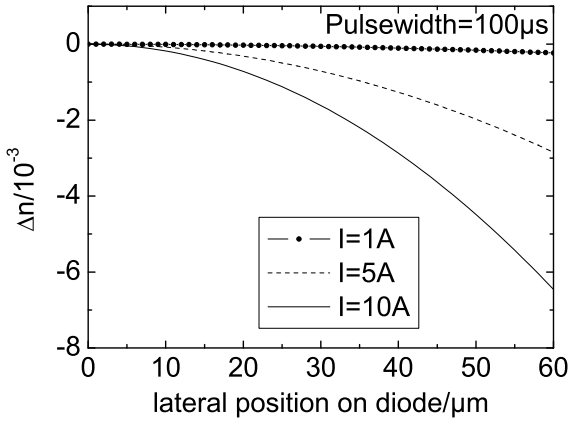
Pulsewidth=100µs
Δn/10-3
I=1A
I=5A
I=10A
lateral position on diode/µm

(c)

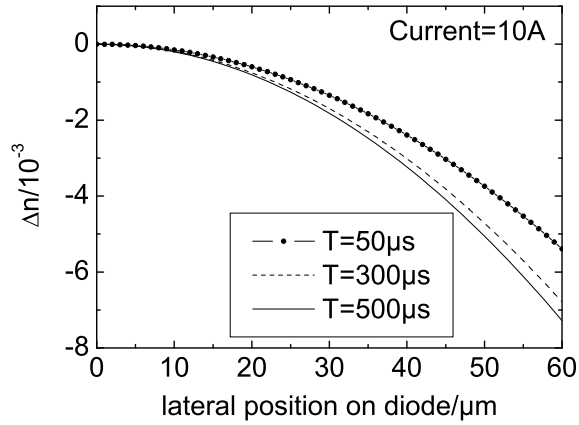
Current=10A
Δn/10-3
T=50µs
T=300µs
T=500µs
lateral position on diode/µm

(d)

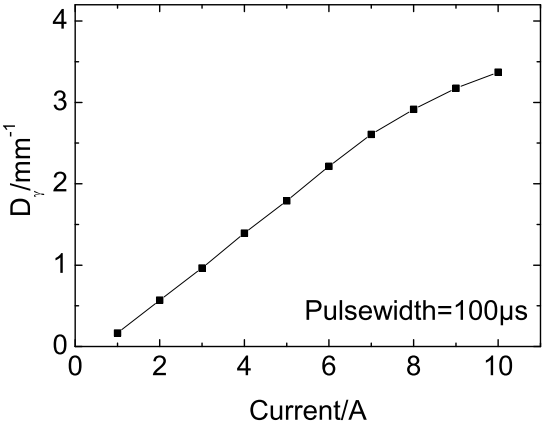
Dγ/mm-1
Pulsewidth=100µs
Current/A

(e)

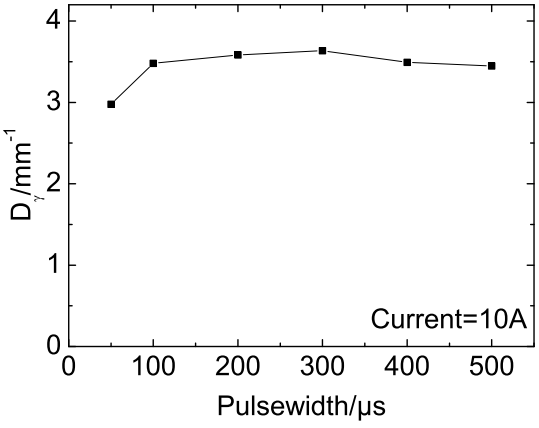
Dγ/mm-1
Current=10A
Pulsewidth/µs

(f)

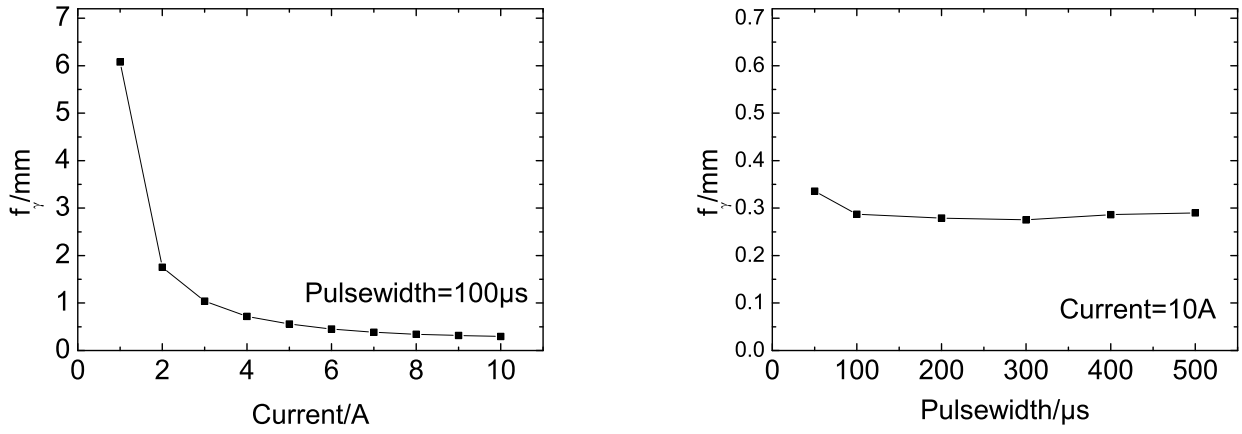

Figure 5.6: Experimentally determined thermal lens parameters as a function of current(left column):(a) Thermal lens coefficient (γ),(c) Refractive index change (Δn),(e) Refractive power (D_γ),(g) Focal length (f_γ); and as a function of pulse width (right column):(b) Thermal lens coefficient (γ),(d) Refractive index change (Δn),(f) Refractive power (D_γ),(h) Focal length (f_γ)

5.5 Validation of the experimental results

The thermal lens arising in the test amplifier has been measured at different injection currents and pulse widths. These results are meant to be applied to the laser diode used in the design of the external cavity laser. However, it is important to verify the validity of the thermal lens coefficient values obtained in the experiment. This is, on the one hand, achieved by relating the M^2 value of a free running laser to the thermal lens influencing it. By measuring the former and comparing it to the expected values, a method is obtained that indicated the reliability of the measurement of the thermal lens coefficient. On the other hand, a simulation of the heat transfer inside the structure of the test amplifier is carried out as a function of the pulse width. It is meant to compare with the experimental results obtained by varying the pulse width at a constant current of 10 A. From there, not only a validation of the measurement technique of the thermal lens can be extracted, but also a better understanding of the process that induces the thermal gradients, and thus, the thermal lens inside the diode.

5.5.1 Estimation of the beam quality of a laser diode

Under the influence of a thermal lens, a free running laser diode fulfills the conditions for the setup of a stable resonator between the two plane mirrors deposited on its facets. The treatment, with the ABCD-matrix formulation, of such a case has been detailed in equations 3.34-3.37, in chapter three. The M^2 value of the emission is estimated by comparing the diameter of the fundamental mode to that of the highest order mode that is allowed to oscillate, in this case taken to be limited by the width of the active zone of the diode (W_x), as represented in the sketch in figure 5.7(a). The M^2 value thus obtained is related to the thermal lens coefficient γ, through the effective refractive

index of the active zone of the diode (n_0) and the emission wavelength (λ):

$$M^2 \approx \frac{\pi n_0 \gamma {W_x}^2}{4\lambda} \tag{5.7}$$

The M^2 values, calculated at different pump currents, are compared with experimental data coming from a broad area laser diode in all points similar to the test amplifier used in the determination of the thermal lens coefficient, except that its facets are coated 5 % on the front and 95 % on the rear. The results are shown in figure 5.7(b). A good agreement is to be seen between the estimated and measured values of the M^2. At lower currents, the curves show a bigger divergence than at higher current. This is expected of a resonator, while at lower M^2 values, aberrations tend to have a more pronounced influence on the beam quality [98]. These results confirm the validity of the measurement technique in the determination of the thermal lens parameters in semiconductor lasers.

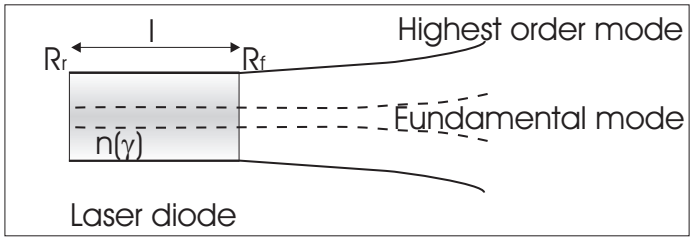

(a)

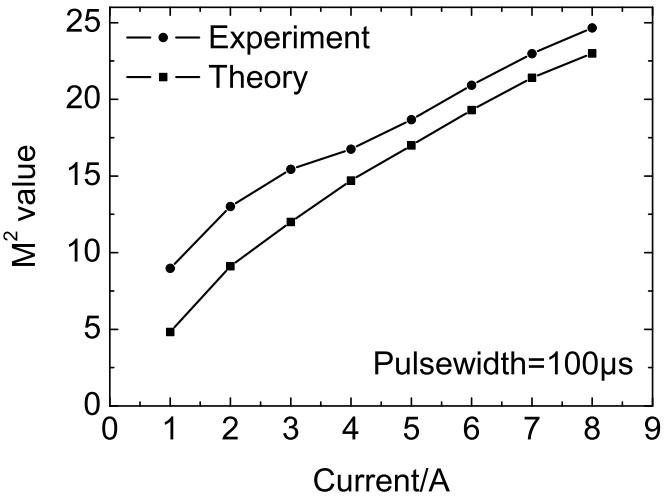

(b)

Figure 5.7: (a) Sketch of a laser diode showing the fundamental mode and the highest order mode of the stable resonator (between the two coated facets) under the influence of a thermal lens, (b) Estimated (dots) and measured (squares) M^2 value of a 1.3mm long laser diode coated 5 % on the front facet and 95 % on the rear facet. The values of the parameters are as follows: n_0=3.33, λ=1.053 μm, W_x=0.1 mm.

5.5.2 Validation through simulation

The two-dimensional temperature distribution in the transverse cross section of the laser diode is calculated by solving the time-dependent linear heat equation [99] with the

help of the MSC Patran/Nastran software package (simulation courtesy of Dr. Frank Schnieder, Ferdinand-Braun-Institute). The heat flux in the epitaxial layer structure, in the sub mount and in the heat sink is accounted for, as shown in figure 5.8. Table 5.2 lists the different layers, with their respective geometries and material parameters [100] relevant to the simulation. All parameters are assumed to be temperature independent.The complete heat source, modeled as an area heat source, is placed in the plane of the active region with a real thickness of about 30 nm, neglected in the simulation. The temperature at the bottom of the Cu heat sink is kept constant. At all other boundaries, zero heat flux is assumed. The temperature distribution versus time is initially calculated for an arbitrary loss power (Q) of 10 W.

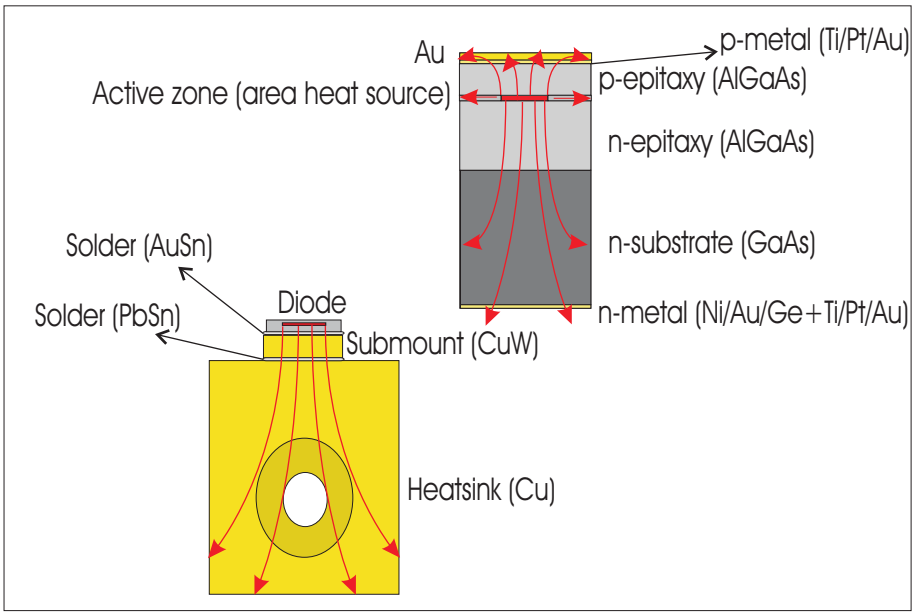

Figure 5.8: Sketch of the layers consisting the system to be thermally modeled (left), with a zoom on the laser chip depicted on the right side. The red arrows show schematically the propagation of heat in the system (from active zone outwards, without crossing the interface with air)

The true loss power and hence the absolute temperature values are then determined as follows: first, the shift of the maximum of the amplified spontaneous emission (ASE) spectrum is recorded in dependence on the pulse width at a current of 10 A. With the wavelength shift as a function of temperature ($\frac{d\lambda}{dT}$) calculated to be 0.41 nmK^{-1} for this structure, the mean temperature change inside the active zone ($\langle \Delta T \rangle_{AZ}$) at the peak emission wavelengths λ_i and λ_{i+1} corresponding to two successive pulse widths reads:

$$\langle \Delta T \rangle_{AZ} = (\lambda_{i+1} - \lambda_i) \frac{\partial T}{\partial \lambda} \tag{5.8}$$

In a next step, the simulated arbitrary temperature distribution inside the active zone of the diode is used to infer the difference in temperature ($\langle \Delta T \rangle_{AZ}$) for two successive pulse widths. In order to reflect the temperature rise that is experimentally determined, the simulated temperature rise is spatially averaged over the lateral span of the active region, that is, from 0 μm to 50 μm. The values are compared with those obtained in equation 5.8. From there, an actual loss power of 5.8 W at a current of 10 A is derived. Knowing

Layer	Material	Thickness $/mm$	Width $/mm$	Thermal conductivity $/WK^{-1}mm^{-1}$	Heat capacity $/Jg^{-1}K^{-1}$	Density $/gmm^{-3}$
Gold	Au	0.003	0.4	0.32	0.129	0.019
p-electrode	composite metal	0.00001	0.4	0.1	0.38	0.012
p-epitaxy	AlGaAs	0.0013	0.4	0.012	0.366	0.00485
Active region		0	0.1			
n-epitaxy	AlGaAs	0.0045	0.4	0.012	0.366	0.00485
n-substrate	GaAs	0.12	0.4	0.044	0.327	0.00532
n-electrode	composite metal	0.00055	0.4	0.1	0.38	0.012
Solder	AuSn	0.006	0.4	0.057	0.17	0.0145
Submount	CuW	0.53	2	0.2	0.175	0.0161
Solder	Pb0.4Sn0.6	0.02	2	0.050	0.27	0.0089
Heatsink	Cu	5	6.4	0.384	0.383	0.0089

Table 5.2: Layer structure (p-up mounting) of the modeled cross section of the semiconductor laser amplifier which is symmetric with respect to the lateral direction

that only heat conduction is considered in the simulation (all the boundaries with air are considered to have no heat exchange), the temperature rise inside the diode is taken to be proportional to the heat power of the source [101]. Therefore, the temperature distribution is scaled with the actual loss power.
The obtained lateral temperature profiles, as a function of current pulse width, are shown in figure 5.9(a). These profiles, taken at the position of the active region, are obtained by a temporal average of the lateral profiles evolving during the pulse. The temperature increases with longer pulse widths. However, the temperature difference between two successive pulses decreases as they get longer. For current pulse widths larger than 100 μs, the temperature difference between the center of the active region and its edge (located at 50 μm) remains almost constant. As a result, the thermal lens coefficient also remains constant. This explains the behavior shown in figure 5.6(b). In order to determine the lateral index profile from the simulated temperature profiles the dependence of the (effective) refractive index on the temperature ($\frac{dn}{dT}$) is used. Its value for the present structure has already been calculated to be 2.5 x $10^{-4}\,K^{-1}$. Figure 5.9(b) shows the change in lateral refractive index profile resulting from the temperature rise inside the chip.

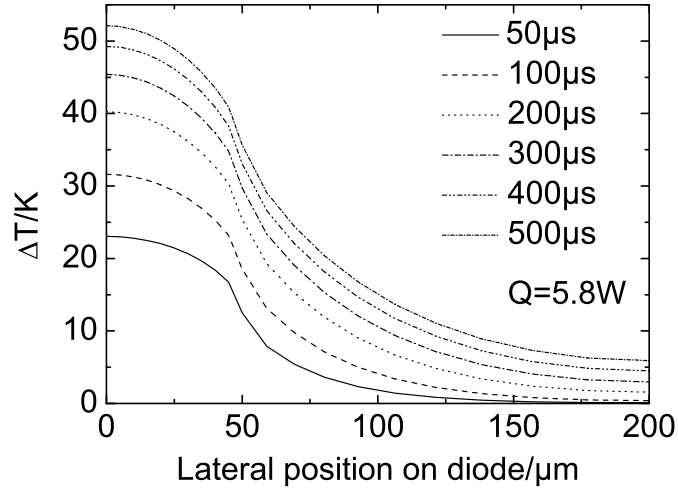

(a)

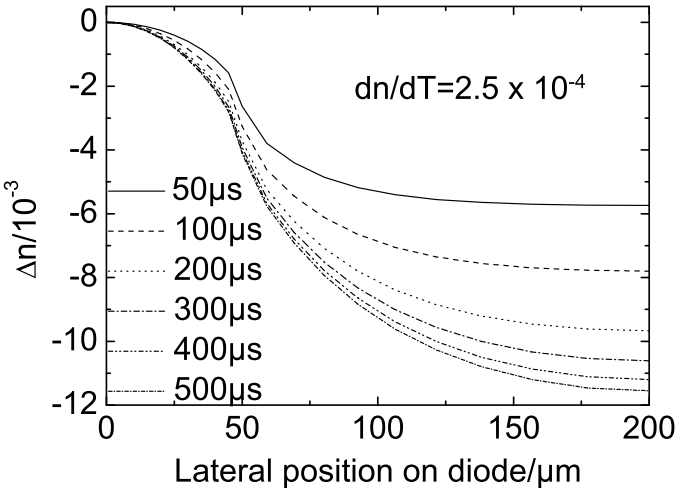

(b)

Figure 5.9: (a) Simulated lateral temperature change (ΔT) in the laser amplifier at a constant current of 10A for several pulse widths, (b) Inference of the refractive index change (Δn) along the width of the amplifier.

From the simulated refractive index change inside the diode, an estimate of the thermal lens coefficient can be inferred. In fact, it is known from equation 5.6 that the refractive index change can be written as:

$$\Delta n(x) = -\frac{n_0 \gamma^2 x^2}{2} \tag{5.9}$$

By making the substitution $x^2{=}X$, the refractive index change can be rewritten as a linear function of X and the fitted slope gives the value of the thermal lens coefficient (γ):

$$\Delta n(X) = \beta X, \qquad \gamma = \sqrt{\frac{-2\beta}{n_0}} \tag{5.10}$$

The linear fit of the refractive index change is carried out over the lateral width falling under the current injection stripe of the diode in order to reflect the measurement conditions, where the probe beam is propagated within this region. The thermal lens coefficient obtained from measurement and simulation are compared for different pulse widths of the current injection, as shown in figure 5.10 below.

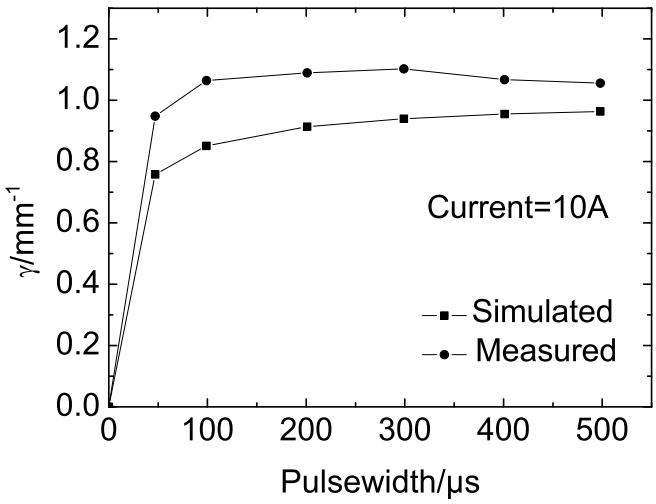

Figure 5.10: Comparison between the measured and simulated thermal lens coefficient (γ) for several pulse widths at a constant current of 10A

As expected, the curve representing the simulated values of γ shows the same saturation behavior as the measurements when the pulse width is increased. The validation of the measured thermal lens coefficient is achieved by the simulation, despite discrepancies between the two set of values, with a maximum difference of approximately 20 $\%$ occuring at a pulse width of 100 μs.

The thermal lens coefficient for the diode laser structure used in the implementation of the external cavity laser has been quantified. The experimental results have been validated by two methods, namely via the influence of the thermal lens on the beam quality of a free running laser and via the simulation of the temperature distribution inside the laser chip. The latter has also allowed to get a better understanding of the behavior of the thermal lens with increasing current pulse width. From now on, the measured values of the thermal lens coefficient can be injected in the design of the external resonator, and an implementation of the concept can ensue.

Chapter 6

Implementation of the external resonator laser

6.1 The experimental setup

Based on the theory developed in chapter three, an external resonator laser is implemented. Its geometry and constitutive elements are sketched in figure 6.1. A 1.3 mm long BA laser diode with a stripe width of 100 μm is used as gain medium. As seen before, its effective refractive index, in the absence of perturbations, is taken to be 3.33. The front facet of the diode, which also serves as output coupler of the ECL has a reflectivity of 5 $\%$. The rear facet is AR-coated and faces an aspheric lens with a focal length of 8 mm (working distance of 5.9 mm) and a numerical aperture of 0.5. The primary function of the lens is the collimation of the fast axis of the emission of the diode. Following the asphere is a cylindrical lens with a focal length of 50 mm that influences the beam only in the lateral direction. It is positioned in such a way that it forms a confocal pair with the asphere. Both lenses are AR-coated at the emission wavelength of the laser. The setup is completed by a plane mirror with a reflectivity of 95 $\%$. It is placed at a distance d from the surface of the cylindrical lens.

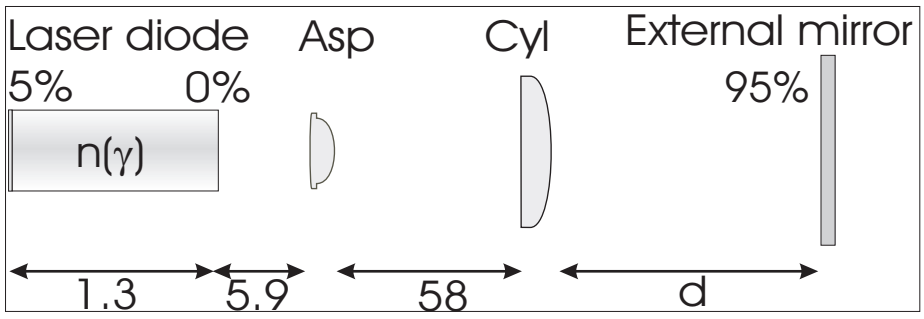

Figure 6.1: Sketch of the implementation of the external resonator laser. 'Asp' is an aspheric lens with a focal length of 8 mm and 'Cyl' is a cylindrical lens (in the lateral direction) with a focal length of 50 mm. The distances given at the bottom are all in millimeter.

The operating conditions of the laser are identical to those detailed in the previous chapters, that is, the diode is mounted p-side up on a CuW sub-mount, which is in turn mounted on a C-mount. The latter is fixed to a copper heat sink that is kept at a temperature of 25 $^{\circ}C$ by a water circulator. Current pulses with a temporal width of 100 μs are injected at a repetition rate of 25 Hz in the diode. The measurement of the output beam follows the description given in chapter four.

It has been discussed in chapter three that a critical issue in the external resonator is the collimation of the beam in the vertical axis, so that the back coupling efficiency in that direction is maximized. The two factors that principally influence the latter are the axial misalignment (δ) of the collimation lens and the accuracy with which the vertical tilt (α) of the external mirror can be adjusted. From equations 3.9 and 3.13, the back coupling efficiency (η) of the vertical mode into the waveguide is given by:

$$\eta = \frac{1}{\sqrt{1+\left(\frac{\delta}{z_R}\right)^2}} \exp\left[\frac{-(2f_1\alpha)^2}{w^2}\right], \tag{6.1}$$

where f_1 is the focal length of the collimation lens, z_R the Rayleigh length of the emission and w the radius of the mode. In the experimental setup, the collimation lens is mounted on a translation stage with an accuracy of 1.5 μm in the axial direction whereas the mount of the external mirror can adjust the tilt angle down to an accuracy of 15 μrad. The values of f_1, z_R and w are already known to be 8 mm, 8.4 μm and 1.68 μm, respectively. These values yield a back coupling efficiency of approximately 96 $\%$.

The requirements on the positioning of the elements in the lateral resonator are not so stringent. In fact, the modes are coupled back into an aperture of 100 μm, some twenty times wider than the aperture in the vertical axis. However, care is taken that the beam in the lateral direction is reflected parallel to the optical axis. The accuracy with which the lateral tilt of the mirror can be adjusted is equal to that in the vertical direction, that is, 15 μrad. Both the external mirror and the cylindrical lens are mounted on linear translation stages that enable axial movement in steps as low as 10 μm. However, the accuracy of the absolute positioning of these elements is around 0.5 mm (accuracy of a ruler).

6.2 Stability of the resonator and output power

Based on the mathematical model of the external resonator developed in chapter three, and the values of the thermal lens coefficient measured in chapter five, a map of the stability range of the laser, as represented in figure 6.1, is plotted in figure 6.2(a). The lower and upper stability limits (SL_l and SL_u respectively), the optimal position of the external mirror for fundamental mode operation (d_{opt}) and the thermal lens coefficient (γ) are plotted against the injection current. As the latter increases, the stability range shrinks and the curves for SL_u and d_{opt} melt into each other. Between a current of 1 A and approximately 3 A, the resonator remains stable beyond d_{opt}, where the fundamental mode is then truncated at the rear facet of the diode. Above 3 A, the laser will have to be operated at its stability limit in order to fit the fundamental mode exactly into

its active zone in the lateral dimension. How far this can be achieved is going to the investigated in the next sections.

The power-current characteristics of the external resonator (P_{Res}) are recorded for d=50 mm. At this particular distance of the external mirror from the cylindrical lens, the resonator is stable for the whole range of injection currents between 1 A and 8 A. The results are shown in figure 6.2(b). The power-current characteristics of a free running laser (P_{FRL}), as described in chapter two, are also plotted as a comparison, as well as the fraction P_{Res}/P_{FRL}. It can be deduced that, in average, the external resonator achieves approximately 87 $\%$ of the output power of the free running laser. However, the instabilities in the curve tend to indicate that misalignments of the cavity occur during the recording of the power-current characteristics, particularly at the extremities. Above 6 A, the power of the external resonator saturates, unlike that of the free running laser, where, due to thermal rollover, the curve tends to saturate approximately at a current of 8 A. The measurement of the power of the external resonator is stopped at 7 A in order to avoid any eventual damage to the laser chip. The saturation of the curve could have been caused by an increased heating inside the diode indirectly caused by a further misalignment of the optical elements. In fact, an off-axis backcoupling of the beam into the diode can lead to an increase in both the non-radiative recombination inside the gain medium and absorption at its borders. Since no posterior adjustments are made during the experiment, the risk that the power-current characteristics do not reflect the optimal case cannot be neglected. However, it is sufficient to get an estimation of the mechanical stability of the setup and the induced losses. The effective output power of an optimized cavity shall be assessed in particular cases where the beam quality shall also be measured.

Using the power-current characteristics of the external resonator between the threshold current and 6 A (avoiding the saturation of the power), a slope efficiency of 0.82 WA^{-1} is extracted, as compared to 0.94 WA^{-1} for the free running laser in the same current range. Using equations 2.5 and 2.6 (refer to chapter two), the additional losses in the external resonator are found to be 1.94 cm^{-1}, distributed on the length of the laser diode. Still according to the simulations in chapter two, the threshold current is then expected to be 0.67 A. It is measured on the experimental curve to be 0.60 A, and it has already been measured on the free running laser to be also 0.60 A. The experimental value is close to the theory, within the resolution of the current steps, which is 50 mA in this case. In general, although the external resonator suffers from misalignments during the recording of the power-current characteristics, both the percentage power achieved with respect to the free running laser and the similar threshold current tend to indicate that the losses in the external cavity are small.

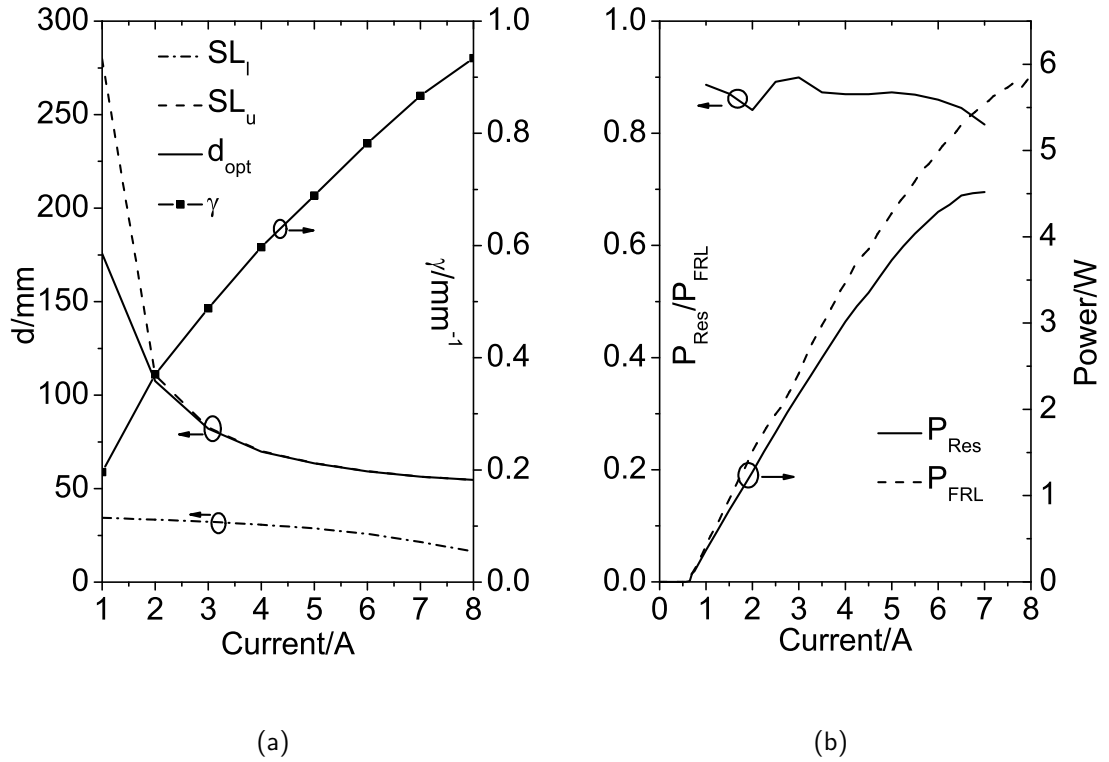

(a) (b)

Figure 6.2: (a) Stability diagram of the external resonator as a function of current. The lower stability limit (SL_l), the upper stability limit (SL_u), the optimal mirror position that theoretically yields fundamental mode operation (d_{opt}) and the thermal lens coefficient (γ) are shown, (b) Power-current characteristics (right-hand axis) of the external resonator (P_{Res}) and of a free running laser (P_{FRL}). The fraction of the output power of the external resonator to that of the free running laser (P_{Res}/P_{FRL}) is also plotted on the left-hand axis.

6.3 Influence on the beam quality

6.3.1 The active zone as modal filter

The external resonator is tested by measuring the beam quality and the output power for several positions of the external mirror at a current of $1\,A(1.67\,I_{th})$. The experiment is carried out relatively close to the laser threshold such that nonlinear effects inside the gain medium are minimized. The thermal lens coefficient measured at this value of the current is $0.20\,mm^{-1}$, and the resonator is stable for d, the distance between the cylindrical lens and the external mirror, in the range between $35\,mm$ and $275\,mm$. However, the fundamental mode is expected to fill exactly into the width of the active region when d is in the region of $175\,mm$, and positioning the external mirror further away would cause the beam to be truncated at the aperture of the diode. d is made to vary from $70\,mm$ to $175\,mm$, and the measured power and beam quality are shown in figure 6.3. The power is plotted on the right-hand axis, whereas the M^2 value is plotted on the left-hand axis. It is measured according to the methods of second moments (2^{nd} Mom.) and the knife-edge method (K.E) at $95\,\%$, $90\,\%$, and $80\,\%$ of the total power. The theoretical M^2 values according to the model developed in chapter three are also traced.

The output power decreases as d is increased, with a difference in power of approximately 10 % between the start point and the end point of the experiment. However, the initial power (d=70 mm) is recorded to be 0.41 W, which is closer to the 0.42 W of the free running laser than the 0.37 mW measured in the power-current characteristics of the external resonator. This confirms the hypothesis that the latter suffered from misalignments during the recording of the power, and that optimization of the coupling into the diode is possible.

As d is increased, the M^2 value decreases. However, when the second moments M^2 is considered, its values lie very far from the theoretical curve. As for the knife-edge M^2 measurements, the values come closer to the trend followed by the theory as the criteria for the percentage of power enclosed is decreased.

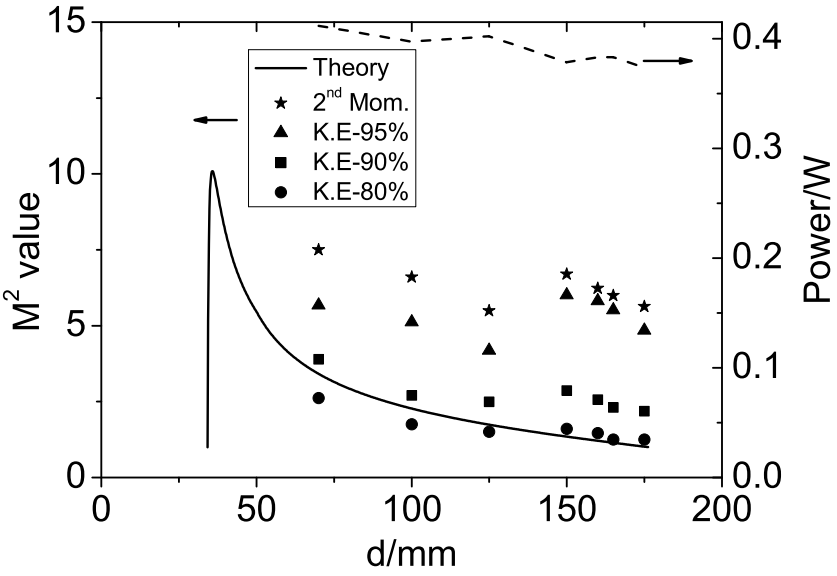

Figure 6.3: M^2 value and output power of the beam in the external resonator as the position of the external mirror is varied. The current is kept constant at 1 A.

This behavior is better understood when the near-field and far-field profiles of the beam at different positions of d are investigated. The near-field and far-field profiles of the beam for d equal to 70 mm, and 175 mm are depicted in figure 6.4. As expected, the near-field of the beam does not change much as d travels towards the stability limit. In both cases, the beam width is around 100 μm and the profiles do not differ too much from each other.

A marked decrease in the divergence angle of the beam is observed when d is increased, proving that filtering of higher order modes by the aperture of the diode takes place. However, the foot of the intensity distributions remains relatively wide. At d equal 175 mm, the upper fraction of the profile is very close to that of the diffraction-limited beam (0.77 °), but the lower fraction is broadened and contains some ripples on either side of the central lobe. This explains the high values for the M^2 measured by the method of second moments, and the progressive decrease in the M^2 values as the criteria of the power enclosed in the knife-edge measurements is lowered. An explanation for such a behavior of the beam could be an ineffective mode discrimination at the aperture of the diode. In the high-gain active medium, small fractions of higher order modes lying in the wings of the distribution do not experience enough losses in order to decay completely in steady-state operation. Moreover, it is highly probable that non-linearities in the gain medium induce a non-uniform lateral phase front, that could be responsible for the modulations observed in the near-field profiles and the broadening of the far-field.

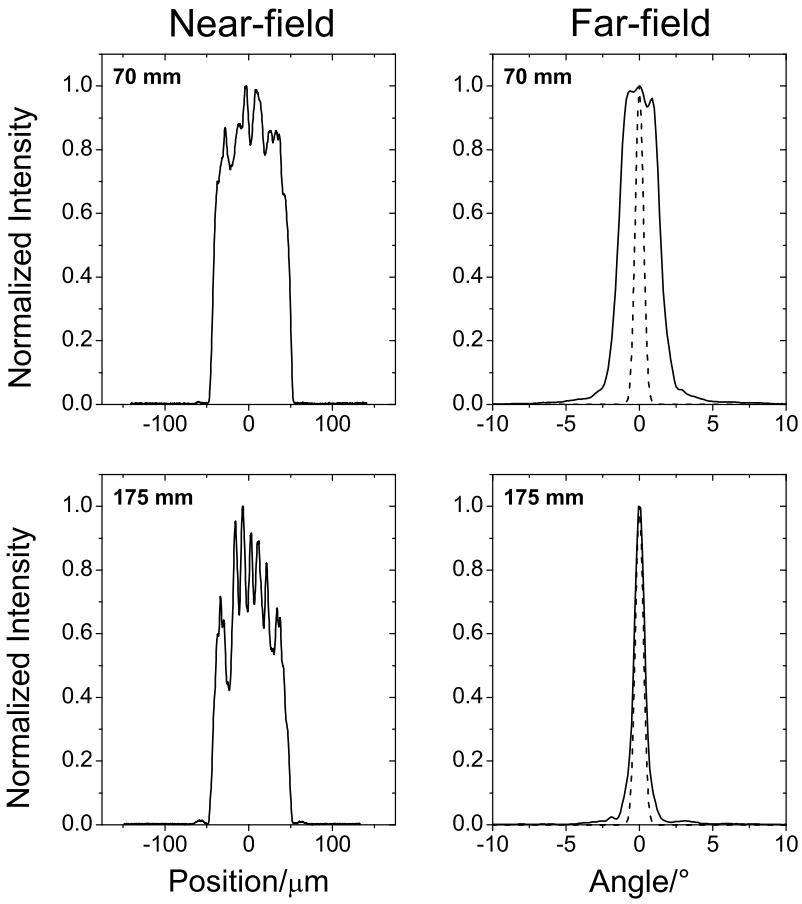

Figure 6.4: Near-field (left) and far-field (right) profiles of the output beam for d= 70 mm, and 175 mm. In each far-field profile, the theoretical diffraction-limited distribution corresponding to a near-field of 100 μm is also traced in dotted lines.

6.3.2 Addition of an intra-cavity slit

A slit with an adjustable lateral size is included in the setup, as sketched in figure 6.5. The influence of the slit on the emission of the external resonator is used for two different purposes:

- To further study the behavior of the external resonator and to compare it with the theoretical model.
- To improve the beam quality by:
  - ensuring that the beam propagates inside the diode without hitting the borders of the active region.
  - providing additional mode filtering.

The theoretical model yields the beam diameter of the fundamental mode at any point inside the stable resonator. Moreover, the diameters of the higher order modes is also known, since they propagate exactly in the same way as the fundamental mode, except that a beam with an M^2 value of 'x' will have a its diameter $\sqrt{x}$ times larger than the latter. By adjusting the size of the slit, the higher order modes can be progressively cut off. Therefore, by observing the effects of closing the slit on the output power and on the beam profiles, the functioning of the resonator can be investigated, and the results are compared with the theory.

Inside the stable resonator, the beam diameter at the facets of the diode fits exactly into the aperture of the latter. Minor misalignments in the optical system can result in the beam hitting the borders of the active region and reflecting off it, causing degradations in the beam quality. This phenomenon has already been shown in chapter five. By an appropriate adjustment of the slit width, the beam back coupling into the laser diode can be made to have a smaller diameter than its active region, and therefore ensure that the propagation within ensues without reflections off the borders. Moreover, the slit width can also be adjusted such that, for instance, all higher order modes suffer losses, and therefore, only the fundamental mode is allowed to oscillate.

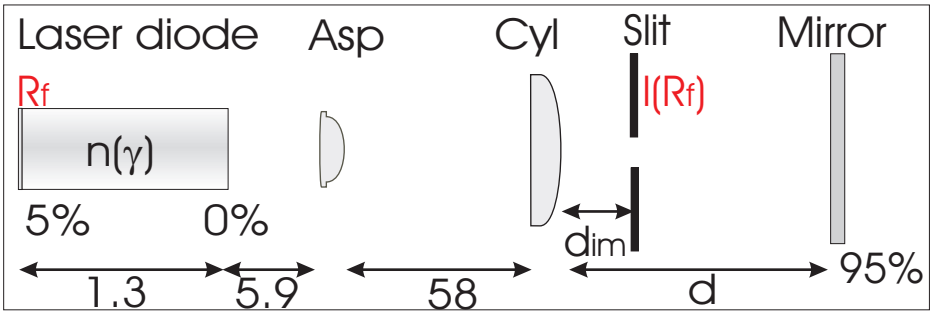

Figure 6.5: Sketch of the external resonator with an intra-cavity slit. R_f represents the plane of the front facet of the diode, while $I(R_f)$ its image plane through the optical system consisting of the diode and the two lenses. d_{im} is the position of $I(R_f)$ behind the cylindrical lens (Cyl).

In order to achieve an easy monitoring of the processes described above, the position of the slit is chosen such that it coincides with the image of the front facet of the diode inside the resonator. Since the front facet of the diode is also the output facet of the laser, the intensity distribution at the position of the slit can be directly inferred by measuring the near-field profile of the output beam.

For the calculation of the image of the front facet of the diode and its magnification, the propagation from the front facet (in air) through the optical system consisting of the diode, the aspheric lens and the cylindrical lens is considered. Assuming the paraxial approximation to be valid, the ABCD-matrix of the optical system is derived. From the knowledge that the B-element of the ABCD-matrix of an imaging system is equal to zero, and that the magnification factor is given by the A-element of the matrix [26], the position of the image behind the cylindrical lens (d_{im}) and the lateral magnification factor (m_{im}) are found to be:

$$d_{im} = f_2\left(1 - \frac{f_2 \tan(\gamma l)}{{f_1}^2 \gamma n_0}\right) \tag{6.2}$$

$$m_{im} = f_1 \gamma n_0 \sin(\gamma l)\left(\frac{d_{im}}{f_2} - 1\right) - \frac{f_2 \cos(\gamma l)}{f_1}, \tag{6.3}$$

where f_1 and f_2 are the respective focal lengths of the aspheric and cylindrical lenses, n_0 and l are, respectively, the effective refractive index and the length of the diode and γ is the thermal lens coefficient. At an injection current of $1\,A$, where γ has been measured to be $0.20\,mm^{-1}$, d_{im} is equal to $34\,mm$ and m_{im} is found to be equal to -6.5.

The adjustable slit is implemented inside the cavity, $34\,mm$ away from the cylindrical lens. At full opening, it has a width of $2.65\,mm$ and at one full turn of the adjustment screw, it is closed by $0.44\,mm$. During the experiments, it is closed in steps of a quarter-turn, and the near-field and far-field of the output beam, as well as the power, are recorded at each step. This procedure is carried out for each of the lengths of the external resonator that have been previously investigated. However, the analysis of the experiments with the slit will be confined to one specific length of the external resonator, namely with d equal to $175\,mm$.

The beam width and output power

Figure 6.6 shows the evolution of the beam diameter (second moments) as the slit is progressively closed. The position of the external mirror (d) is equal to $175\,mm$. The theoretical beam diameter at the position of the slit is found to be $0.65\,mm$, and its evolution as the slit size is reduced is also traced in dotted lines. It is observed that the slit cuts into the beam earlier than expected, but as it is closed further, the theoretical and measured beam diameters are in good agreement.

While the slit is meant to help improve the beam quality of the external resonator laser by filtering out higher order modes, it is, at the same time, also responsible for a decrease in the output power. As it cuts into the beam, the slit blocks the modes that have a diameter larger than its opening. These eventually decay, leaving only the modes with a smaller diameter than its aperture unaffected. The overlap between the beam and the gain area of the stable resonator is thus reduced, causing the output power to decrease.

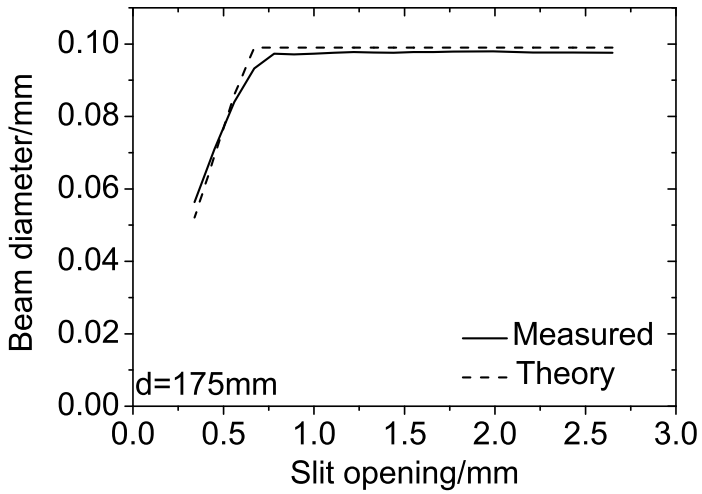

Figure 6.6: Influence of the slit size on the output beam diameter for the resonator with d=175 mm: measured values (full lines) and theoretical values (dotted lines).

By assuming the gain in the lateral direction of the diode to be uniform, the decrease in output power of the stable resonator is therefore proportional to the reduction in the beam diameter caused by the closing of the slit. However, when the latter starts cutting into the fundamental mode, the output power drops sharply due to the progressive decay of the last remaining mode, and the relationship between power and mode diameter is no more proportional. This criterion is used to identify the point where the slit starts to block the fundamental mode. The ratio of the output power to the diameter of the beam is determined, and the point where it starts to drop indicates that the fundamental mode begins to be obscured by the slit. Figure 6.7(a) shows a comparison between the output power (P) and the ratio of the power to the beam diameter ($R_{P/D}$) as a function of the slit size for the resonator with d equal to 175 mm.

It is observed that the power starts to drop when the slit size is 0.78 mm, although the theoretical beam diameter is calculated to be 0.65 mm. This is consistent with the observations of figure 6.5, where the beam width also started to drop at the same slit opening. This could be due to small intensity lobes in the wings of the beam being cut off by the slit. As for $R_{P/D}$, it starts to drop sharply when the slit is 0.67 mm wide, which is close to the calculated diameter of the fundamental mode. In order to confirm the validity of these hypotheses, the experiment with the slit is carried out for various lengths of the external resonator, and, in each case, the beam diameter at the point where the slit is meant to cut into the fundamental mode is recorded. These values are compared with the diameter of the fundamental mode at the position of the slit given by the theory of the stable resonator, as shown in figure 6.7(b). Within the uncertainty of the measurement, which has been estimated to be approximately 10 $\%$ for the beam diameter (refer to chapter four), the experimental results correspond to the theoretical curve. Therefore, $R_{P/D}$ can be used as an indication to whether the fundamental mode is hindered by the slit.

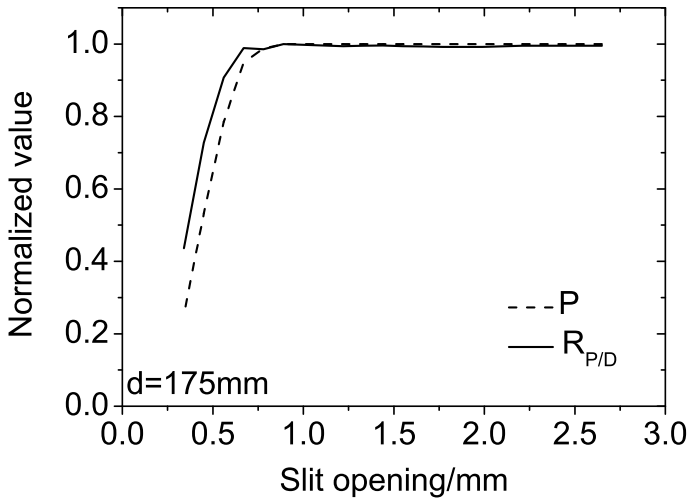

(a)

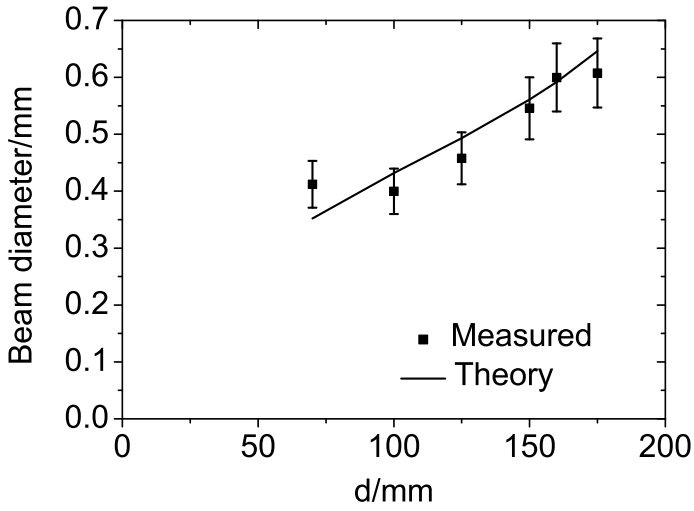

(b)

Figure 6.7: (a)Normalized values of the output power P (dotted lines) and the ratio of the power over the beam diameter $R_{P/D}$ (full lines) in the resonator with d=175 mm, (b) comparison between theory (full line) and experiment (squares) for the beam diameter of the fundamental mode at different lengths of the resonator.

Evolution of the beam quality

By using $R_{P/D}$, the slit can now be adjusted to the width of the fundamental mode, and the corresponding M^2 value of the beam can be measured in order to check if the beam quality is effectively improved. Figure 6.8(a) shows the evolution of the M^2 value of the beam as the slit opening is varied. As long as the opening of the slit is larger than the beam diameter, the M^2 value remains close to that measured in the resonator without slit. The small deviations in the successive values are due to measurement error. As the power starts to decrease, a light improvement is observed in the M^2 value. At the point where $R_{P/D}$ starts to drop, corresponding to the slit cutting into the fundamental mode, the M^2 value experiences a sharp improvement. As the slit is further closed, the M^2 value continues to improve, but by a smaller amount. This behavior can be

explained by observing the evolution of the near-field and the far-field of the emission, as shown in figure 6.8(b). As seen before, the near-field decreases proportionally to the width of the slit. As for the far-field, it decreases slowly between a slit opening of $1\,mm$ and $0.78\,mm$, following the pattern of the near-field. As stated before, this could be due to the slit cutting off small lobes in the wings of the distribution. Then, as $R_{P/D}$ starts to drop, the far-field experiences a sharp improvement. At this point, the slit has approximately the same width as the fundamental mode, and higher order modes are blocked. When the slit is further closed, the far-field angle increases again, due to diffraction of the fundamental mode by the slit and increased amplified spontaneous emission (ASE) coming from regions of the active medium that are no more encountered by the beam. However, since the near-field diameter is also decreasing, a net decrease in the M^2 value is observed.

In order to confirm the behavior of the beam described above, the near-field and far-field profiles at three different widths of the slit (when it is fully open ($2.65\,mm$), at the point where $R_{P/D}$ starts to drop ($0.67\,mm$), and at its smallest opening ($0.34\,mm$)) are shown in figure 6.9. The near-field profile at the slit opening of $2.65\,mm$ is identical to the case without a slit. When the slit is closed to $0.67\,mm$, no significant changes are observed except that the small side lobes on the near-field disappear. At a slit opening of $0.34\,mm$, the fundamental mode is clearly obscured, and the profile is dominated on either side by ASE. The intensity that goes through the slit experiences enough gain to continue oscillating. These manipulations on the beam translate into the far-field. Am improvement in observed when the slit is closed to $0.67\,mm$. However, the latter is not effective enough so as to eliminate all intensity lobes in the wings. Closing the slit further severely degrades the far-field, with the apparition of side lobes and a base line of ASE in the profile.

The brightness of the external resonator laser

The slit brings an improvement in the beam quality, but to the expense of the output power. Since both quantities cannot be maximized simultaneously, a comprise point of operation has to be met. In order to identify this particular point of operation, a means of quantifying the performance of the resonator by taking both the output power (P) and the beam quality into account is required. The measurement of the brightness (B_0) suits the purpose. It is defined as the power emitted per unit surface area and per unit solid angle. It can be written in the form [6]:

$$B_0 = \frac{P}{M_x^2 M_y^2 \lambda^2}, \tag{6.4}$$

where x and y denote the lateral and the vertical direction, respectively, and λ is the emission wavelength. In the present study, M_y^2 and λ are considered invariant, be it in the free running laser or the external resonator with different lengths. Therefore, in the comparison between the power and the lateral beam quality of the different laser setups, a reduced brightness (B_r) can be defined:

$$B_r = \frac{P}{M_x^2} \tag{6.5}$$

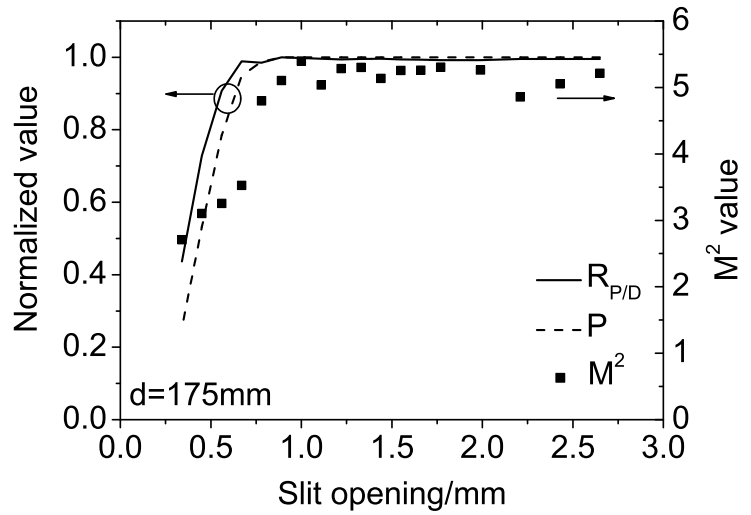

(a)

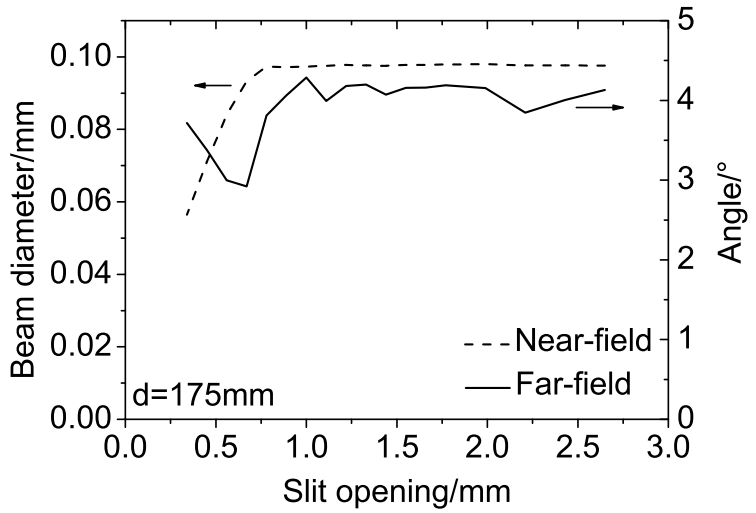

(b)

Figure 6.8: (a) Influence of the slit size on the M^2 value of the output beam (squares) of the resonator with d=175 mm (full lines). The normalized values of $R_{P/D}$ (full lines) and the power (P) (dotted lines) are also plotted, (b) Near-field diameter (dotted lines) and far-field angle (full lines) as a function of slit opening.

The value of B_r is calculated using exclusively the lateral M^2 value of the beam according to the second moments definition. Figure 6.10 below shows the reduced brightness (B_r) as a function of slit opening for a resonator having d equal to 175 mm. $R_{P/D}$ is also shown, as well as B_r for the free running laser at the same injection current, that is, 1 A. For d equal to 175 mm, the external resonator, even without a slit, improves B_r approximately by a factor 1.4 with respect to the free running laser. When the slit is progressively closed, B_r increases, and then decreases again. In this case, its maximum corresponds with the point where $R_{P/D}$ begins to drop. This is conceivable since, at that particular slit size, it has been found that the M^2 value drops sharply, whereas the power drop is much smaller in proportion.

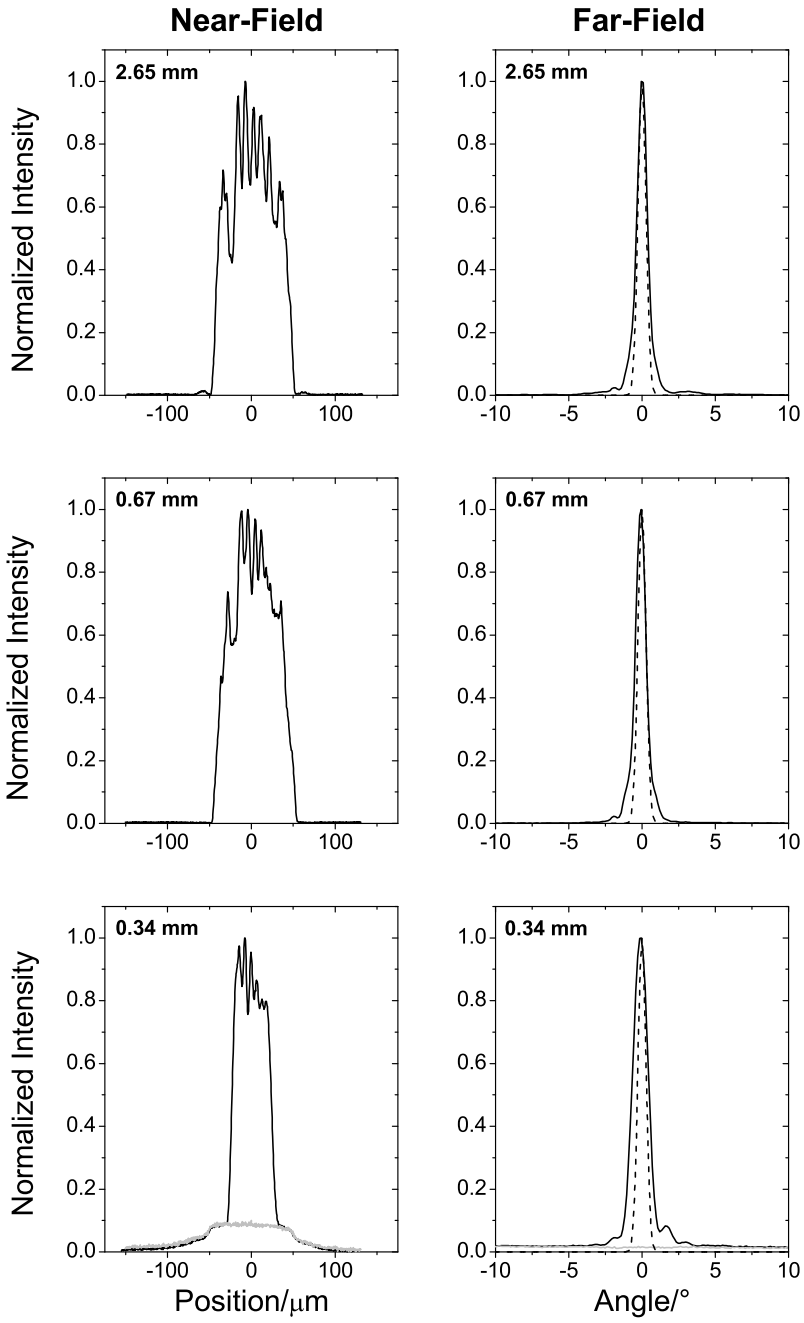

Figure 6.9: Near-field (left) and far-field (right) profiles at the different openings of the slit: 2.65 mm, 0.67 mm and 0.34 mm. In each far-field profile, the theoretical diffraction-limited distribution corresponding to a near-field of 100 μm is also traced in dotted lines. Additionally, in the bottom figure (slit opening of 0.34 mm), the amplified spontaneous emission (ASE) curve is also shown (grey). The cylindrical lens-mirror distance d of the resonator is 175 mm and the injection current is 1 A.

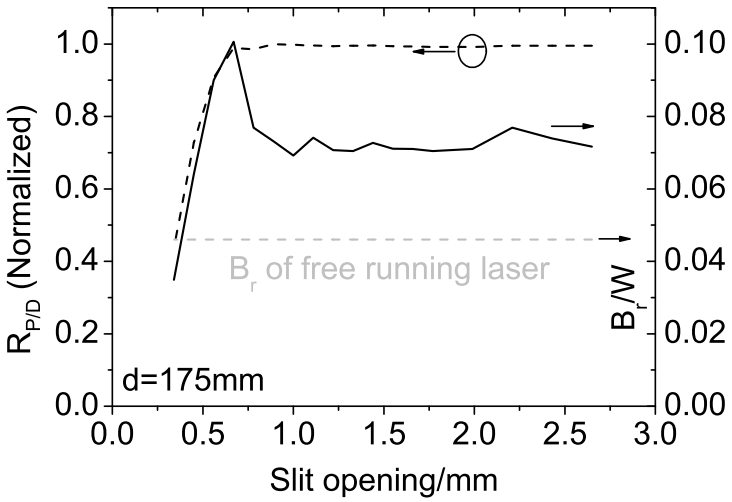

Figure 6.10: Influence of the slit size on the reduced brightness (B_r) of the resonator with d=175 mm (full lines). $R_{P/D}$ (dotted lines) and the reduced brightness of the free running laser (grey) are also indicated.

The results achieved by the external resonator laser, with and without intra-cavity slit, are compared to those of the free running laser. In all three cases, the injection current is 1 A. The respective output powers, M^2 values, and reduced brightness are presented in table 6.1. In addition to the standard M^2 measured by the method of the second moments, the values obtained by the knife-edge method at 95 %, 90 %, and 80 % of the total power enclosed are also shown.

	P/W	M^2 2^{nd} mom.	M^2 K.E-95 %	M^2 K.E-90 %	M^2 K.E-80 %	B_r/W
Free running laser	0.42	9.0	7.4	4.6	3.4	0.05
External resonator	0.37	5.6	4.9	2.2	1.2	0.07
External resonator and slit	0.35	3.5	2.8	1.9	1.0	0.10

Table 6.1: Power (P), M^2 value according to the second moments definition (2^{nd} mom.) and the knife-edge (K.E) definition at 95 %, 90 %, and 80 %, and the reduced brightness (B_r) achieved by the free running laser, the external resonator alone, and the external resonator with a slit. B_r is calculated according to the second moments definition of the beam quality. The distance d for the external resonators in both cases is 175 mm and the injection current is 1 A.

Following the theory of the passive resonator developed in chapter three, spatial mode filtering is achieved by the active zone of the laser diode. The addition of an intra-cavity slit enables the further reduction of the M^2 value. However, even with the use of a slit as filter, it has not been possible to completely cut off the higher order modes. As a result, the second moments M^2 values remain relatively high, with 3.5 as best value. From observations of the intensity profiles of the beam, it can be concluded that low-lying intensity lobes in the wings of the far-field distribution contribute to the degradation of the beam quality. This is confirmed by the M^2 values measured by the method of the knife-edge. As the criterion for the percentage of the total power enclosed is reduced,

the recorded M^2 value decreases sensibly since the sensitivity to small parasitic intensity pockets in the foot of the far-field intensity distribution is also reduced. A best value of 1.0, which corresponds to the fundamental mode, is obtained for the knife-edge M^2 at 80 % of the total power enclosed.

The improvement in beam quality is accompanied by a reduction of the output power. The best performance of the external resonator is assessed by the reduced brightness, which weights the loss in output power with the reduction in the M^2 value. In that respect, the operation of the external resonator with a slit has once again given the best results, with a two-fold improvement of the reduced brightness with respect to the free running laser.

The study of the external resonator at an injection current of 1 A has been very instructive on its mode of operation. The results obtained have shown to which extent the expected performance can be achieved. Moreover, the ratio of the power over the mode diameter and of the reduced brightness have proved to be useful tools in the determination of the resonator length and beam diameter that provide optimized performance. This knowledge can now be applied in the study of the external resonator at higher injection currents.

6.4 The resonator at an injection current of 5A

6.4.1 The active zone as modal filter

It is in the scope of the present work to achieve high output power and good beam quality with the external resonator laser. While the experiments at a current of 1 A (1.67 I_{th}) have provided an insight inside its functioning, the resonator is now driven at a current of 5 A (8.33 I_{th}) in order to assess its performance at high power. The thermal lens coefficient (γ) measured at this injection current is 0.69 mm^{-1}, and it is predicted that the resonator remains stable for d, the distance between the cylindrical lens and the external mirror, between 31 mm and 64 mm. During the experiment, d is varied between 48 mm and 90 mm, and the power, near-field profile and far-field profile of the beam are recorded at each step. Figure 6.11 shows the evolution of these quantities as a function of the resonator length. The output power is plotted in dotted lines. As in the previous measurements at 1 A, the M^2 value of the beam is calculated using the second moments definition (2^{nd} Mom.) (stars), and the knife-edge (K.E) definition at 95 % (triangles), 90 % (squares) and 80 % (circles) of the power enclosed. The simulated (Sim.) M^2 values for γ equal to 0.69 mm^{-1} are shown in full lines. As an indication, the simulated M^2 values for a hypothetical γ of 0.59 mm^{-1} are also shown in fine-dotted lines.

The maximum output power inside the resonator is 3.76 W, which is 88 % of the power of the free running laser at the same current. It stays almost constant between 48 mm and 70 mm, and starts to drop as d is increased. It attains its minimum value at 90 mm, where only 3.15 W are extracted. As for the M^2 values, they drop constantly between 48 mm and 70 mm, achieve a trough until 75 mm, and then start to increase again. Both the behaviors of the output power and the beam quality tend to indicate that the resonator reaches its stability limit between 70 mm and 75 mm. However, the theoretical value lies way before at 64 mm, and the one observed would rather correspond to γ in the range of 0.59 mm^{-1}. Even by using this hypothetical value of the thermal lens

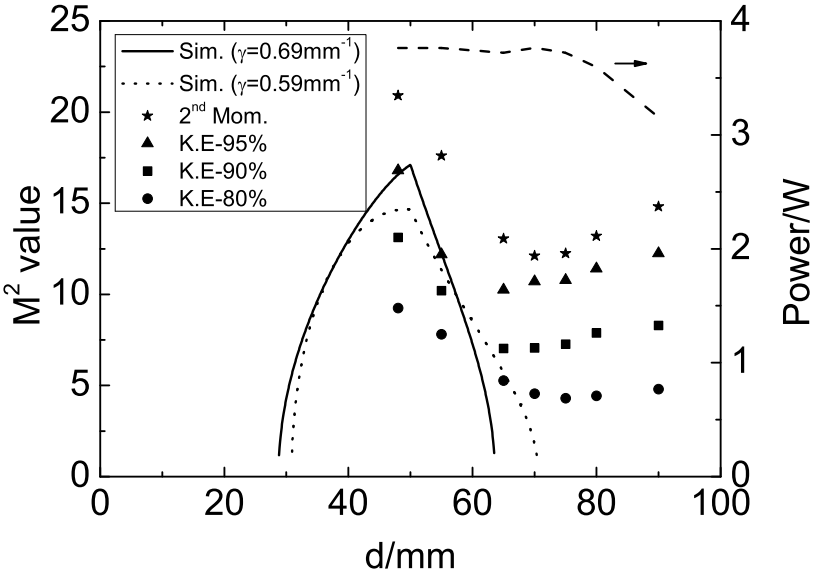

Figure 6.11: M^2 value and output power of the beam in the external resonator as the position of the external mirror is varied. The current is kept constant at 5 A.

coefficient, the trend of the simulated M^2 values is not met by the experimental data.

The analysis of the near-field and far-field profiles at different lengths of the resonator (d= 48 mm, 75 mm, 90 mm), as depicted in figure 6.12, gives an indication of the behavior of the M^2 value as d is varied. The near-field distribution increases slightly as d is increased. This is mainly due to small side lobes that appear at 75 mm, and that grow bigger and move closer to the main lobe when d is equal to 90 mm . As for the far-field, a significant improvement is observed when d is increased from 48 mm to 75 mm, indicating that mode filtering at the active region of the diode takes place to some extent. As for the profile at 90 mm, although the upper part is smaller than at 75 mm, the lower part is, however, broader. The knife-edge measurements of the M^2 value confirm this, since, as the criterion for the enclosed power is reduced, so does the difference in M^2 between the beams recorded at the two values of d of 75 mm and 90 mm.

Even in the vicinity of the stability limit, which, theoretically, also corresponds to the region where the beam quality is best improved, the emission remains multi-mode. With the high gain and the enhanced nonlinearities at an injection current of 5 A, the mode-selective ability of the external resonator design is sensibly affected.

6.4.2 Addition of an intra-cavity slit

The distance d in the external resonator is fixed to 75 mm (best improvement in the beam quality obtained at this position) and a slit is introduced in the image plane of the front facet of the laser diode. Using equations 6.2 and 6.3, the position of the slit and the magnification factor of the image are found to be 28.7 mm and -10.0, respectively. The value of the thermal lens coefficient used for the calculations is 0.69 mm^{-1}. Owing to the large deviations between the measured properties of the external resonator and those predicted by the theory, a detailed study of the beam formation with the help of

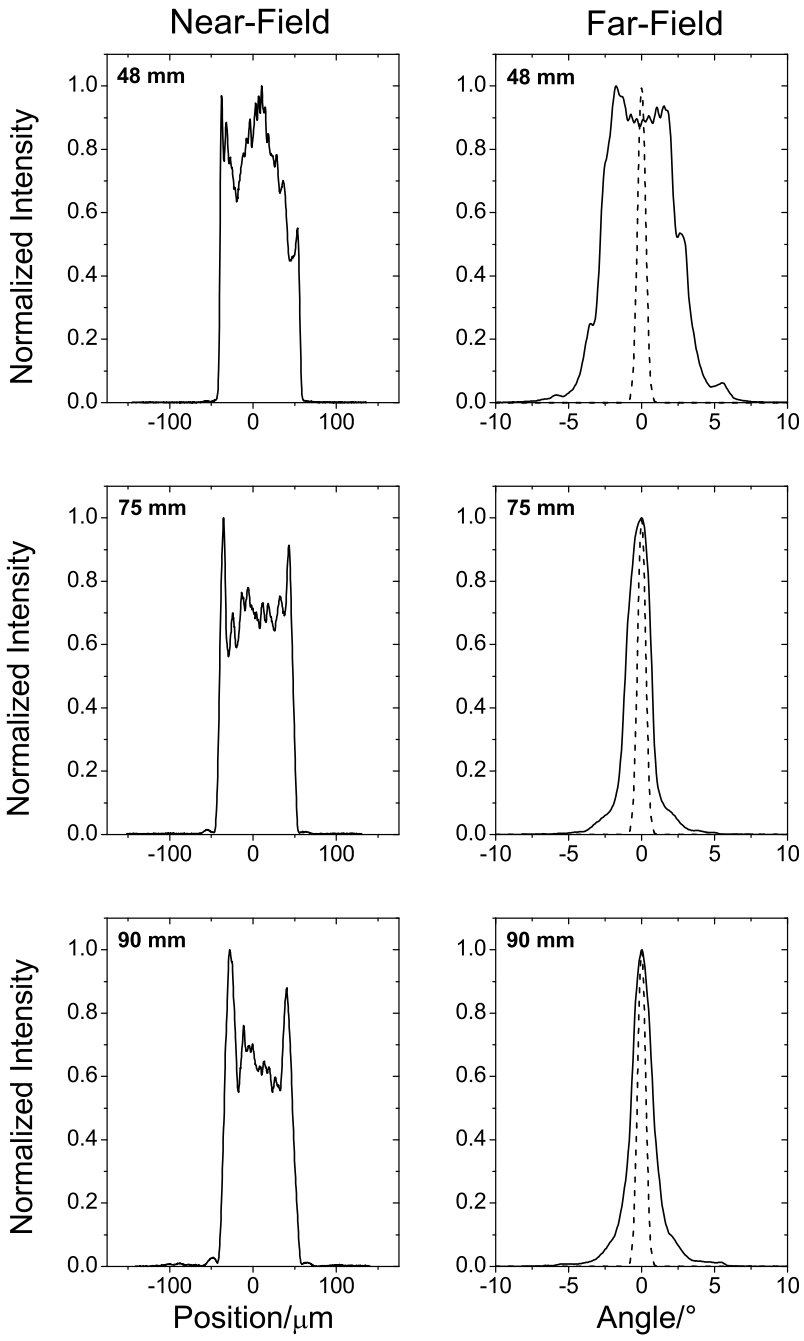

Figure 6.12: Near-field and far-field profiles of the output beam for d= 48 mm, 75 mm and 90 mm. In each far-field profile, the theoretical diffraction-limited distribution corresponding to a near-field of 100 μm is also traced in dotted lines.

the slit cannot be carried out as in the case of an injection current of $1\,A$. However, the ability of the slit to improve the beam quality is still investigated.

The slit is closed from a width of $2.65\,mm$ to a width of $0.23\,mm$ in steps of $0.11\,mm$. The output power, near-field profile and far-field profile of the beam at each step are recorded. Figure 6.13 shows the measured output power and the near-field (NF) diameter as the slit is progressively closed. The expected beam width on the facet is also traced. As the slit is closed to $1.22\,mm$, the near-field starts to decrease. Obscuration of the beam starts, and the power is reduced accordingly. However, the comparison between measurement and calculated values shows that the near-field starts to drop earlier, and that it is throughout larger than expected.

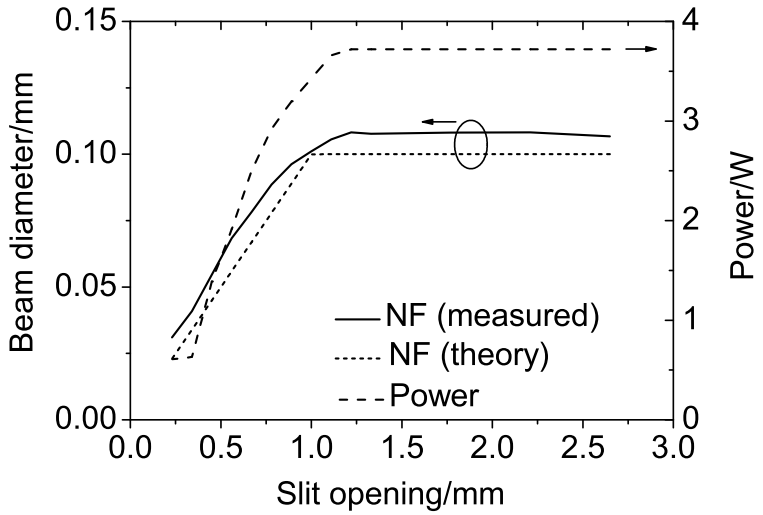

Figure 6.13: The near-field (NF) diameter measured (full line) and simulated (short-dotted lines), and the output power (dotted lines) of the external resonator as a function of the slit opening.

The ratio of the power over the beam diameter ($R_{P/D}$) has previously been used to identify the point where the slit cuts into the fundamental mode. It is, in the present case, also measured, and it is interesting to verify if its behavior is similar as when the diode is driven with a current of $1\,A$. Additionally, the reduced brightness (B_r) is the criterion with which the slit size that yields optimal performance of the external resonator laser is determined. Figure 6.14 shows the evolution of $R_{P/D}$ and B_r as a function of the slit opening. At a slit opening of $0.67\,mm$, $R_{P/D}$ has a sharp drop, and at the same point, the maximum value of B_r is observed. Its value is approximately 1.5 times higher than the external resonator without slit and twice as high as that of the free running laser. However, the near-field diameter is $0.078\,mm$, showing that the maximum relative brightness does not occur at a point where the beam occupies the whole gain area of the diode. As a result, only $67\,\%$ of the output power of the external resonator without slit, and $59\,\%$ of the power of the free running laser are extracted.

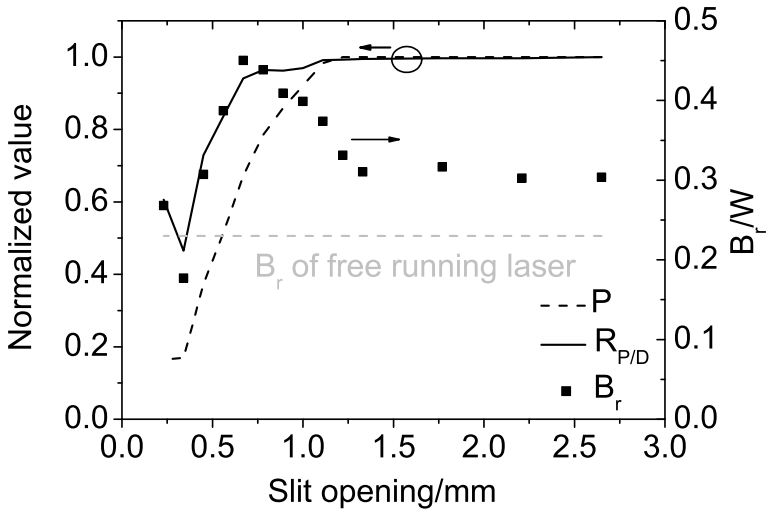

Figure 6.14: Ratio of power over beam diameter $R_{P/D}$ (full line), reduced brightness B_r (squares) and output power P (dotted lines) of the resonator as a function of slit opening. The reduced brightness B_r of the free running laser at a current of $5\,A$ is also shown (grey). P and $R_{P/D}$ are normalized.

The influence of the slit on the M^2 value of the beam is depicted in figure 6.15. The normalized near-field and far-field are also shown. Following the drop in near-field and far-field, the M^2 value also decreases when the slit is closed onto the beam. It is observed that a slit opening of $0.67\,mm$ corresponds to the point where the far-field achieves its minimum, before starting to increase again. This is in agreement with what is observed with $R_{P/D}$ and B_r, since at that slit opening, the former is on the point of dropping sharply and the latter attains its maximum value. At this point, the M^2 value is 5.6. When the slit is further closed, the far-field divergence angle increases again. However, since the near-field diameter is still decreasing, the net effect is a further reduction of the M^2 value.

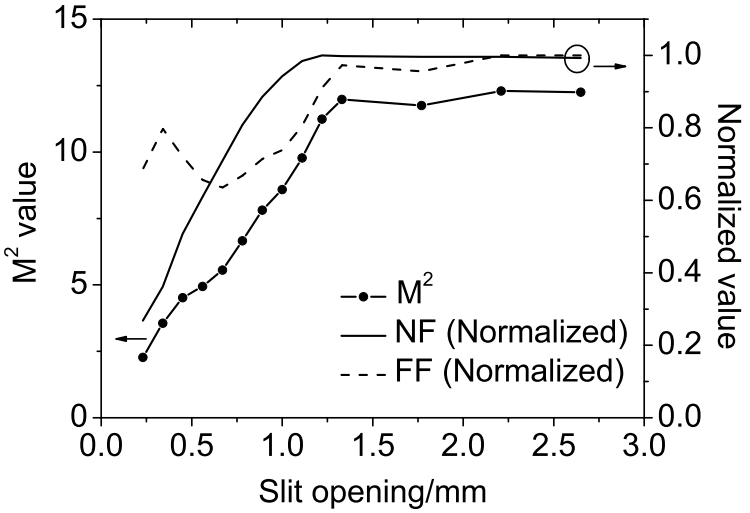

Figure 6.15: M^2 value (circles) of the external resonator as a function of the slit opening. The normalized near-field (NF) (full line) and far-field (FF) (dotted lines) are also shown.

The near-field and far-field profiles of the beam for a full open slit (2.65 mm) and at a slit size of 0.67 mm, corresponding to the optimal reduced brightness, are shown in figure 6.16. The reduction of approximately 20 $\%$ in the near-field diameter is clearly seen at the smaller slit opening, as well as the additional mode filtering of the slit is also characterized by the reduction of the far-field divergence angle. However, the emission remains multi-mode. Moreover, just as in the experiment at a current of 1 A, the wings of the far-field distribution are significantly broader than those expected of a Gaussian distribution.

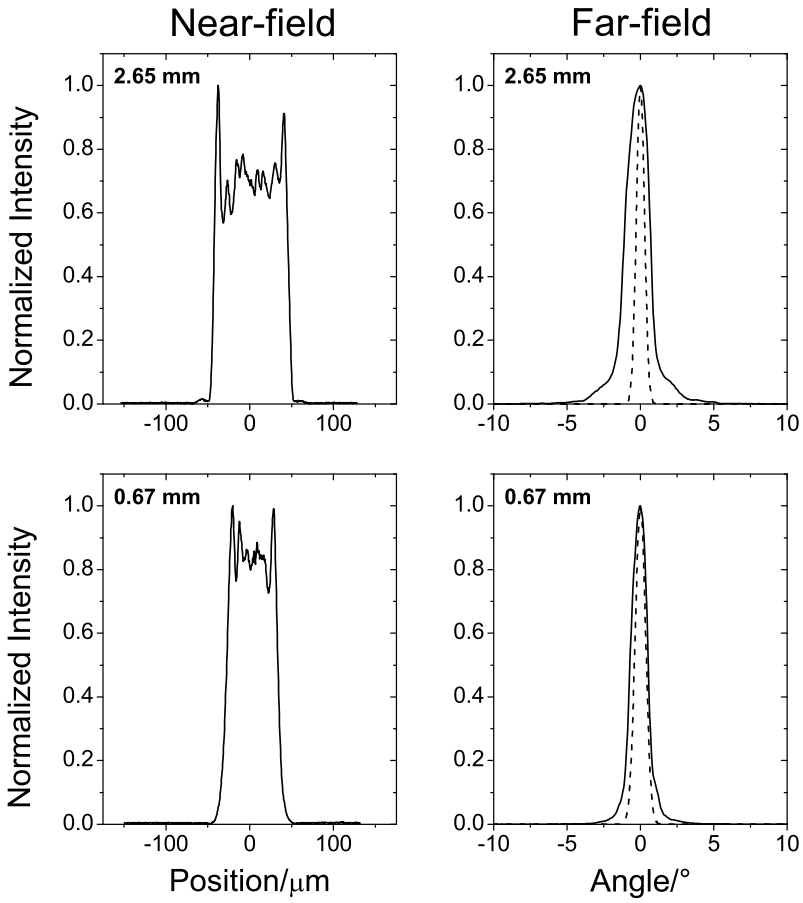

Figure 6.16: Near-field and far-field profiles of the output beam for slit openings of 2.65 mm and 0.67 mm. In each far-field profile, the theoretical diffraction-limited distribution, corresponding to a near-field of 100 μm for the upper case and 78 μm for the lower case, is also traced in dotted lines.

The behavior of the output beam of the external resonator laser at an injection current of 5 A has shown a significant deviation from the theory of the passive resonator. The characteristic drop in output power and degradation of the beam quality at the stability limit have been observed for a position of the external mirror that is some 10 mm beyond the predicted value, namely 75 mm away from the cylindrical lens. However, the best improvement in the M^2 value of the emission has been recorded there. Therefore, the experiments including the use of a slit as additional modal filter have been carried out at this particular resonator length.

Unlike in the experiments at a current of 1 A, a detailed comparison between the measured beam inside the resonator and the theoretical predictions has not been possible. Nonetheless, a similar behavior of the ratio of power over beam diameter ($R_{P/D}$) and the reduced brightness (B_r) has been observed. A sharp drop in the former has coincided with the maximum value of the latter. At 1 A, this has been the point where the slit size has matched the diameter of the fundamental mode, although the M^2 value is not close to one, due to a broadening in the foot of the far-field intensity distribution. In the present case, because the model of the passive resonator does not apply, there is no theoretical reference value for the diameter of the fundamental mode at a given resonator length. As a result, it cannot be verified if the sharp drop in $R_{P/D}$ actually corresponds to the fundamental mode being blocked by the slit. However, the maximum value of B_r as criterion for the optimal performance of the external resonator is still valid.

The reduced brightness is maximized when the slit opening is 0.67 mm. A marked improvement in the M^2 value is observed, but the extracted power is only 67 % of the initial value without slit, caused principally by the reduction of 20 % of the beam diameter inside the diode. The values of the output power, M^2 value (second moments and knife-edge at 95 %, 90 %, and 80 % of the total power enclosed), and maximum reduced brightness of each of the free running laser, the external resonator, and the external resonator with a slit are compared in table 6.2.

	P/W	M^2 2^{nd} mom.	M^2 K.E-95 %	M^2 K.E-90 %	M^2 K.E-80 %	B_r/W
Free running laser	4.27	18.7	13.3	11.1	8.4	0.23
External resonator	3.72	12.2	10.8	7.3	4.3	0.30
External resonator and slit	2.50	5.6	4.6	3.2	1.9	0.45

Table 6.2: Power (P), M^2 value according to the second moments definition (2^{nd} mom.) and the knife-edge (K.E) definition at 95 %, 90 %, and 80 %, and the reduced brightness (B_r) achieved by the free running laser, the external resonator alone, and the external resonator with a slit. B_r is calculated according to the second moments definition of the beam quality. The distance d for the external resonators in both cases is 75 mm and the injection current is 5 A.

The theoretical model of the passive resonator has been observed to lose its validity at an injection current of $5\,A$. A detailed study of the mode formation inside the external resonator has not been possible, but the position of the external mirror, and subsequently, the width of the intra-cavity slit have been experimentally optimized such that the maximum reduced brightness is obtained. Its value has been found to be approximately twice bigger than that of the free running laser at the same injection current. Its M^2 value, according to the second moments definition, is then 5.6 and the power penalty is around $40\,\%$. The M^2 value measured by the knife-edge method at $80\,\%$ of the total power enclosed is found to be 1.9. In the present case, it has not been possible to match the level of filtering of higher order modes that has been achieved in the experiments at a current of $1\,A$, although a significant fraction of the output power has been sacrificed in the process.

Chapter 7

Conclusion

The ability of an external resonator configuration to improve the lateral beam quality of BA laser diodes while minimizing the losses at high power operation has been investigated. A simple, 'on-axis' external resonator setup consisting of the BA laser diode as gain medium, a lens, and an external mirror has been considered. In this concept, discrimination against higher order modes is achieved by forcing them to have a diameter larger than the aperture of the active region of the laser diode.

Based on the ABCD-matrix treatment of the Gaussian beam in a passive stable resonator, a model for the determination of the diameter of the fundamental mode at any point inside the lateral resonator as a function of its the geometry is developed. Thermal lensing, the main contribution to non-linearities inside the gain medium of the system, is incorporated in the model. With the help of the simulation, it has been inferred that:

- the ability of the chosen concept to provide single mode operation is limited to lasers diodes under the influence of a weak thermal lens.
- an alternative resonator concept comprising an additional lens achieves fundamental mode operation for both weak and strong thermal lenses in the laser diode. In that case, there exists, for a given thermal lens coefficient, one length of the external resonator that produces a fundamental mode whose beam diameter fits exactly into the limiting aperture of the active zone of the laser diode, and whose overlap with the active area is maximized.

The thermal lens arising in the BA laser diode used as gain medium in the external resonator has been quantified at different injection currents and pulse widths. For this purpose, a novel experimental procedure has been devised and implemented. The measurement results have been validated by a comparison with the measurement of the thermal lens dependent M^2 value of a free running BA laser with a similar structure. Moreover, the observed saturation of the thermal lens coefficient as the injection current and the pulse width are increased has been investigated with the help of the simulation of the temperature distribution inside the laser diode at different pulse widths. It is found that even if the temperature increases with longer pulses, the temperature gradient between the active region and the extremities of the laser chip saturates, due to the heating up of the regions outside the current stripe. As a consequence, the thermal lens coefficient also saturates.

With the values of the thermal lens coefficient inside its gain medium known, the ECL comprising the two lenses and the external mirror has been implemented. An intra-cavity slit with adjustable width has been inserted in the setup in order to monitor the beam diameter inside the resonator. At the same time, it has been used as an additional spatial filter. The dependence of the output power and of the M^2 value on the resonator length and on the width of the slit at injection currents of $1\,A$ (close to laser threshold) and $5\,A$ (high power operation) has been studied.

The behavior of the external resonator follows the pattern of the theoretical predictions at an injection current of $1\,A$, whereas at $5\,A$, it deviates significantly from the simulated values. In both cases, the M^2 value is significantly improved, but single mode operation is, however, not achieved. The use of the slit as additional spatial filter improves the M^2 value further, but, in the process, the loss of output power can be significant. The maximization of the reduced brightness, defined as the output power weighted by the lateral M^2 value, is then used to identify the optimal performance of the external resonator. The best results achieved by the ECL, as compared to the free running laser, are:

- a two-fold improvement of the reduced brightness at an injection current of $1\,A$. The lateral M^2 value is improved from 9.0 to 3.5. The output power is $0.35\,W$, representing a reduction of $17\,\%$ with respect to the free running laser at the same injection current.
- equally a two-fold improvement of the reduced brightness at an injection current of $5\,A$. In this case, the lateral M^2 value is improved from 18.7 to 5.6, at an output power recorded to be $2.50\,W$, which is a $40\,\%$ loss with respect to the output power of the free running laser at the same injection current.

At both injection currents, the main obstacle to a further improvement of the M^2 value is the inability of the spatial filters to effectively cut off low-lying intensity lobes that broaden the foot of the far-field intensity distribution of the emission. Moreover, at the injection current of $5\,A$, the relatively higher gain and non-linear effects tend to render the process of spatial filtering less effective. Therefore, as compared to the resonator at a current of $1\,A$, the power penalty is much higher for an improvement of the beam quality of approximately the same order.

The $2.5\,W$ of output power and an M^2 value of 5.6 achieved by the present ECL compares with the best results reported in the literature for the operation in the Watt range of a BA laser diode in an external resonator [1]. However, the significant power penalty that accompanies the process remains the biggest obstacle against the further exploitation of the concept at higher injection currents. In that respect, the standards set by other high-power semiconductor laser concepts, especially the tapered laser, cannot be met by the ECL studied in this work. In fact, owing to its inherent lateral geometry, where only the fundamental guided mode is allowed to propagate in the ridge-waveguide

[1] In a rival claim to $2.46\,W$ of output power in a nearly-diffraction-limited beam for a BA laser operated in an external resonator [10], the criteria used for the determination of the divergence angle of the emission are not specified. However, in the light of the published far-field intensity profiles, it is evident that the contribution of a significant fraction of the intensity contained in the wings of the distribution has been neglected.

region and where the large-gain tapered region is adapted to the divergence angle of the given fundamental mode, the tapered laser achieves a more efficient discrimination against higher order modes than the broad area laser in an external resonator. However, as a result of this same geometry, the maximum output power of the tapered laser lies much lower than that of the broad area counterpart with identical dimensions. For this reason, the broad area laser remains the most promising device when it comes to very high output power.

As it has been seen, the biggest challenge facing the broad area laser with an external resonator is the efficient discrimination against higher order modes. In that respect, further information is required on the exact interactions that occur between the gain medium and the optical field inside the diodes at high power operation. A consistent model that takes the multiple non-linear effects (both in the steady-state and the dynamic regimes) into account is required. Simultaneously, experimental methods that enable the isolation of individual non-linear effects and their subsequent measurement have to be developed. Only then is the optimization of the laser structures and of the ensuing external resonators possible.

List of abbreviations and symbols

Abbreviations

α-DFB	Angled Distributed Feedback
2^{nd} Mom.	Second Moments
AR/HR	Anti-Reflection/High-Reflection
ARROW	Anti-Resonant Reflective Optical Waveguide
ASE	Amplified Spontaneous Emission
Asp.	Aspheric lens
BA	Broad Area
BW/NF/FF	Beam-Waist/Near-Field/Far-field
CCD	Charge-Coupled Device
CL	Cladding
COMD	Catastrophic Optical Mirror Damage
CTE	Coefficient of Thermal Expansion
CW/QCW	Continuous Wave/Quasi Continuous Wave
Cyl.	Cylindrical lens
DBR	Distributed Bragg Reflector
DL	Diffraction-Limit
DQW	Double Quantum Well
ECL	External Cavity Laser
FAC	Fast Axis Collimator
FEM	Finite Element Method
FWHM	Full Width at Half Maximum
ISO	International Organization for Standardization
K.E	Knife-Edge
LOC/ASLOC	Large Optical Cavity/Asymmetric Large Optical Cavity
MOPA/MBA-MOPA	Master Oscillator Power Amplifier/Monolithic MOPA with a BA laser as MO
MOVPE	Metal Oxide Vapor Phase Epitaxy
OSA	Optical Spectrum Analyzer
PBC	Photonic Bandgap Crystal
RIBE	Reactive Ion Beam Etching
RW	Ridge Waveguide
SCH	Separate Confinement Heterostructure
SCOWL	Slab-Coupled Optical Waveguide Laser
VBG	Volume Bragg Grating
WG	Waveguide

Physical constants

h	Planck's constant	(6.63 x $10^{-34}\,Js$)
q	Elementary charge of the electron	(1.60 x $10^{-19}\,As$)

Symbols

α	Tilt angle of the external mirror of the ECL.
α_i	Internal losses of a laser diode.
α_m	Mirror losses of a laser resonator.
A, B, C, D	Elements of an ABCD-matrix.
β	Slope of the linear fit in equation 5.10.
B_0	Brightness of a laser.
B_r	Reduced brightness of a laser.
d	Distance between the outermost lens and the external mirror in the ECL.
δ	Deviation in the axial position of an object.
D_γ	Refractive power of the thermal lens.
Δ_x	Lateral pixel size of the CCD camera.
η	Efficiency of a process.
η_i	Internal efficiency of a laser diode.
E_0	Electric field at the start point of a round-trip inside the external resonator.
E_{rt}	Electric field after a round-trip inside the external resonator.
E_g	Band gap energy.
E_c, E_v	Energy level of the conduction band and of the valence band, respectively.
E_{Fc}, E_{Fv}	Quasi-Fermi levels for the electrons and the holes, respectively.
f_i, f_{ib}	Focal length, respectively back focal length of lens i.
f_γ	Focal length of the thermal lens.
g, g_0, g_{th}	Gain, differential gain, and threshold gain of a laser.
γ	Thermal lens coefficient.
Γ	Confinement factor of a laser structure.
h_γ	Principal plane of the thermal lens.
I, I_{th}, I_{tr}	Injection current, threshold current, transparency current.
$I(i)$	Image of plane i.
$I(x,y)$	Intensity of a beam perpendicular to the optical axis.
J, J_{th}, J_{tr}	Current density, threshold current density, transparency current density.
l	Length of a laser diode.
Li	Lens i.
λ	Emission wavelength of a laser.
m	Magnification of a lens system.
M	Matrix.
n, n_0	Refractive index, effective refractive index.
n_N, n_T	carrier dependent refractive index, temperature dependent refractive index.
ν	Frequency of the photon.
N	Carrier density.
N_x	Number of lateral pixels on the CCD camera.
P, P_{th}	Optical power, heat power.

Symbols-continued

q_0	q-parameter at the start point of a round-trip inside the external resonator.
q_{rt}	q-parameter after a round-trip inside the external resonator.
Q	Arbitrary heat source.
r	Radial coordinate.
R	Radius of curvature of a Gaussian beam.
R_f, R_r	Reflectivity at the front facet and at the rear facet of a diode, respectively.
R_s	Series resistance.
R_{th}	Thermal resistance.
$R_{P/D}$	Ratio of output power to beam diameter.
σ_{wx}	Standard deviation of the measured lateral beam radius.
S	Slope efficiency.
SL_l, SL_u	Lower stability limit, upper stability limit.
T_0, T_1	Characteristic temperatures of a laser diode.
θ	Full divergence angle of a beam.
V, V_0	Voltage across a laser diode, junction voltage.
w, W	Beam radius, beam diameter.
W_0	Beam waist diameter.
x, y, z	Lateral, vertical and axial coordinates.
z_0	Position of the beam waist.
z_R	Rayleigh length.

Bibliography

[1] J. J. Lim, S. Sujecki, L. Lang, Z. Zhang, D. Paboeuf, G. Pauliat, G. Lucas-Leclin, P. Georges, R. C. I. MacKenzie, P. Bream, S. Bull, K. H. Hasler, B. Sumpf, H. Wenzel, G. Erbert, B. Thestrup, P. M. Petersen, N. Michel, M. Krakowski, and E. C. Larkins, "Design and Simulation of Next-Generation High-Power, High-Brightness Laser Diodes," *IEEE Journal of Selected Topics in Quantum Electronics*, vol. 15, no. 3, May/June 2009.

[2] R. Diehl, Ed., *High-Power Diode Lasers (Fundamentals, Technology, Applications)*. Springer-Verlag, 2000.

[3] *ISO/FDIS 11146-1, ISO/FDIS 11146-2, ISO/TR 11146-3, "Laser and laser-related equipment-Test methods for laser beam widths, divergence angles and beam propagation ratios*. Deutsches Institut für Normung e.V, 2004.

[4] D. Botez, "Design considerations and analytical approximations for high continuous-wave power, broad-waveguide diode lasers," *Applied Physics Letters*, vol. 74, no. 21, March 1999.

[5] H. Wenzel, F. Bugge, M. Dallmer, F. Dittmar, J. Fricke, K. H. Hasler, and G. Erbert, "Fundamental-Lateral Mode Stabilized High-Power Ridge-Waveguide Lasers With a Low Beam Divergence," *IEEE Photonics Technology Letters*, vol. 20, no. 3, February 2008.

[6] H. Wenzel, B. Sumpf, and G. Erbert, "High brightness diode lasers," *C. R. Physique 4*, pp. 649–661, 2003.

[7] P. Crump, G. Blume, K. Paschke, R. Staske, A. Pietrzak, U. Zeimer, S. Einfeld, A. Ginolas, F. Bugge, K. Häusler, P. Ressel, H. Wenzel, and G. Erbert, "20W continuous wave reliable operation of 980nm broad-area single emitter diode lasers with an aperture of 96μm," *Proc. of SPIE*, vol. 7198, 2009.

[8] J. R. Marciante and G. P. Agrawal, "Nonlinear Mechanisms of Filamentation in Broad-Area Semiconductor Lasers," *IEEE Journal of Quantum Electronics*, vol. 32, no. 4, April 1996.

[9] R. Hülsewede, J. Sebastian, H. Wenzel, G. Beister, A. Knauer, and G. Erbert, "Beam quality of high power 800 nm broad-area laser diodes with 1 and 2 μm large optical cavity structures," *Optics Communications*, vol. 192, pp. 69–75, 2001.

[10] G. Venus, L. Glebov, V. Rotar, V. Smirnov, P. Crump, and J. Farmer, "Volume Bragg semiconductor lasers with near diffraction limited divergence," *Proc. of SPIE.*, vol. 6216, 2006.

[11] W. Sharfin, J. Seppala, A. Mooradian, B. Soltz, R. Waters, B. Vollmer, and K. Bystrom, "High-power, diffraction-limited, narrow-band, external-cavity diode laser," *Appl. Phys. Lett.*, vol. 54, no. 18, May 1989.

[12] Siegman, *Lasers*. University science books, 1986.

[13] H. Kroemer, "A Proposed Class of Hetero-junction Injection Lasers," *Proceedings of the IEEE*, pp. 1782–1783, December 1963.

[14] H. Kressel and J. Butler, *Semiconductor Lasers and Heterojunction LEDs*. Associated Press, 1977.

[15] W. W. Chow, S. W. Koch, and M. Sargent III, *Semiconductor-Laser Physics*. Springer-Verlag, 1994.

[16] W. B. Joyce and R. W. Dixon, "Electrical characterization of heterostructure lasers," *J. Appl. Phys.*, vol. 49, no. 7, July 1978.

[17] M. G. A. Bernard and G. Duraffourg, "Laser Conditions in Semiconductors," *Physica Status Solidi (b)*, vol. 1, no. 7, pp. 669–703, 1961.

[18] R. Dingle, W. Wiegmann, and C. H. Henry, "Quantum States of Confined Carriers in Very Thin $Al_xGa_{1-x}As - GaAs - Al_xGa_{1-x}As$ Heterostructures," *Physical Review Letters*, vol. 33, no. 14, September 1974.

[19] F. Bugge, G. Erbert, J. Fricke, S. Gramlich, R. Staske, H. Wenzel, U. Zeimer, and M. Weyers, "12 W continuous-wave diode lasers at 1120 nm with InGaAs quantum wells," *Applied Physics Letters*, vol. 79, no. 13, September 2001.

[20] J. J. Coleman, "Strained Layer InGaAs Quantum Well Heterostructure Lasers," *IEEE Journal on Selected Topics in Quantum Electronics*, vol. 6, no. 6, November 2000.

[21] M. Weyers, "GaAs-based high power laser diodes ," 2005.

[22] W. Streifer, R. D. Burnham, and D. R. Scifres, "Modal analysis of separate-confinement heterojunction lasers with inhomogeneous cladding layers," *Optics Letters*, vol. 8, no. 5, May 1983.

[23] G. Erbert, F. Bugge, B. Eppich, J. Fricke, K. H. Hasler, K. Paschke, A. Pietrzak, H. Wenzel, and G. Tränkle, "High brightness diode lasers with very narrow vertical divergence," *Proc. of SPIE*, vol. 6909, 2008.

[24] M. Sanayeh, P. Brick, W. Schmidt, B. Mayer, M. Müller, M. Reufer, K. Streubel, S. Schwirzke-Schaaf, J. W. Tomm, A. Danilewski, and G. Bacher, "Defect investigation and temperature analysis of high-power AlGaInP laser diodes during catastrophic optical damage," *Journal of Material Science*, vol. 19, pp. 155–159, 2008.

[25] P. Ressel, G. Erbert, U. Zeimer, K. Häusler, G. Beister, B. Sumpf, A. Klehr, and G. Tränkle, "Novel Passivation Process for the Mirror Facets of Al-Free Active-Region High-Power Semiconductor Diode Lasers," *IEEE Photonics Technology Letters*, vol. 17, no. 5, May 2005.

[26] N. Hodgson and H. Weber, *Optical resonators, Fundamentals, advanced concepts and applications*. Springer, 1997.

[27] H. Numai, Ed., *Fundamentals of Semiconductor Lasers*. Springer Verlag, 2004.

[28] H. Wenzel, G. Erbert, A. Knauer, A. Oster, K. Vogel, and G. Tränkle, "Influence of current spreading on the transparency current density of quantum-well lasers," *Semicond. Sci. Technol.*, vol. 15, 2000.

[29] G. Zhang, M. Pessa, and D. Ahn, "Gain Characetristics of Strained-Layer InGaAs/GaAs Quantum Well Lasers," *Phys. stat. sol. (b)*, vol. 176, 1993.

[30] P. Mc Ilroy, A. Kurobe, and Y. Uematsu, "Analysis and Application of Theoretical Gain Curves to the Design of Multi-Quantum-Well Lasers," *IEEE. Journal of Quantum Electronics*, vol. 21, no. 12, December 1985.

[31] M. Rattunde, C. Mermelstein, J. Schmitz, R. Kiefer, W. Pletschen, M. Walther, and J. Wagner, "Comprehensive modeling of the electro-optical-thermal behavior of (AlGaIn)(AsSb)-based 2.0 μm diode lasers," *Applied Physics Letters*, vol. 80, no. 22, June 2002.

[32] A. Salhi, Y. Rouillard, A. Perona1, P. Grech, M. Garcia, and C. . Sirtori, "Low-threshold GaInAsSb/AlGaAsSb quantum well laser diodes emitting near 2.3 μm," *Semicond. Sci. Technol.*, vol. 19, pp. 260–262, 2004.

[33] F. Bugge, M. Zorn, U. Zeimer, A. Pietrzak, G. Erbert, and M. Weyers, "MOVPE growth of InGaAs/GaAsP-MQWs for high-powerl aser diodes studied by reflectance anisotropy spectroscopy," *Journal of Crystal Growth*, vol. 311, pp. 1065–1069, 2009.

[34] A. Knauer, G. Erbert, R. Staske, B. Sumpf, H. Wenzel, and M. Weyers, "High-power 808 nm lasers with a super-large optical cavity," *Semicon. Sci. Technol.*, vol. 20, pp. 621–624, April 2005.

[35] M. Afromowitz, "Refractive index of $Ga_{1-x}Al_xAs$," *Solid State Communications*, vol. 15, pp. 59–63, 1974.

[36] H. Wenzel and H. Wünsche, "A Model for the Calculation of the Threshold Current of SCH-MQW-SAS Lasers," *Phys. Stat. Sol. (a)*, vol. 120, p. 661, 1990.

[37] F. Nash, "Mode guidance parallel to the junction plane of double-heterostructure GaAs lasers," *J. Appl. Phys.*, vol. 44, no. 10, October 1973.

[38] L. Goldberg, D. Mehuys, M. Surette, and D. Hall, "High-Power, Near-Diffraction-Limited Large-Area Traveling-Wave Semiconductor Amplifiers," *IEEE Journal of Quantum Electronics*, vol. 29, no. 6, June 1993.

[39] Z. Dai, R. Michalzik, P. Unger, and K. Ebeling, "Numerical Simulation of Broad-Area High-Power Semiconductor Laser Amplifiers," *IEEE Journal of Quantum Electronics*, vol. 32, no. 12, December 1997.

[40] J. Marciante and G. Agrawal, "Spatio-Temporal Characteristics of Filamentation in Broad-Area Semiconductor Lasers," *IEEE Journal of Quantum Electronics*, vol. 33, no. 7, July 1997.

[41] L. M. Tilton, G. C. Dente, A. H. Paxton, J. Cser, R. K. DeFreez, C. E. Moeller, and D. Depatie, "High-power, nearly diffraction-limited output from a semiconductor laser with an unstable resonator," *IEEE Journal of Quantum Electronics*, vol. 27, no. 9, pp. 2098–2108, September 1991.

[42] C. Lindsey, P. Derry, and A. Yariv, "Tailored-Gain Broad-Area Semiconductor Laser with Single-Lobed Diffraction-Limited Far-Field Pattern," *Electronic Letters*, vol. 21, no. 16, pp. 671–673, August 1985.

[43] L. J. Mawst, D. Botez, C. Zmudzinsky, and C. Tu, "Antiresonant reflecting optical waveguide-type, single-mode diode lasers," *Appl. Phys. Lett.*, vol. 61, no. 5, August 1992.

[44] A. P. Napartovich, N. N. Elkin, A. G. Sukharev, V. N. Troshchieva, D. V. Vysotsky, M. Nesnidal, E. Stiers, L. J. Mawst, and D. Botez, "Comprehensive Above-Threshold Analysis of Antiresonant Reflecting Optical Waveguide Edge-Emitting Diode Laser," *IEEE Journal of Quantum Electronics*, vol. 42, no. 6, pp. 589–599, June 2006.

[45] R. K. Huang, J. P. Donnelly, L. J. Missaggia, C. T. Harris, B. Chan, A. K. Goyal, A. Sanchez-Rubio, T. Y. Fan, and G. W. Turner, "High Brightness Slab-Coupled Optical Waveguide Lasers," *Proc. of SPIE*, vol. 6485, 2007.

[46] K. Paschke, R. Güther, J. Fricke, F. Bugge, G. Erbert, and G. Tränkle, "High power and high spectral brightness in 1060 nm α-DFB lasers with long resonators," *Electronic Letters*, vol. 39, no. 4, February 2003.

[47] K. Paschke, A. Bogatov, A. E. Drakin, R. Güther, A. A. Stratonnikov, H. Wenzel, G. Erbert, and G. Tränkle, "Modelling and measurement of the radiative characteristics of high-power α-DFB lasers," *IEEE. Journal of Selected Topics in Quantum Electronics*, vol. 9, no. 3, May 2003.

[48] K. Posilovic, T. Kettler, V. A. Schukin, S. S. Ledentsov, U. W. Pohl, D. Bimberg, J. Fricke, A. Ginolas, G. Erbert, G. Tränkle, J. Jönsson, and M. Weyers, "Ultrahigh-brightness 850 nm GaAs/AlGaAs photonic crystal laser diodes," *Appl. Phys. Lett.*, vol. 93, 2008.

[49] S. O'Brien, D. Mehuys, D. Welch, R. Parke, R. Lang, and D. Scifres, "High-Power Diffraction-Limited Monolithic Broad Area Master Oscillator Power Amplifier," *IEEE Photonics Technology Letters*, vol. 5, no. 5, May 1993.

[50] C. Fiebig, G. Blume, C. Kaspari, D. Feise, J. Fricke, M. Matalla, W. John, H. Wenzel, K. Paschke, and G. Erbert, "12W high-brightness single-frequency DBR tapered diode laser," *Electronics Letters*, vol. 44, no. 21, October 2008.

[51] O. B. Jensen, P. Andersen, B. Sumpf, K. H. Hasler, G. Erbert, and P. M. Petersen, "1.5 W green light generation by single-pass second harmonic generation of a single-frequency tapered diode laser," *Optics Express*, vol. 17, no. 8, April 2009.

[52] C. Chang-Hasnain, J. Berger, D. Scifres, W. Streifer, and J. Whinnery, "High power with high efficiency in a narrow single-lobed beam from a diode laser array in an external cavity," *Appl. Phys. Lett.*, vol. 50, no. 21, May 1987.

[53] R. Waarts, A. Hardy, D. Mehuys, W. Streifer, and D. Welch, "Coherent radiation from a Broad Area Semiconductor Laser in an External Cavity," *Proc. SPIE*, vol. 1219, 1990.

[54] V. Raab and R. Menzel, "External resonator design for high power laser diodes that yields 400 mW of TEM_{00} power," *Optics Letters*, vol. 27, no. 3, February 2002.

[55] A. Jechow and R. Menzel, "Efficient blue light generation by frequency doubling of a broad-area diode laser in a compact external cavity," *Applied Physics B*, vol. 89, no. 4, December 2007.

[56] A. Jechow, V. Raab, R. Menzel, M. Cenkier, S. Stry, and J. Sacher, "1W tunable near diffraction limited light from a broad area laser diode in an external cavity with a line width of 1.7 MHz," *Optics Communications*, vol. 277, pp. 161–165, 2007.

[57] V. Raab, D. Skoczowsky, and R. Menzel, "Tuning high-power laser diodes with as much as 0.38 W of power and $M^2 = 1.2$ over a range of 32 nm with 3-GHz bandwidth," *Optics Letters*, vol. 27, no. 22, November 2002.

[58] S. MacCormack and J. Feinberg, "High-brightness output from a laser-diode array coupled to a phase-conjugate mirror," *Optics Letters*, vol. 18, no. 3, February 1993.

[59] S. J. Jensen, M. Loebel, and P. Petersen, "Stability of the single-mode output of a laser diode array with phase conjugate feedback," *Applied Physics Letters*, vol. 76, no. 5, January 2000.

[60] M. Loebel, P. Petersen, and P. Johansen, "Single-Mode High-Power Semiconductor Lasers Using Phase Conjugation," *Journal of the Danish Optical Society (DOPS-NYT)*, vol. 3, 1998.

[61] S. Zhouping, L. Qihong, D. Jingxing, Z. Jun, and W. Runrong, "Beam quality improvement of laser diode array by using off-axis external cavity," *Optics Express*, vol. 15, no. 19, September 2007.

[62] B. Thestrup, C. Mingjun, B. Sass, and P. Petersen, "High brightness laser source based on polarization coupling of two diode lasers with asymmetric feedback," *Appl. Phys. Lett.*, vol. 82, no. 5, February 2003.

[63] E. Samsoe, P. Malm, P. Andersen, P. Petersen, and S. Andersson-Engels, "Imrpovement of brightness and output power of high-power laser diodes in the visible spectral region," *Optics Communications*, vol. 219, pp. 369–375, 2003.

[64] E. Samsoe, N. Kjaergaard, H. Lausen, P. Andersen, and P. Petersen, "An external-cavity laser diode at 635 nm for laser display applications," *Optics Communications*, vol. 245, pp. 333–339, 2005.

[65] C. Mingjun, N. Bogh, B. Thestrup, and P. Petersen, "Improvement of the beam quality of a broad-area diode laser using double feedback from two external mirrors," *Appl. Phys. Lett.*, vol. 85, no. 7, August 2004.

[66] E. Samsoe, P. Andersen, S. Andersson-Engels, and P. Petersen, "Improvement of spatial and temporal coherence of a broad area laser diode using an external-cavity design with double grating feedback," *Optics Express*, vol. 12, no. 4, February 2004.

[67] J. Chen, X. Wu, J. Ge, A. Hermerschmidt, and H. Eichler, "Broad-area laser diode with 0.02 nm bandwidth and diffraction limited output due to double external cavity feedback," *Appl. Phys. Lett.*, vol. 85, no. 4, July 2004.

[68] C. Liu, J. Ge, and J. Chen, "Study on a broad-area laser diode with external cavity feedback," *Optics and Laser Technology*, vol. 39, no. 1, pp. 169–173, February 2007.

[69] S. Wolff, D. Messerschmidt, and H. Fouckhardt, "Fourier-optical selection of higher order transverse modes in broad area lasers," *Optics Express*, vol. 5, no. 3, April 1999.

[70] G. Mowry and J. Leger, "Large-area, single-transverse-mode semiconductor laser with diffraction-limited super-Gaussian output," *Appl. Phys. Lett.*, vol. 66, no. 13, March 1995.

[71] S. Yiou, F. Balembois, P. Georges, and J. Huignard, "Improvement of the spatial beam quality of laser sources with an intracavity Bragg grating," *Optics Letters*, vol. 28, no. 4, February 2003.

[72] S. Mailhot, Y. Champagne, and N. McCarthy, "Single-mode operation of broad-area semiconductor laser with an anamorphic external cavity: experimental and numerical results," *Applied Optics*, vol. 39, no. 36, December 2000.

[73] W. Sharfin, A. Mooradian, C. Harding, and R. Waters, "Lateral-Mode Selectivity in External-Cavity Diode Lasers with Residual Facet Reflectivity," *IEEE Journal of Quantum Electronics*, vol. 26, no. 10, October 1990.

[74] Y. Zheng, A. Watanabe, T. Morita, and H. Kan, "High-Brightness Narrow-Bandwidth Operation of a Broad-Area Laser Diode with a Rear External Cavity," *Japanese Journal of Applied Physics*, vol. 45, no. 38, pp. 1025–1026, 2006.

[75] K. Jentsch, M. Sondermann, and T. Ackemann, "Analysis and optimization of coupling to external cavities in feedback experiments with vertical-cavity surface-emitting lasers," *Optics Communications*, vol. 281, pp. 1396–1400, 2008.

[76] H. Kogelnik and T. Li, "Laser Beams and Resonators," *Proceedings of the IEEE*, vol. 54, no. 10, October 1966.

[77] R. Hunsperger, *Integrated Optics*. Springer, 2002.

[78] Bronstein, Semendjajew, Musiol, and Mühlig, *Taschenbuch der Mathematik*. Verlag Harri Deutsch, 2001.

[79] P. Baues, "Huygen's Principle in Inhomogeneous, Isotropic Media and a General Integral Equation Applicable to Optical Resonators," *Opto-Electronics 1*, pp. 37–44, 1969.

[80] A. Bogatov, A. Drakin, A. Stratonnikov, and V. Konyaev, "Brightness and filamentation of a beam from powerful cw quantum-well $In_{0.2}Ga_{0.8}As/GaAs$ lasers," *Quantum Electronics*, vol. 30, no. 5, pp. 401–405, 2000.

[81] H. Wenzel, M. Dallmer, and G. Erbert, "Thermal lensing in high-power ridge-waveguide lasers," *Optical and Quantum Electronics*, vol. 40, no. 5, pp. 379–384, May 2008.

[82] W. Rideout, B. Yu, J. LaCourse, P. York, K. Beernick, and J. Coleman, "Measurement of the carrier dependence of differential gain, refractive index, and linewidth enhancement factor in strained-layer quantum well lasers," *Appl. Phys. Lett.*, vol. 56, no. 8, February 1990.

[83] A. Ukhanov, A. Stintz, P. Eliseev, and K. Malloy, "Comparison of the carrier induced refractive index, gain, and linewidth enhancement factor in quantum dot and quantum well lasers," *Appl. Phys. Lett.*, vol. 84, no. 7, February 2004.

[84] C. Carter and J. Harris, "Comparison of models describing the thermal lens effect," *Applied Optics*, vol. 23, no. 3, February 1984.

[85] J. Andrews, "Variable focusing due to refractive-index gradients in a diode-array traveling-wave amplifier," *J. Appl. Phys.*, vol. 64, no. 4, August 1988.

[86] L. Casperson and A. Yariv, "The Gaussian mode in optical resonators with a radial gain profile," *Appl. Phys. Lett.*, vol. 12, no. 10, May 1968.

[87] A. E. Siegman, "New developments in laser resonators," *Proc. SPIE*, vol. 1224, no. 2, 1990.

[88] H. Weber, "Some historical and technical aspects of beam quality," *Optical and Quantum Electronics*, vol. 24, pp. 861–864, 1992.

[89] N. Reng and B. Eppich, "Definition and measurements of high power laser beam parameters," *Optical and Quantum Electronics*, vol. 24, pp. 973–992, 1992.

[90] J. A. Tatum, R. Staszewski, D. L. MacFarlane, and H. B. Serreze, "Beam quality of high-power broad-area visible diode lasers," *Optical and Quamtum Electronics*, vol. 26, pp. 911–928, 1994.

[91] A. E. Siegman, G. Nemes, and J. Serna, "How to (Maybe) Measure Laser Beam Quality," in *DPSS (Diode Pumped Solid State) Lasers: Applications and Issues*. Optical Society of America, 1998.

[92] F. M. Dickey and S. C. Holswade, *Laser beam shaping, theory and techniques*. Marcel Dekker, Inc., 2000.

[93] B. Eppich, "Measurements of beam parameters with 2D matrix camera arrays," *Proc. SPIE*, vol. 2870, no. 31, 1996.

[94] P. Chan, K. Pipe, J. Plant, R. Swint, and P. Juodawlkis, "Temperature mapping and thermal lensing in large-mode, high-power laser diodes," *Applied Physics Letters*, vol. 89, 2006.

[95] D. Hall, L. Goldberg, and D. Mehuys, "Interferometric Measurement of Lateral Phase Profile and Thermal Lensing in Broad-Area Diode Amplifiers," *IEEE Photonics Technology Letters*, vol. 5, no. 8, August 1993.

[96] F. Hoos, S. Li, T. Meyrath, B. Braun, and H. Giessen, "Thermal lensing in an end-pumped Yb:KGW slab laser with high power single emitter diodes," *Optics Express*, vol. 16, no. 9, pp. 6041–6049, 2008.

[97] S. Amarande and M. Damzen, "Measurement of the thermal lens of grazing-incidence diode-pumped $Nd : YVO_4$ laser amplifier," *Optics Communications*, vol. 265, pp. 306–313, 2006.

[98] U. Wittrock, Ed., *Adaptive Optics for Industry and Medecine- Proceedings of the 4th international workshop*. Springer Verlag, 2005.

[99] G. Romo, T. Smy, D. Walkey, and B. Reid, "Modeling facet heating in ridge lasers," *Microelectronics Reliability*, vol. 43, pp. 99–110, 2003.

[100] E. Kowalczyk, L. Ornoch, Z. Gniazdowski, and B. Mroziewicz, "Dynamics of thermo-optical properties of semiconductor lasers," *Proc. of SPIE*, vol. 6456, 2007.

[101] L. Bechou, O. Rehioui, Y. Deshayes, O. Gilard, G. Quadri, and Y. Ousten, "Measurement of the thermal characteristics of packaged double-heterostructure light emitting diodes for space applications using spontaneous optical spectrum properties," *Optics and Laser Technology*, vol. 40, pp. 589–601, 2008.